Nuclear Physics
Dipartimento di Fisica
Università degli Studi di Milano
2021-22

from September 2021

Contents

1 The nucleon-nucleon (NN) interaction **7**
- 1.1 Elementary notions on the NN interaction 8
- 1.2 Structure of the NN interaction 11
- 1.3 The NN interaction from meson exchange 15
  - 1.3.1 Warm-up: the interaction range and Yukawa potential 16
  - 1.3.2 The one-pion exchange potential (OPEP) 18
  - 1.3.3 Two pion exchange potential 21
  - 1.3.4 The short-range repulsion 23
  - 1.3.5 The three-body force 24
- 1.4 Chiral forces 25

2 Nuclear bulk properties and shell structure: effective interactions for mean-field and Density Functional Theory **29**
- 2.1 Generalities on the nuclear mean-field 29
  - 2.1.1 Empirical potentials: Woods-Saxon 31
  - 2.1.2 Empirical estimate of the shell gap 34
- 2.2 Hartree-Fock theory 35
- 2.3 Effective interactions for Hartree-Fock 39
  - 2.3.1 Symmetric nuclear matter with a simplified Skyrme force 40
- 2.4 Nuclear Density Functional Theory (DFT) 43

3 Nuclear superfluidity **47**
- 3.1 BCS theory 48
- 3.2 Derivation of the BCS equations 51
- 3.3 Solution of the BCS equations in schematic cases 56
  - 3.3.1 Solution for equally spaced levels 57
  - 3.3.2 Solution for a single j-shell 57
- 3.A Appendices 59

3.A.1 Matrix elements of use for the BCS theory 59

4 Spectroscopy of even-even nuclei and collective vibrations 61
4.1 Spectra of vibrational and rotational nuclei 62
4.2 Phenomenology of nuclear vibrations 64
4.3 Linear response theory for nuclear vibrations 68
4.4 Solution of the TDA equations in a schematic model 72

5 Nuclear deformation and collective rotations 75
5.1 Introduction to nuclear shapes 75
5.2 Intrinsic shape and orientation 77
5.3 Rotational bands of an axial even-even nucleus 79
5.4 Electromagnetic transitions and exctraction of the intrinisic β 82
5.5 Moments of inertia 86
5.6 Motion of a particle in a deformed potential: simple features . 86

6 Electromagnetic moments and transitions 89
6.1 Multipole expansion of the electromagnetic interaction 90
6.2 Electric multipole operators and moments 91
6.3 Electric multipole transitions and single-particle units 93
6.4 The magnetic sector 95
6.5 Lifetimes 97

7 Direct nuclear reactions 99
7.1 Introduction and classification of reactions 99
7.2 Formal theory 102
7.2.1 The Lippmann-Schwinger equation 104
7.2.2 The scattering amplitude and the cross section 106
7.3 Elastic scattering 107
7.3.1 Kinematics 107
7.3.2 Cross section within the Born approximation 108
7.3.3 Absorbtion and the optical potential 111
7.3.4 Eikonal approximation 113
7.4 Inelastic scattering 115
7.4.1 General considerations and kinematics 115
7.4.2 The Distorted Wave Born Approximation (DWBA) . . 117
7.4.3 Coulomb excitation 119

7.4.4 Plane Wave Born Approximation (PWBA) with a zero-range force . . . 121
7.A Appendices . . . 122
7.A.1 Tranformation between the LAB and COM system for the incident energy . . . 122

8 Compound nucleus reactions 125
8.1 Neutron reactions . . . 125
8.2 Charged particles reactions . . . 129
8.3 Experimental findings and the nuclear temperature . . . 132

9 Selected topics in Nuclear Astrophysics 135
9.1 Nuclear reactions inside stars . . . 135
9.1.1 The origin of the energy emitted by the sun . . . 135
9.1.2 Hydrostatic equilibrium and average properties of the sun . . . 136
9.1.3 Nuclear reactions in the sun . . . 138
9.1.4 The case of other stars . . . 138
9.2 The Gamow peak . . . 139
9.3 The nucleosynthesis problem . . . 142
9.4 Neutron stars . . . 144
9.4.1 A crude argument . . . 145
9.4.2 The Tolman-Oppenheimer-Volkov (TOV) equation . . . 146
9.4.3 Brief discussion of the neutron star structure . . . 148

10 Fusion and fission reactions 151
10.1 Heavy-ion fusion reactions . . . 151
10.1.1 Classical approximation . . . 153
10.1.2 Sub-barrier fusion and Wong's formula . . . 154
10.1.3 Failure of potential models below the barrier: fusion enhancement . . . 156
10.2 Nuclear fission . . . 156
10.2.1 General aspects . . . 156
10.2.2 The case of U and the role of pairing . . . 160
10.2.3 The fission chain reaction . . . 161
10.3 Appendix: relation between b and l . . . 163

Chapter 1

The nucleon-nucleon (NN) interaction

The first part of this manuscript deals with nuclear structure, namely with the branch of physics that aims at understanding all properties of nuclei. This study is often extended to uniform nucleonic matter which, strictly speaking, does not exist and yet is a very useful ideal system on which basic ideas and sophisticated theories can be tested. The fresh student can immediately appreciate the comparison with the case of Coulomb systems, as the uniform electron gas plays a similar role in that context. Moreover, this system is less artificial that it may seem at a first glance, because some layers of neutron stars are very similar to uniform nuclear matter (we shall discuss some features of neutron stars in Chapter 9).

There is no standard model for nuclear structure physics but rather a variety of approaches, and each of them is based on a Hamiltonian together with a more-or-less-approximate many-body method to solve the Schrödinger equation. In this text, we shall restrict ourselves to methods based on non-relativistic quantum mechanics, although relativistic or covariant approaches do exist.

A basic distinction should be made between the so-called *ab initio* approaches and the others. Note that the very definition of *ab initio* has changed during the time, and this may still continue. *Ab initio* approaches use some technique to solve the many-body problem that is in principle exact, or systematically improvable, and can provide a reliable estimate of the theoretical error of the predicted quantities. Up to 10-15 years ago, any *realistic* Hamiltonian that includes two- or three-nucleon interactions and it is fitted to

reproduce few-body observables would have been considered sufficient. This involves substantial phenomenological assumptions. Many current practitioners seek to avoid this limitation by requiring that the Hamiltonian should be derived, in some controlled way, from the basic theory of strong interaction, that is quantum chromodynamics (QCD).

In any event, there is no unique Hamiltonian. This would not be a problem at all, if there were different Hamiltonians that predict compatible values for the different observables. So far, the different Hamiltonians are not accurate enough and there are discrepancies between the results of different Hamiltonians when used within a given many-body method. Nevertheless, this is an active field of research and progress is continuously made: we can expect that the picture will become more clear in the coming years.

The computational methods to solve the many-body Schrödinger equation that lie at the core of *ab initio* theory are also a field of very active research. We mention the most widely used ones, for the sake of completeness, and we provide some references: Quantum Monte Carlo (QMC) [1, 2], In-Medium Similarity Renormalization Group (IM-SRG) methods [3], Coupled Cluster (CC) approach [4], Self-Consistent Green's Function (SCGF) theory [5], Brueckner-Hartree-Fock (BHF) theory [6], and No-Core Shell Model (NCSM) [7]. The reason why we do not discuss them is that it would require the student to be more conversant with many-body physics than we can safely assume. However, one can find useful pedagogic descriptions of all these methods in [8, 9].

In this Chapter we focus on the simpler task of understanding the main features of the bare nucleon-nucleon (NN) interaction. Many of these features will be common to the effective Hamiltonians that are employed in other contexts than *ab initio*. In this respect, reading this Chapter is instrumental also for the understanding of the mean-field methods that are the subject of the following Chapters, as well as of general symmetries and properties of nuclear forces in a general sense.

1.1 Elementary notions on the NN interaction

There are a number of general features of the interaction between nucleons that can be easily inferred from the phenomenology. We briefly recall them

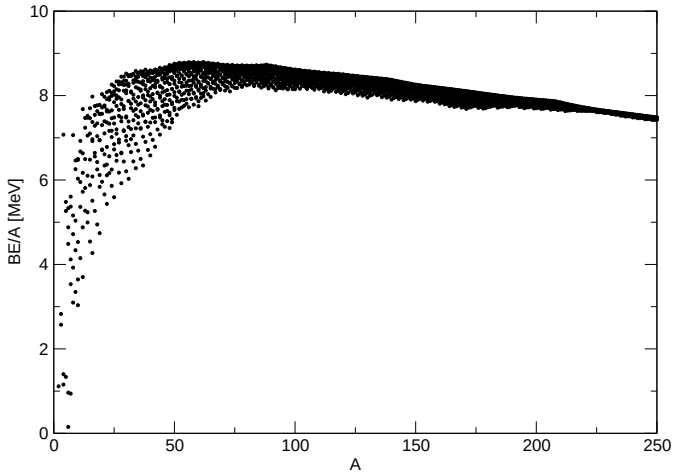

Figure 1.1: Binding energy per particle B/A as a function of the mass number A. Figure taken from Ref. [10] and data from Refs. [11, 12].

in what follows.

- *Short range.* The short-range nature of the NN interaction is well-known. It can be simply guessed in the following manner.

Nucleus	BE/A [MeV]
^{2}H $\equiv d$	1.112
^{3}He	1.493
^{4}He $\equiv \alpha$	7.073

Table 1.1: Binding energies per particle of the lightest nuclei.

In Table 1.1, we display the binding energy per particle BE/A of the lightest nuclei. The same quantity in the whole range of A is shown in Fig. 1.1. The figure is meant to remind the well-known fact that BE/A saturates at a value around ≈ 8 MeV. From the table, we see that the α-particle displays a value of BE/A that, although smaller, is still comparable to the saturation value. The widely accepted interpretation is that BE/A in nuclei saturates because each nucleon interacts only with its nearest neighbours; thus, we can conclude that this happens already, roughly speaking, when four nucleons are bound together. Along this

line, we can make a first estimate of the range of the NN force, which should be of the order of the radius of the α-particle. Looking at the experimental finding for this quantity [13], we can say that

$$\text{Range } \approx 1.5 \text{ fm}. \tag{1.1}$$

- *Hard core.* The scattering data indicate that the NN force has a strongly repulsive component, dubbed as hard core, for relative distances of the order of $\approx$ 0.4-0.5 fm. This is not quite relevant for low-energy nuclear structure. As we will discuss below, nucleons hardly find themselves at these distances in normal conditions.

- *Spin-dependence.* The two-nucleon system can be in the three different states pp, nn and pn. Only the pn system displays a bound state. How do we reconcile this fact with the charge independence property of the nuclear force, that is known to hold since the Coulomb force and the charge-breaking terms of the NN force are relatively weak? The solution lies in the spin-dependence of the NN force, together with the role of the Pauli principle.

  To a very good approximation, the NN two-body potential commutes with isospin,

  $$\left[V_{NN}, T^2\right] = 0, \quad [V_{NN}, T_z] = 0. \tag{1.2}$$

  The consequence is that the two-nucleon system must be in a state with good quantum numbers T, T_z. Since the neutron and proton states can be taken as[1], respectively, $|t = 1/2, t_z = 1/2\rangle$ and $|t = 1/2, t_z = -1/2\rangle$, the two-nucleon system can in principle be in the states $T = 0, 1$. However, for the pp and nn systems T_z is equal to 1 and -1 respectively, and thus these two systems can only be found in the $T = 1$ state. On the other hand, the pn system can also be in a $T = 0$ state. The other quantum numbers for the two-particle states can be the orbital angular momentum L and spin S. At low energy we can limit our discussion to $L = 0$ states. Since the total wave function must be antisymmetric, and the $L = 0$ part is symmetric, it is clear that $T = 1$ implies $S = 0$, while $T = 0$ implies $S = 1$. The NN interaction in the $T = 1, S = 0$ channel must be equal in the pp, nn, and pn cases, and it turns out

[1] The convention we use here is the most common in nuclear physics. In particle physics, the opposite convention for t_z is instead more common.

to be not strong enough to bind the two particles. The pn system can also exist in the $T = 0, S = 1$ state and has a bound state. Therefore, we can deduce that, for $L = 0$,

$$V(S = 1, T = 0) \text{ is more attractive than } V(S = 0, T = 1). \quad (1.3)$$

In the literature one often employs the spectroscopic notation $^{2J+1}L_S$ and writes

$$V(^3S_1) \text{ is more attractive than } V(^1S_0). \quad (1.4)$$

In general, quite a lot can be understood in nuclear structure by assuming that the pn interaction is dominant and the interaction between particles of the same kind (pp and nn) is negligible [14]. Only one example here: as a function of the neutron number, ^{24}O is the last bound O isotope ($Z = 8$); if we add just one proton and move to F ($Z = 9$), we can bind seven more neutrons as the last bound F isotope is ^{31}F!

- *Spin-orbit component.* This component must exist in the NN interaction since we need it in many contexts like e.g. in the analysis of scattering data. Moreover, in nuclear stucture it is known that the magic numbers of nuclei cannot be explained without a strong spin-orbit force (having opposite sign with respect to the atomic case).

- *Tensor component.* The deuteron is not spherical but has a positive electric quadrupole moment. We also need a component of the NN interaction that explains this phenomenon. As will be discussed in the following, the so-called tensor component is needed to explain why $L = 0$ and $L = 2$ mix together. We will also show that this component emerges naturally from the simplest field theory for the nucleus: nucleons, pions, and their coupling.

1.2 Structure of the NN interaction

In a phenomenological approach, we can assume that the two-body NN interaction is the most general function of the position, momentum and spin of the two particles that fulfils the requirements of being invariant under translations, Galilean boosts, rotations, parity and time-reversal, as well as under

the exchange of the two nucleons. The consequences of these requirements are best seen if we use the center-of-mass and relative distance coordinates,

$$\begin{cases} \mathbf{R} = \dfrac{\mathbf{r}_1 + \mathbf{r}_2}{2}, \\ \mathbf{r} = \mathbf{r}_1 - \mathbf{r}_2, \end{cases} \tag{1.5}$$

with the corresponding conjugate momenta

$$\begin{cases} \mathbf{P} = \mathbf{p}_1 + \mathbf{p}_2, \\ \mathbf{p} = \dfrac{\mathbf{p}_1 - \mathbf{p}_2}{2}. \end{cases} \tag{1.6}$$

We leave aside for the moment the charge-dependence, or isospin-dependence, of the NN interaction: we shall return to this at the end of this Section. The NN potential is, therefore, a function

$$V = V(\mathbf{R}, \mathbf{P}, \mathbf{r}, \mathbf{p}, \sigma_i), \tag{1.7}$$

with $i = 1, 2$. Translations (Galilean boosts) are transformations in which $\mathbf{r}_i \to \mathbf{r}_i + \mathbf{a}$ ($\mathbf{p}_i \to \mathbf{p}_i + \mathbf{p}_0$). They do not change $\mathbf{r}$ and $\mathbf{p}$; if the potential must be invariant under them, it must be independent both of $\mathbf{R}$, that becomes $\mathbf{R} + \mathbf{a}$, and of $\mathbf{P}$, that becomes $\mathbf{P} + 2\mathbf{p_0}$. Rotational invariance implies that the potential must be a scalar. With two of the vectors $\mathbf{A}$, $\mathbf{B}$ among those that we have at our disposal $(\mathbf{r}, \mathbf{p}, \sigma_i)$, we can form:

$$\begin{cases} \mathbf{A} \cdot \mathbf{B}, & \text{scalar product;} \\ \mathbf{A} \pm \mathbf{B}, \mathbf{A} \times \mathbf{B}, & \text{sum or difference and vector product;} \\ \mathbf{A} \otimes \mathbf{B} \equiv \frac{1}{2}\left(A_i B_j + A_j B_i\right) - \frac{1}{3}\delta_{ij}\mathbf{A} \cdot \mathbf{B}. & \text{rank two-tensor product or tensor product.} \end{cases} \tag{1.8}$$

The quantities defined in the upper three lines transform, under rotations, as scalars, vectors and tensors, respectively. The only way to obtain an overall scalar is to make combinations of the type scalar-scalar, vector-vector or tensor-tensor. In the case at hand, the operators $\mathbf{r}$ and $\mathbf{p}$ act on the space part of the wave functions while the spin operators act on their spin part. Therefore, we can conclude that the simplest ways to form a scalar V correspond to combine a scalar, vector, or tensor formed with space operators, with a scalar, vector, or tensor, respectively, formed with spin operators. These combinations must respect the parity and time-reversal invariance that we have not exploited yet. Thus, we now sort these combinations out.

We remind that under parity P,

$$\begin{cases} \mathbf{r} \to -\mathbf{r} \\ \mathbf{p} \to -\mathbf{p} \\ \sigma_i \to \sigma_i, \end{cases} \tag{1.9}$$

whereas under time-reversal

$$\begin{cases} \mathbf{r} \to \mathbf{r} \\ \mathbf{p} \to -\mathbf{p} \\ \sigma_i \to -\sigma_i. \end{cases} \tag{1.10}$$

We label by + (-) combinations of operators that are even (odd) under a given transformation. The result is in Table 1.2.

	P	T		P	T
r^2	+	+	1	+	+
p^2	+	+	$\sigma_1 \cdot \sigma_2$	+	+
$\mathbf{r} \cdot \mathbf{p}$	+	-			
$\mathbf{r}$	-	+	$\sigma_1 \times \sigma_2$	+	+
$\mathbf{p}$	-	-	$\sigma_1 \pm \sigma_2$	+	-
$\mathbf{r} \times \mathbf{p}$	+	-			
$\mathbf{r} \otimes \mathbf{r}$	+	+	$\sigma_1 \otimes \sigma_2$	+	+
$\mathbf{p} \otimes \mathbf{p}$	+	+			
$\mathbf{r} \otimes \mathbf{p}$	+	-			

Table 1.2: Scalar, vector and tensor combinations of the space and spin operators, together with their properties under the transformations P and T.

From Table 1.2 we now easily read the simplest possible combinations that produce acceptable terms of the NN potential V. We list and comment them here below.

- Scalar-scalar combinations.

  1. A simple function of r^2 (or r) is possible. We call it *central potential* $V_C(r)$. It can be a function of p as well.
  2. A function V_S of r (or, in principle, of p) can be multiplied by $\sigma_1 \cdot \sigma_2$. We call it *spin potential* $V_S(r)\ \sigma_1\sigma_2$.

- Vector-vector combinations.

  3. The only possibility is to combine $\mathbf{r} \times \mathbf{p}$ with $\sigma_1 + \sigma_2$ (note that combining with $\sigma_1 - \sigma_2$ is not possibile because it would not provide a term which is invariant under exchange $1 \leftrightarrow 2$). A function of scalars $V_{LS}(r)$ [or $V_{LS}(p)$], multiplied by $2\,(\mathbf{r} \times \mathbf{p})\,(\sigma_1 + \sigma_2) \equiv \mathbf{L}{\cdot}\mathbf{S}$, is called *spin-orbit potential*.

- Tensor-tensor combinations.

  4. We can consider

$$\begin{aligned}
[\mathbf{r} \otimes \mathbf{r}]\,[\sigma_1 \otimes \sigma_2] &= \left(\frac{1}{2} r_i r_j + \frac{1}{2} r_j r_i - \frac{1}{3}\delta_{ij} r^2\right)\left(\frac{1}{2}\sigma_{1i}\sigma_{2j} + \frac{1}{2}\sigma_{1j}\sigma_{2i} - \frac{1}{3}\delta_{ij}\sigma_1 \cdot \sigma_2\right) \\
&= (\sigma_1 \cdot \mathbf{r})\,(\sigma_2 \cdot \mathbf{r}) - \frac{1}{3}\sigma_1 \cdot \sigma_2 r^2 \equiv \frac{r^2}{3} S_{12}(\hat{r}), \qquad (1.11)
\end{aligned}$$

     where in the last step the so-called tensor operator S_{12} has been defined. A function of other scalars V_T times this quantity $S_{12}(\hat{r})$ is called *tensor potential*. In principle we can form the same combination with the momentum p, and we can introduce another function $V_{T'}$ times $S_{12}(\hat{p})$.

We can, then, ask ourselves the question whether more complicated combinations of space and spin operators can produce new terms in the NN potential. It is clear that powers of r^2, p^2 do not provide anything new, and the same can be said for powers of $\sigma_1 \cdot \sigma_2$ (try yourself, and remember that $\sigma^2 = 3$ because the square of each Pauli matrix is 1). On the other hand, two new combinations of scalars can be introduced.

5. $(\mathbf{r} \cdot \mathbf{p})^2$ generates a possible new term of the potential because it is invariant under P and T. From simple vector algebra,

$$\begin{aligned}
L^2 &= (\mathbf{r} \times \mathbf{p})\,(\mathbf{r} \times \mathbf{p}) = r^2 p^2 - (\mathbf{r} \cdot \mathbf{p})^2 \quad \Rightarrow \\
(\mathbf{r} \cdot \mathbf{p})^2 &= r^2 p^2 - L^2, \qquad (1.12)
\end{aligned}$$

   so that a function of $(\mathbf{r} \cdot \mathbf{p})^2$ can be replaced by a function of L^2. Consequently, we can introduce a function of other scalars V_L times L^2. This term does not carry any special name, and is simply dubbed L^2 *term*.

6. By the same argument, and from Table 1.2, we can introduce a function of other scalars times $L^2\sigma_1 \cdot \sigma_2$.

It is rather tedious to check if new combinations appear or not by combining more vectors or more tensors. We state without proof that the only new term that appears as a candidate for a term in the NN potential is the following.

7. The so-called *quadratic spin-orbit potential* is given by a function V_Q of other scalars times the combination $(\mathbf{L} \cdot \mathbf{S})^2$. It arises from $(\mathbf{r} \cdot \mathbf{p})(\mathbf{r} \otimes \mathbf{p})(\sigma_1 \otimes \sigma_2)$.

In conclusion, the general form of the NN potential $V_{NN}(1,2)$ turns out to be the sum of all the terms we have described.

For each term, we have a pp (or nn) plus a pn term. If we work in isospin representation, for each term we have the possibility to multiply by the identity (in isospin space) or by $\tau_1 \cdot \tau_2$. All this gives 14 terms. One of the most famous and widely used potentials, the so-called Argonne potential AV18 [15], contains 18 terms that are the 14 we have just discussed, plus four charge-symmetry breaking term that we do not discuss here. This potential has been fitted using 4301 scattering data, at laboratory energy smaller than 350 MeV. The reduced χ^2 is 1.09, testifying to the great accuracy of such potential. Many other phenomenological potentials exist on the market.

It should be stressed that one could re-express the 14 terms we have just discussed in different forms. Eq. (1.12) clarifies that one can use in fact functions of $\mathbf{r}$ and $\mathbf{p}$. We shall return to this point in the following discussion.

1.3 The NN interaction from meson exchange

In a microscopic picture, the interaction between particles arises from the exchange of another particle that acts as a mediator, that is, of a particle that transfers the energy and the quantum numbers associated with the interaction. Field theory is the fundamental theory of all forces when they are treated in this manner. Different types of fields are associated with the interacting particles and with the mediators (like e.g. Dirac and Klein-Gordon fields). In the best known quantum field theory, quantum electrodynamics (QED), photons are the bosons that mediate the electromagnetic force between charged particles like the electrons.

The strong force is far more challenging than the electromagnetic force. The theory that describes it at best, as of today, is QCD. This theory is,

unfortunately, highly non-perturbative at the low-energy scale which is of interest for nuclear structure. In the past, it has been often said that QCD is needed when dealing with quarks and gluons, that is, at an energy (length) scale which is much higher (lower) than the nuclear scale. At the nuclear scale, quarks are *confined* into baryons (like the nucleons) and mesons.

Nucleons can be treated in a simpler way, if we do not aim to derive the NN interaction from QCD, but we describe it in terms of mesons exchanged between nucleons. We will follow this idea in this Section, and discuss in Sec. 1.4 to which extent the recent developments have altered this picture, by rooting better the NN interactions in QCD.

1.3.1 Warm-up: the interaction range and Yukawa potential

In elementary courses, it is often hinted that if an interaction is mediated by a particle having mass μ, the interaction range is

$$\text{Range } \approx \frac{\hbar}{\mu c}. \tag{1.13}$$

We suggest that the student checks that he or she can derive this simple equation using the uncertainty principle. We also use it to introduce the fact that in this part of the manuscript devoted to microscopic NN interactions (and only here) we shall employ natural units. In these units, $\hbar = c = 1$. A useful mnemonic trick to get acquainted with these units consists in remembering that the range associated with a pion (μ around 140 MeV) is ≈ 1.4 fm. Note the consistency with Eq. (1.1), which is obviously not accidental. The pion is the lightest meson that can be exchanged between nucleons, and a meson whose mass is 2 or 5 times larger will give rise to a component in the NN force with a range which is 2 or 5 times smaller.

In addition to knowing the range, we also need to know the radial dependence of an interaction which is mediated by a meson with mass μ. The meson wave fuction ϕ must satify the Klein-Gordon equation, that is, in the vacuum

$$\left(\Box + \mu^2\right) \phi(\vec{r}, t) = \left(\frac{\partial^2}{\partial t^2} - \nabla^2 + \mu^2\right) \phi(\vec{r}, t) = 0. \tag{1.14}$$

If the meson is coupled to a density ρ of given particles,

$$\left(\Box + \mu^2\right) \phi(\vec{r}, t) = \left(\frac{\partial^2}{\partial t^2} - \nabla^2 + \mu^2\right) \phi(\vec{r}, t) = 4\pi\rho(\vec{r}, t). \tag{1.15}$$

The student should note that if the mass μ is set to 0, as it happens for the photon, this is the equation for the electromagnetic potential[2] that he or she knows already. Thus, we may be content with this heuristic discussion.

If we move to the static case by negecting the time-dependence in the latter equations, (1.15) becomes

$$\left(-\nabla^2 + \mu^2\right) \phi(\vec{r}) = 4\pi\rho(\vec{r}). \tag{1.16}$$

Inhomogeneous equations like the latter one can be solved by using the Green's function or propagator G, that is the solution of

$$\left(\nabla^2 - \mu^2\right) G(\vec{r}, \vec{r}\,') = -\delta^{(3)}(\vec{r} - \vec{r}\,'). \tag{1.17}$$

The solution of this equation is easier in momentum space. If $G(\vec{k})$ is the Fourier transform of $G(\vec{r}, \vec{r}\,')$, we can obtain

$$G(\vec{k}) = \frac{1}{k^2 + \mu^2}, \tag{1.18}$$

and, from this[3],

$$G(\vec{r}, \vec{r}\,') = \frac{e^{-\mu|\vec{r} - \vec{r}\,'|}}{4\pi|\vec{r} - \vec{r}\,'|}. \tag{1.19}$$

One should be reminded that the Green's function allows to write the solution ϕ of the inhomogeneous equation (1.16) in terms of one solution ϕ_0 of the corresponding homogeneous equation as

$$\phi(\vec{r}) = \phi_0(\vec{r}) + 4\pi \int d^3r'\; G(\vec{r}, \vec{r}\,')\rho(\vec{r}\,') = \phi_0(\vec{r}) + \int d^3r'\; \frac{e^{-\mu|\vec{r} - \vec{r}\,'|}}{|\vec{r} - \vec{r}\,'|}\rho(\vec{r}\,'). \tag{1.20}$$

The latter equation shows how we can interpret the Green's function, in this case, as the meson-nucleon potential. In fact, the quantity in Eq. (1.19) is the well-known Yukawa potential V_{Yukawa}, and Eq. (1.18) is the same potential in momentum space (aside from 4π-factors).

Before we move to the pion-exhange potential, we end this warm-up by saying that matrix elements of the potentials could be represented by Feynman diagrams. Although we do not strictly need any of them in what follows, we display in Fig. 1.2 the diagram associated with the potential (1.18) in momentum space.

[2] In the Lorenz gauge.

[3] The students are encouraged to perform the calculations in detail. Eq. (1.18) is straightforward while deriving Eq. (1.19) requires the use of the residue theorem to solve integrals.

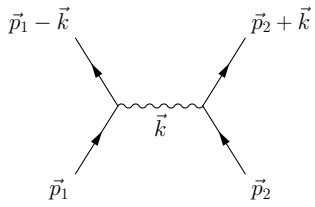

Figure 1.2: Feynman diagram associated with the exchange of a meson (wavy line) between nucleons (lines with arrows). The labels indicate the momenta of the particles. In this case, the wavy line represents the potential of Eq. (1.18).

1.3.2 The one-pion exchange potential (OPEP)

In the considerations made in the previous subsection, we have assumed that the exchanged meson is purely scalar. Mesons have spin and can have scalar, pseudo-scalar, vector, pseudo-vector, tensor and pseudo-tensor couplings with nucleons. Moreover, they possess isospin. Then, in general, the potential will have an operator structure which is less simple than just the identity operator as in Eq. (1.19).

As we said, the lightest meson that can be exchanged between nucleons is the pion ($m_\pi \approx 140$ MeV). The pion (i) is pseudo-scalar ($J^\pi = 0^-$); and (ii) it belongs to an isospin (or charge) triplet. As a consequence of (i), each pion-nucleon vertex must include a scalar operator that changes the parity: such operator must be $\sigma \cdot \mathbf{k}$, since the momentum $\mathbf{k}$ is equal to $-i\nabla$ and the gradient changes the parity of any wave function. As a consequence of (ii), each pion-nucleon vertex must include an isospin operator. These facts provide us with a clear guidance to write down the operator structure, and generalise appropriately Eqs. (1.18) and (1.19):

$$V_{\rm OPEP}(\mathbf{k}) = -\frac{f_\pi^2}{m_\pi^2}\frac{(\sigma_1\cdot\mathbf{k})\,(\sigma_2\cdot\mathbf{k})}{k^2+m_\pi^2}\,(\tau_1\cdot\tau_2)\,, \tag{1.21}$$

$$V_{\rm OPEP}(\mathbf{r}) = \frac{f_\pi^2}{m_\pi^2}\,(\sigma_1\cdot\nabla)\,(\sigma_2\cdot\nabla)\,\frac{e^{-m_\pi r}}{4\pi r}\,(\tau_1\cdot\tau_2)\,. \tag{1.22}$$

Two comments are in order. Those who know Dirac theory can attempt to derive this form of the coupling from what is known to be the Lagrangian describing the pion-nucleon coupling[4]. The coupling constant $f_\pi^2 = 0.08$ can be deduced from data on pion-nucleon interactions (for details, and more precise values of this coupling constant, cf. Ref. [16]).

[4] $\mathcal{L} = i\frac{f_\pi}{m_\pi}\bar{\psi}(x)\gamma_5\vec{\tau}\psi(x)\cdot\vec{\pi}(x)$, where ψ is the Dirac nucleon field and π is the pion field. Arrows refer here to vectors in isospin space.

To clarify the structure of Eq. (1.22), we can perform the following steps. We start from the identity

$$(\sigma_1 \cdot \nabla)(\sigma_2 \cdot \nabla) = \frac{1}{3}(\sigma_1 \cdot \sigma_2)\nabla^2 + \frac{1}{3}\left[3(\sigma_1 \cdot \nabla)(\sigma_2 \cdot \nabla) - (\sigma_1 \cdot \sigma_2)\nabla^2\right],$$

and verify that the contribution from ∇^2 ($\nabla_i \nabla_j$ with $i = j$) cancels when working out the term in the square brackets. Using elementary formulas from vector algebra, together with $\nabla^2(1/r) = -4\pi\delta^{(3)}(r)$, we can evaluate the following derivatives:

$$\begin{aligned} \nabla^2 \frac{e^{-m_\pi r}}{r} &= m_\pi^2 \frac{e^{-m_\pi r}}{r} - 4\pi\delta^{(3)}(r), \\ (\sigma \cdot \nabla)\frac{e^{-m_\pi r}}{r} &= \left(-m_\pi \sigma \cdot \frac{\vec{r}}{r} - \sigma \cdot \frac{\vec{r}}{r^2}\right)\frac{e^{-m_\pi r}}{r}. \end{aligned}$$

Finally, by inserting all this into (1.22), we arrive at the standard form of the OPEP:

$$\begin{aligned} V_{\rm OPEP}(r) &= f_\pi^2 m_\pi \tau_1 \cdot \tau_2 \left[S_{12}\left(\frac{1}{(m_\pi r)^3} + \frac{1}{(m_\pi r)^2} + \frac{1}{(3m_\pi r)}\right) e^{-m_\pi r} + \right. \\ &+ \left. \frac{\sigma_1 \cdot \sigma_2}{3}\frac{e^{-m_\pi r}}{m_\pi r} - \frac{4\pi}{3m_\pi^3}\delta^{(3)}(r)\sigma_1 \cdot \sigma_2 \right], \end{aligned} \tag{1.23}$$

where S_{12} has been defined in (1.11). The last term (i.e. the contact one) is neglected in the following discussion, because we will show below that other terms dominate at short distances and that they can incorporate this contact term.

Values of the OPEP in the different channels can be estimated if one is reminded that

$$\langle S|\sigma_1 \cdot \sigma_2|S\rangle = \begin{cases} -3 & S = 0; \\ +1 & S = 1, \end{cases} \tag{1.24}$$

and that the same holds for $\langle T|\tau_1 \cdot \tau_2|T\rangle$. If we neglect the tensor part, S_{12}, the spin part of (1.23) in the ${}^1S_0$ channel is shown in the left panel of Fig. 1.3. Units have been converted to usual ones (fm and MeV). For the sake of completeness, we show in the right panel of the same figure the $l = 0$ phase shifts δ_0 associated with the same potential[5]. Looking at the left panel,

[5]Look back at your introductory quantum mechanics course to be reminded about phase shifts.

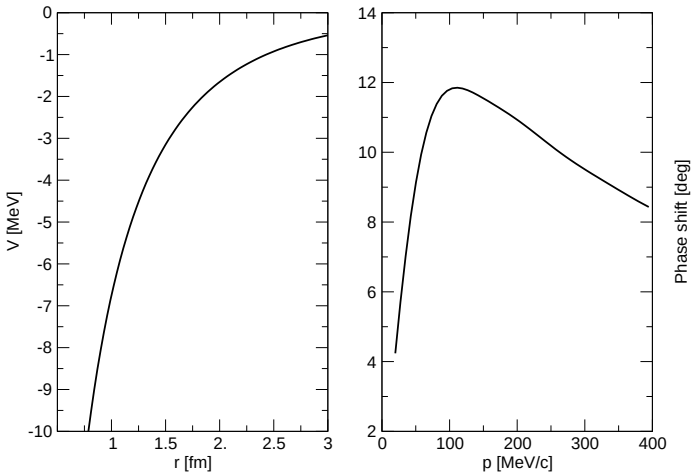

Figure 1.3: (Left panel) Spin part of the OPEP potential [cf. Eq. (1.23)] in the ${}^1S_0$ channel. (Right panel) Phase shifts associated with the potential of the left panel (see the analogous Fig. A.1 in [17]).

let us focus on the region around 1.4 fm, as we have already stressed that other components of the potential become dominant at smaller distances. We can compare the value of potential in that region with the kinetic energy associated with the relative motion of two nucleons at the same distance. This, in turn, can be estimated from the uncertainty principle as

$$\Delta p \approx \frac{\hbar}{\Delta r} \quad \Rightarrow \frac{(\Delta p)^2}{2m} = \frac{(\hbar c)^2}{2mc^2\,(\Delta r)^2} \approx 10 \text{ MeV} \tag{1.25}$$

(where m is the nucleon mass). The relative weakness of the potential can be judged with respect to this value of the kinetic energy. Note that this statement remains true for the potential in the ${}^3S_1$ channel.

One should also inspect the tensor part of the OPEP. Because of the presence of the position operator in S_{12}, a precise estimate of the expectation values of this component requires the knowledge of the two-particle wave function. However, it is easy to infer from the form of S_{12} that, if the two-particle wave function has spherical symmetry, the tensor contribution vanishes. We can make a qualitative estimate of the tensor component of the OPEP in a deformed configuration, with the help of Fig. 1.4.

From the expression of S_{12} and the relative orientation of the relative vector and of the two spins, one can easily deduce the expectation values of

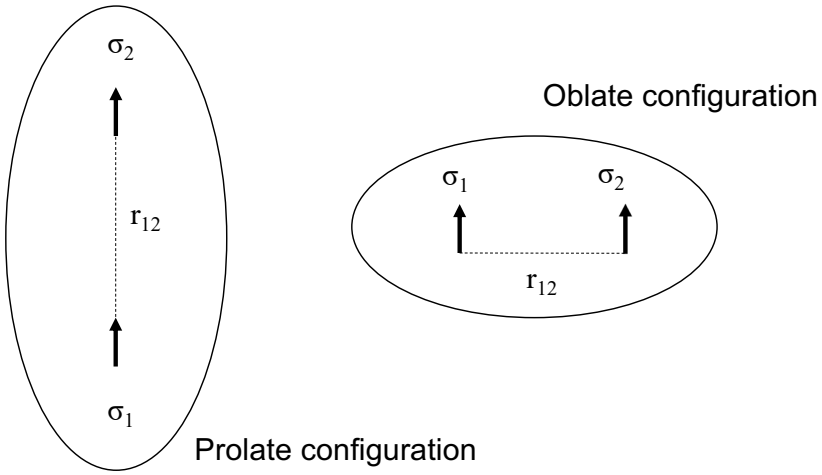

Figure 1.4: Schematic picture of the configurations in which the spins are either aligned with (prolate configuration) or perpendicular to (oblate configuration) the relative distance vector **r**.

the tensor operator in the two configurations of Fig. 1.4:

$$S_{12} = \begin{cases} -1 & \text{if the spins are orthogonal to } \hat{r} \text{ (oblate configuration);} \\ +2 & \text{if the spin are parallel to } \hat{r} \text{ (prolate configuration).} \end{cases} \tag{1.26}$$

It must be stressed that in the case of the deuteron, that is, neutron and proton in the $T = 0$ channel, we easily see from Eqs. (1.23) and (1.26) that the prolate configuration is favoured. This explains the exerimental fact that the deuteron has a positive electric quadrupole moment, $Q = 0.28590$ e fm^2.

1.3.3 Two pion exchange potential

The main shortcomings of the OPEP are: (i) it lacks a central part, and (ii) it is unlikely to provide enough binding, as we have discussed in the previous subsection. One expects a contribution to the NN potential from (correlated) two-pion exchange, with a range $\approx 1/(2m_\pi) \approx 0.7$ fm. A microscopic calculation of this potential is tough and may be affected by theoretical uncertainites, since several Feynman diagrams contribute. A few of them are drawn in Fig. 1.5 for the mere sake of illustration.

We do not attempt detailed estimates. Rather, we follow second-oder perturbation theory that tells us that the contribution to the energy shift of

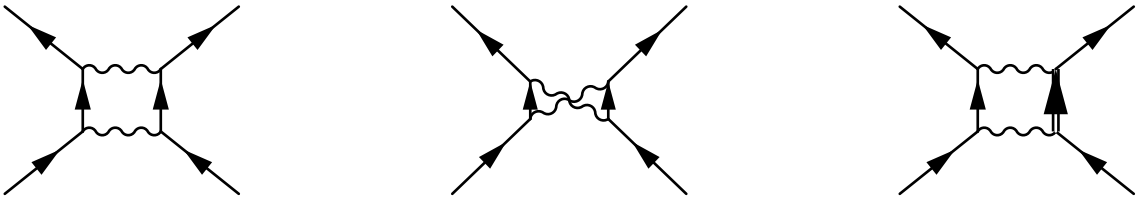

Figure 1.5: A few examples of Feynman diagrams involving two-pion exchange. The double arrowed line denotes a nucleon excitation like, for instance, a Δ-isobar (cf. the main text).

a state $|n\rangle$, due to the coupling with other states $|m\rangle$, reads

$$\Delta E_n = \sum_m \frac{\langle n|V|m\rangle\langle m|V|n\rangle}{E_n - E_m}, \tag{1.27}$$

where V is the coupling potential. Accordingly, the amplitudes associated with the diagrams in Fig. 1.5 can be seen as "squares" of the OPEP divided by the energy denominator associated with the difference between the initial and intermediate states. In some of the diagrams the intermediate state $|m\rangle$ is close in energy to the initial state, while if one Δ-isobar[6] is excited, the energy is increased by ≈ 300 MeV. We can take an average energy denominator $\bar{E} \approx$ -150 MeV.

We can use the following equations (that are easy to deduce from the properties of the operators), namely

$$(\tau_1 \cdot \tau_2)^2 = 3 - 2\tau_1 \cdot \tau_2,$$

and

$$S_{12}^2 = 6 + 2\sigma_1 \cdot \sigma_2 - 2S_{12},$$

to support the statement that the two-pion exchange potential contains, in addition to spin and tensor terms, central terms as well! In fact, we can write down the structure of the two-pion exchange potential by means of the square of the OPEP divided by $\bar{E}$:

$$\begin{aligned} V_{2\pi} &= \frac{1}{\bar{E}} f_\pi^4 m_\pi^2 (3 - 2\tau_1 \cdot \tau_2) \Big[(6 + 2\sigma_1 \cdot \sigma_2 - 2S_{12}) f^2(r) + \\ &\quad \frac{1}{9}(3 - 2\sigma_1 \cdot \sigma_2) g^2(r) + 2S_{12} \frac{\sigma_1 \cdot \sigma_2}{3} f(r) g(r) \Big], \end{aligned} \tag{1.28}$$

[6]The Δ particle or isobar is a baryon with $J^\pi = \frac{3}{2}^-$ and mass equal to 1232 MeV/c^2. It can be seen as the lowest excited state of the nucleon.

where f and g correspond to the radial functions associated with the first two terms in the square brackets of Eq. (1.23) (the zero-range term, namely the last one, has been dropped). We neglect the terms that include S_{12}, to avoid the estimate of the relative weight of oblate and prolate components, so that

$$V_{2\pi} \approx \frac{1}{\bar{E}} f_\pi^4 m_\pi^2 \left(3 - 2\tau_1 \cdot \tau_2\right) \left[\left(6 + 2\sigma_1 \cdot \sigma_2\right) f^2(r) + \frac{1}{9}\left(3 - 2\sigma_1 \cdot \sigma_2\right) g^2(r)\right]. \tag{1.29}$$

It is straightforward to see that the first term in the square brackets of (1.29), estimated in the $S = 1$, $T = 0$ channel at a distance corresponding to the OPEP range (so that we can compare it with the OPEP itself), provides a contribution

$$V_{2\pi} \approx -\frac{1}{150} 0.08^2 \times 140^2 \times 9 \left(8 \times \frac{49}{9e^2}\right) \approx -40 \text{ MeV}. \tag{1.30}$$

The second term in square brackets provides a smaller contribution. Although our estimate is rough, the two-pion exchange potential is stronger than the OPEP.

We recall here what we said before in Sec. 1.2. In the derivation of explicit one-pion or two-pion exchanges, the dependence on $\mathbf{r}$ and $\mathbf{p}$ appears while that on the angular momentum does not appear naturally. The same holds for the chiral forces that we shall discuss in 1.4.

1.3.4 The short-range repulsion

We treat this part in a less mathematical, more intuitive fashion. The pion is the lightest meson that can be exchanged among nucleons. Another possible exchange among nucleons is that of the ρ and ω mesons: their mass is around 700-800 MeV, so that the corresponding range should be around 0.3 fm or less. These mesons have angular momentum and parity 1^-, so they are vector mesons. The structure of the interaction they mediate is expected to be similar to the structure of the electromagnetic force since the photon has the same quantum numbers. Consequently, we draw simple conclusions without resorting to any estimate of Feynman diagrams:

- the main part of the interaction will be like the Coulomb force between two identical charges, namely a strongly repulsive one;

- we also expect a spin-orbit force of the type

$$\frac{1}{r}\frac{dV}{dr}\mathbf{L}\cdot\mathbf{S}. \tag{1.31}$$

  Since V is repulsive, the spin-orbit force has the opposite sign than in the atomic case, and because of the large absolute value of V and of its derivative, it is also a much more intense force: as discussed in the next Chapter, it creates the difference between the atomic and nuclear shell closures.

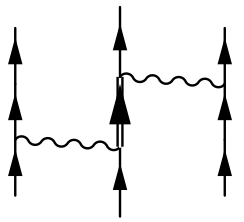

Figure 1.6: Feynman diagram corresponding to one of the most important contributions to the three-body force, that is, the so-called Fujita-Miyazawa process. The intermediate double-arrowed line represents a Δ-isobar, like in Fig. 1.5.

1.3.5 The three-body force

Three body forces appear in nuclei as in other quantum systems, and yet they are particularly strong and play a very crucial role for nuclear binding and other nuclear properties. They reflect irreducible elementary processes that involve more than one pair of particles. In this respect, the so-called Fujita-Miyazawa process depicted in Fig. 1.6 (which is believed to be one of the most imprtant) is quite illustrative. It is analogous to the force with which tides on the surface of the earth affect the motion of a satellite, since tides are caused by the effect of the moon. In other words, we can imagine that the three lines of Fig. 1.6 are, from left to right respectively, the moon, the earth and the satellite: the first interaction line represent the fact that the moon induces tides, if we allow ourselves to imagine the Δ-isobar excitation of the nucleon as the earth with ocean tides, and the second interaction line is the effect of these induced tides on the satellite.

As soon as one moves from the two-body nucleon system to the three body systems, whether bound systems like ^{3}H or ^{3}He or reactions like (d,p) etc., it turns out that no sensibile calculation can be made without three-body forces: any model including only two-body forces will not fit the experimental data. The accurate NN potentials mentioned at the end of Sec. 1.2 must be complemented with three-body forces. The improvement of three-body forces and the quest for possible four-body forces are active fields of research in nuclear physics [18].

1.4 Chiral forces

We have already mentioned that, at the end of the day, nuclear forces should be derived from QCD. The force among nucleons should be viewed as a residual force among systems of bound quarks. The analogy with the Van der Waals residual forces between complex molecules could be invoked here, but it is of no practical help. In fact, there is a simple and yet very important difference with the electromagnetic case. QCD is the strong interaction theory in the same manner as Quantum Electrodynamics (QED) is the fundamental theory for electromagnetism. But at variance with QED, whose coupling constant $\alpha = \frac{1}{137}$ is small at the energies of interest, QCD is not perturbative at low energies as the corresponding coupling constant becomes large [19].

A non-perturbative solution for the case of baryon-baryon interactions could be, in principle, obtained by means of lattice QCD calculations; however, in the case of the NN interaction, these calculations have not yet been able to provide reliable results (see [20] and references therein for a discussion of the difficulties). At the moment, not even the two-body problem (that is, the deuteron) can be solved within lattice QCD in a satisfactory manner.

An important remark is in order here. Even if in future one may be able to derive the NN interaction from the dynamics of quarks and gluons, this is not definitely an economic and elegant description. As we said at the beginning of the previous Section, this is reflected in the fact that at low-energy the quarks are confined. At low-energy, the actual degrees of freedom are nucleons and the lightest mesons (pions). An effective (both in general and technical sense) theory must focus on these degrees of freedom, which are the only relevant ones at the energy scales of nuclear structure.

The rationale behind this argument can be better understood using an analogy. In the electromagnetic theory, it is known that the fields are

amenable to a multipole expansion. Even a complicated charge distribution, if viewed from a distance which is large with respect to its size, is described by only few multipole moments.

If we treat nucleons and pions as fields, we can build an Effective Field Theory (EFT) by writing the associate Lagrangian. There exist EFTs that neglect pions (so-called pionless EFTs), as well as other EFTs.

In fact, most of the *ab initio* practitioners have turned their attention to effective chiral Lagrangians. These include the nucleon and pion fields and are consistent with the chiral symmetry and its spontaneous symmetry breaking, as we discuss below. Other QFT Lagrangians include nucleons and effective mesons like pions or heavy ones, as well as their coupling with the nucleons. However, **unique aspects of chiral Lagrangians are the systematic application of the separation of energy scales as well as, obviously, chiral symmetry**.

These concepts have been introduced by S. Weinberg [21], who proposed the equivalence between chiral Lagrangians and the QCD Lagrangian at low energy. Low energy means here "low with respect to the energy scale associated with the mass of the nucleon and of the heavy mesons" ($\Lambda_\chi \approx$ GeV). If we restrict our considerations to the u and d quarks, their masses are very light (of the order of few MeV), and if they are set to zero the QCD Lagrangian becomes invariant under chiral transformations. The QCD Lagrangian reads

$$\mathcal{L}_{\rm QCD} = \bar{q}\left(i\gamma^\mu \mathcal{D}_\mu - \mathcal{M}\right) q - \frac{1}{4}\mathcal{G}_{\mu\nu,a}\mathcal{G}_a^{\mu\nu}. \tag{1.32}$$

The gauge-covariant derivative $\mathcal{D}$, the mass matrix $\mathcal{M}$ and the gluon field tensor $\mathcal{G}$ have a non-trivial structure, in which the quark fields q have a color degree of freedom to which the index a is associated, and the gluons interact with themselves. The student who is interested in going deeper into these aspects can read his/her favourite field theory textbook in which the above Lagrangian is compared with the simpler QED Lagrangian,

$$\mathcal{L}_{\rm QED} = \bar{\psi}\left(i\gamma^\mu D_\mu - m\right)\psi - \frac{1}{4}F_{\mu\nu}F^{\mu\nu}.$$

The aspect which is relevant here, though, is that if we restrict ourselves to u and d quarks and neglect their mass in (1.32), the right-handed and left-handed quarks, $P_R q$ and $P_L q$, defined by

$$P_R = \frac{1}{2}\left(1+\gamma_5\right), \qquad P_L = \frac{1}{2}\left(1-\gamma_5\right), \tag{1.33}$$

do not mix. This symmetry goes hand in hand with the isospin symmetry: the overall result is the existence of six conserved currents, that are

$$R_i^\mu = \bar{q}_R \gamma^\mu \frac{\tau_i}{2} q_R, \qquad L_i^\mu = \bar{q}_L \gamma^\mu \frac{\tau_i}{2} q_L. \tag{1.34}$$

These currents can be combined into conserved vector and axial currents,

$$V_i^\mu = R_i^\mu + L_i^\mu = \bar{q} \gamma^\mu \frac{\tau_i}{2} q, \qquad A_i^\mu = R_i^\mu - L_i^\mu = \bar{q} \gamma^\mu \gamma_5 \frac{\tau_i}{2} q. \tag{1.35}$$

According to Weinberg, any other Lagrangian that is consistent with these symmetries (as well as with the general principles of quantum field theory) should provide the same results, for any observable, as the QCD Lagrangian in the limit of vanishing quark masses.

There is something more. The chiral symmetry is, in part, kept (as far as the vector current is conserved) but it is also *spontaneously broken* in the QCD ground state. This is evident in the spectra of the hadrons. The conservation of vector current manifests itself by means of the isospin multiplets. If axial currents were also conserved, one would observe for each of those multiplets a counterpart with opposite parity. This is not observed at all (cf. e.g. the discussion in Ref. [22]).

Then, one proceeds by noting that the spontaneously broken axial symmetry implies the existence of a massless boson due to the Goldstone theorem [23]. The pion is not massless, due to the approximate nature of the chiral symmetry, and yet its mass ($\approx$ 100 MeV) is much smaller than those of the other mesons. In this manner, one understands the separation of scales within the QCD world, between nucleons and heavy mesons with masses around Λ_χ and the Goldstone boson, that is, the pion.

In such a situation, Weinberg's idea is that the most general Lagrangian that includes nucleons and pions and is consistent with chiral symmetry, should provide the same results as the QCD Lagrangian, at least in the low-energy regime up to Λ_χ. Accordingly, the strategy of chiral effective field theory (in short, chiral EFT or χEFT) consists in writing a Lagrangian that includes nucleons and two types of interaction terms. The contributions to the NN (NNN, etc. ...) forces emerge, in fact, from the set of Feynman diagrams with two (three, etc. ...) nucleon asymptotic states. One set of contributions includes all possible exchanges of pions, that are treated explicitly. Another set of contributions corresponds to all other terms allowed by symmetries, in which NN (NNN, etc. ...) couplings are treated as contact terms. Contact terms [proportional to $\delta(\vec{r} - \vec{r}\,')$] can be associated to

exchanged mesons with an infintely large momentum. The student can convince himself/herself by looking at Eq. (1.18): this becomes a constant in momentum space if $k \to \infty$, and its Fourier transform is a δ-force or contact force. In this way, two goals are obtained at the same time: the theory is general enough, and the physics at a large momentum scale larger is implicit.

For the theory to be tractable, the diagrams must be ordered in a hierarchy according to some perturbative parameter. The widely used choice for this parameter is $\frac{Q}{\Lambda_\chi}$, where Q is the typical nucleon momentum. This choice is not completely obvious and is debated in the literature. The power ν at which the expansion in $\left(\frac{Q}{\Lambda_\chi}\right)^\nu$ is stopped defines lowest-order (LO), next-to-lowest-order (NLO), etc. ... potentials. The existence of a NN bound state (the deuteron) shows that this system is not perturbative. Weinberg (see [24] and references therein) suggested that one can obtain a sensible NN potential by applying perturbation theory with (only) nucleon intermediate states. Therefore, chiral NN potentials are constructed solving the Lippmann-Schwinger equation on top of a LO, NLO etc. ... formulation. This equation will be discussed later in this course (when dealing with general reaction theory in Chapter 7).

It has to be noted that the procedure may require the introduction of a regulator (or ultraviolet cutoff) Λ. It eliminates the contributions from higher momenta and makes the actual calculations feasible (it also avoids divergences that can arise in the diagrams). This cutoff Λ is a parameter that should not be confused with the energy scale Λ_χ. In principle, the results should become independent from Λ and this should happen for $\Lambda > \Lambda_\chi$, or even for smaller values of Λ. In practice, the dependence of the results from chiral potentials on the value of this regulator is still an issue that is not fully understood.

Details on chiral forces are discussed in [25, 26, 22].

Chapter 2

Nuclear bulk properties and shell structure: effective interactions for mean-field and Density Functional Theory

2.1 Generalities on the nuclear mean-field

Early scattering experiments have already proven that, in a nucleus, the mean free path of a nucleon is quite large, that is, of the order of the nuclear radius or even larger[1]. For quite some time it has appeared difficult to reconcile this evidence with the very idea of a strongly interacting system. In fact, the solution of the puzzle lies in the fact that the nucleus is not an extremely dense system, as well as in the role played by the Pauli exclusion principle. The nuclear radius is

$$R = r_0 A^{1/3}, \qquad \text{with } r_0 = 1.2 - 1.3 \text{ fm}. \tag{2.1}$$

Consequently, the volume per nucleon is

$$\frac{V}{A} = \frac{\frac{4}{3}\pi r_0^3 A}{A} \approx 4 r_0^3, \tag{2.2}$$

[1] Cf. Sec. 7.3.3 here below. The interested reader can also have a look at Sec. 2.2 of [10] and Refs. [8,18] therein, or at the discussion around Eq. (4.18) in [27].

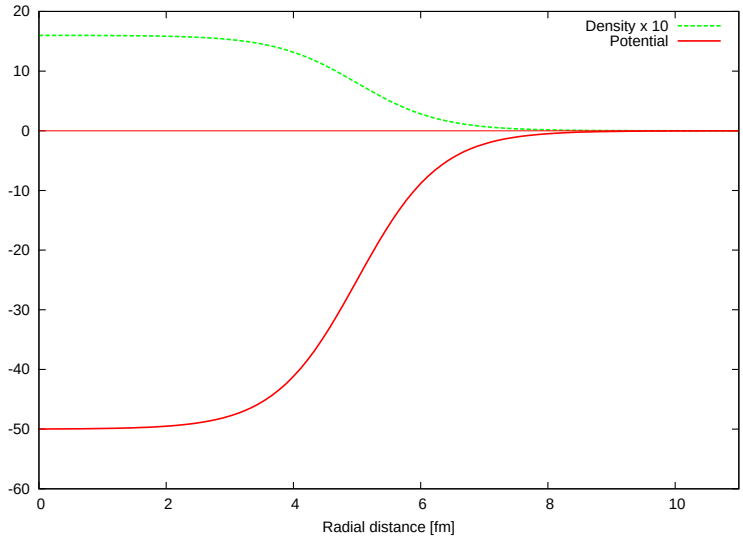

Figure 2.1: Schematic profiles of density (positive y-axis) and potential (negative y-axis) in a nucleus. The density has dimensions fm^{-3} but it has been multiplied by a factor 10 in the figure, while the potential has dimensions of MeV. See the main text for a complete discussion.

and the average distance between nucleons is of the order of ≈ 2 fm. In such conditions, nucleons do not feel during most of the time the strongest part of the NN interaction that we have studied in the previous Chapter.

Electron scattering experiments that measure the charge density, but also other kinds of experiments, consistently point to the fact that the density is approximately constant within the nuclear volume, at least in medium-heavy nuclei. Thus, we can expect that each nucleon feels a relatively smooth potential which is an average of the interactions with all the others (once again, by experiencing only rarely the correlations induced by the strongest component of their mutual force).

All these ideas, together with the evidence of a nuclear single-particle shell structure, have led to the use of empirical mean-field potentials to describe nucleons in the nucleus, starting from the middle of the last century. The empirical potentials and the gross features of the nuclear shells are discussed in this Section. In a very schematic manner, the profiles of the nuclear average potential and of the nucleon density should follow each other as shown in Fig. 2.1. At the edge of the nucleus, where the density drops, the attractive potential drops as well as expected in the case of short-range

forces.

2.1.1 Empirical potentials: Woods-Saxon

All the nuclear phenomenology, starting from the evidence from the binding energies, suggest that, to a first approximation, nucleons occupy orbitals that are grouped in shells like in the atomic case. The nuclear shells differ from the atomic shells as we shall discuss below. The main point is that the atomic shells are mainly governed by an external potential (the Coulomb potential of the atomic nucleus), while nuclear shells are emerging from the complicated behaviour of self-interacting particles.

An empirical potential U that reproduces well the nuclear phenomena is the Woods-Saxon (WS) potential. In the case of spherical nuclei, a widely used parametrization reads

$$U(r) = \frac{-U_0}{1 + e^{\frac{r-R}{a}}}. \tag{2.3}$$

R is the nuclear radius given by Eq. (2.1), and in the usual WS parametrization $r_0 = 1.27$ fm, $a = 0.67$ fm is a parameter that defines the nuclear surface (and is called surface diffuseness), while U_0 is the depth of the potential and often one writes

$$U_0 = \left(51 \pm 33\frac{N-Z}{A}\right) \text{ MeV}$$

(the + and − sign refers to protons and neutrons, respectively). The form of the WS potential is the same as that of a density profile with a form like

$$\rho(r) = \frac{\rho_0}{1 + e^{\frac{r-R}{a}}}, \tag{2.4}$$

with ρ_0 is ≈ 0.16 fm^{-3}. In the context of charge densities, this is called two-parameter Fermi function (cf., for instance, Ref. [28]).

The potential (2.3) must be complemented by the Coulomb potential for protons $U_C(r)$ (that is often taken as that of a uniformely charged sphere), as well as by the spin-orbit potential $U_{LS}(r)$. This latter should be proportional to the radial derivative of (2.3) and the proportionality constant is usually adjusted, so that the results reads

$$U_{LS}(r) = U_0^{LS} \left(\frac{r_0}{\hbar}\right)^2 \frac{1}{r}\frac{d}{dr}\left(\frac{1}{1 + e^{\frac{r-R}{a}}}\right), \tag{2.5}$$

with $U_0^{LS} = 0.44U_0$

Let us start by assuming that the Coulomb and spin-orbit potentials can be treated within first order perturbation theory, namely that they affect the energy of the eigenstates and not their wave functions. The effect of these terms is qualitatively very clear: U_{LS} will split the levels with $j = \ell \pm 1/2$ (by moving the $j = \ell + 1/2$ levels downward and the $j = \ell - 1/2$ levels upward), while U_C will push the all the proton levels upward. The solutions of

$$H = T + U + U_C + U_{LS} \tag{2.6}$$

are spherical wave functions of the form

$$\psi_{n\ell jm}(\mathbf{r}) = \frac{u_{n\ell j}(r)}{r} \left[Y_\ell(\hat{r}) \otimes \chi_{\frac{1}{2}}(\sigma) \right]_{jm}, \tag{2.7}$$

where we have written the standard quantum numbers and used the symbol $\otimes$ to indicate the angular momentum coupling, that is,

$$\left[Y_\ell(\hat{r}) \otimes \chi_{\frac{1}{2}}(\sigma) \right]_{jm} = \sum_{m_\ell, m_s} \langle l m_\ell \frac{1}{2} m_s | jm \rangle Y_{\ell m_\ell}(\hat{r}) \chi_{\frac{1}{2} m_s}(\sigma).$$

If we treat the other terms as a perturbation, as we said, the radial wave functions $u_{n\ell j}(r)$ are the solutions of the reduced Schrödinger equation for the potential U only and they do not depend on j. The reduced Schrödinger equation is

$$\left[-\frac{\hbar^2}{2m} \frac{d^2}{dr^2} + \frac{\hbar^2 \ell(\ell+1)}{2mr^2} + U(r) \right] u_{n\ell}(r) = \varepsilon_{n\ell} u_{n\ell}(r), \tag{2.8}$$

where $\varepsilon_{n\ell}$ is the eigenvalue associated with U. We remind that, as for any central potential, n assumes the values $n = 1, 2, 3 \ldots$ and $n - 1$ corresponds to the number of nodes of the radial wave function, while $\ell = 0, 1, 2 \ldots$ and the spectroscopic notation $s, p, d \ldots$ will be employed.

For pedagogical purposes, we can even assume in some simplified discussion that the wave functions of the Woods-Saxon potential $U(r)$ can be replaced with the eigenfunctions of the harmonic oscillator potential, namely $U = \frac{1}{2} m\omega r^2$, because these are known analytically. We do not actually need to write down their form here[2] but we just remind the corresponding eigenvalues, that are

$$\varepsilon_{n\ell} = \hbar\omega \left(2n + \ell - \frac{1}{2} \right) \equiv \hbar\omega \left(N + \frac{3}{2} \right). \tag{2.9}$$

[2]It can be found in any standard quantum mechanics textbook.

In the case of the spherical harmonic oscillator, $N = 2(n-1) + \ell$ is called the principal quantum number.

The single-particle levels that are solution of the Woods-Saxon potential are depicted in Fig. 2.2.

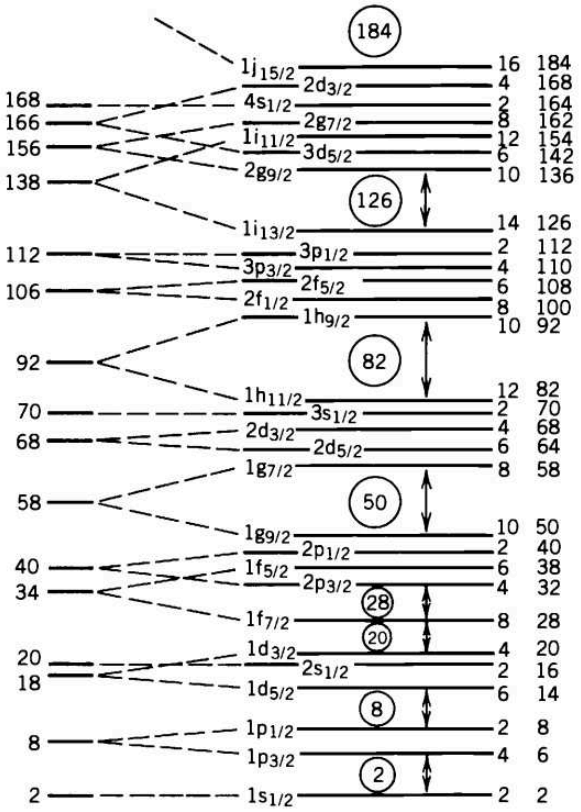

Figure 2.2: Shell model orbitals. In the left part, the solutions of the Schrödinger equation for a WS potential are schematicaly shown (with the cumulative number of particles that can be accommodated when all levels up to a given one are filled). Moving to the right, the spin-orbit splittings and the labels of the resulting levels are displayed. The major gaps between groups of levels, or shells, are highlighted. The degeneracies of each level, $2j + 1$, and the cumulative number of particles that can be accommodated, are visibile at the right side.

From the figure, one should appreciate the following main points. The harmonic oscillator potential (2.9) would be characterised by a high degeneracy between e.g. 1d and 2s levels (in the shell with $N = 2$), 1f and 2p

levels (in the shell with $N = 3$), and so on. In a Woods-Saxon potential, this degeneracy is lifted as it is visible in the left part of the figure (orbitals with lower n and higher ℓ are pushed below). This affects the level ordering but it does not alter the shell structure. The shell structure is strongly affected by the spin-orbit potential that shifts the $j = \ell + 1/2$ levels downward and the $j = \ell - 1/2$ levels upward.

Once this level sequence is defined, in a naïve shell-model picture the nucleons can be disposed on the levels from the bottom up, by respecting the degeneracy of each level, that is, $2j+1$. This concept is very crucial since by using it, and knowing the numbers of neutrons and protons, we immediately see if a system is closed shell or open shells. It must be stressed that all even-even nuclei, and closed-shell nuclei in particular, are characterised by a 0^+ ground-state. The shell-model ordering of the orbitals allows predicting the quantum numbers J^π of the ground-state of nuclei with one-particle or one-hole with respect to closed shells (^{17}O has a $\frac{5}{2}^+$ ground-state, and so on). We now discuss the typical value of the shell gap $\hbar\omega$, going back to the simple harmonic oscillator picture.

2.1.2 Empirical estimate of the shell gap

In this subsection, we derive the harmonic oscillator estimate of the root mean square radius and, by comparing it with the experimental finding, we deduce the optimal value for the shell gap $\hbar\omega$.

We start by recalling that the expectation value of r^2 for an orbital in the harmonic oscillator potential is given by

$$\langle r^2 \rangle_{N\ell} = \frac{\hbar}{m\omega}\left(N + \frac{3}{2}\right). \tag{2.10}$$

Let us now consider a nucleus whose levels are filled up to the shell characterised by the principal quantum number $N_{\max}$. For even values of N, $\ell = 0, 2 \ldots N$ while for odd values $\ell = 1, 3 \ldots N$. In either case, the degeneracy of the shell is given by the sum over the allowed values of ℓ of the degeneracies $2(2\ell + 1)$. It can be shown by a direct calculation that, regardless of the parity of N, one can derive the total shell degeneracy as

$$\sum_\ell 2(2\ell + 1) = (N + 2)(N + 1). \tag{2.11}$$

The total number of particles in all the shells can be also determined by means of an elementary calculation, and it turns out to be

$$\sum_{N=0}^{N_{\max}}(N+1)(N+2) = \frac{1}{3}(N_{\max}+1)(N_{\max}+2)(N_{\max}+3) \approx \frac{1}{3}(N_{\max}+2)^3, \quad (2.12)$$

where the last approximation holds for large values of $N_{\max}$. The root mean square radius of the nucleus can be obtained by making the weighted average of the square radii of the different shells, where the weight is of course the number of particles in the shell. To simplify, we consider an equal number of protons and neutrons that contribute equally to the radius, and this brings an additional factor 2. In summary,

$$\begin{aligned} \langle r^2 \rangle &= \frac{2}{A}\sum_{N=0}^{N_{\max}} \frac{\hbar}{m\omega}\left(N+\frac{3}{2}\right)(N+1)(N+2) \\ &\approx \frac{1}{A}\frac{\hbar}{2m\omega}(N_{\max}+2)^4. \end{aligned} \quad (2.13)$$

The sum could be performed exactly but the second line of the latter equation provides a reasonable approximation, again for large $N_{\max}$. If we now consider that

$$\langle r^2 \rangle = \frac{3}{5}R^2 = \frac{3}{5}r_0^2 A^{2/3},$$

from Eq. (2.1), then Eq. (2.13) can be solved to give the unknown value of $\hbar\omega$:

$$\hbar\omega \approx \frac{5}{4}\left(\frac{3}{2}\right)^{1/3}\frac{\hbar^2}{mr_0^2}A^{-1/3} \approx \frac{41}{A^{1/3}} \quad \text{MeV}. \quad (2.14)$$

This estimate is often used, for instance when evaluating the typical energies needed to excite a particle by one, two, or more shells.

2.2 Hartree-Fock theory

The goal of the Hartree-Fock (HF) theory is to give a microscopic foundation, starting from the Hamiltonian formalism, to the existence of a nuclear mean field. Let us start, then, from an Hamiltonian

$$H = T + V, \quad (2.15)$$

where

$$T = \sum_{\alpha} -\frac{\hbar^2}{2m}\nabla_{\alpha}^2 \tag{2.16}$$

is the kinetic energy, and

$$V = \frac{1}{2}\sum_{\alpha\neq\beta} v(\mathbf{r}_{\alpha}, \mathbf{r}_{\beta}) \tag{2.17}$$

is a two-body interaction between nucleons. α, β are indices that label the nucleons. For the sake of simplicity, we omit here the spin and isospin dependences in V and we also do not consider three-body forces. It is possible to write more general formulas without these pedagogical simplifications.

The assumption of the HF theory is that the total wave function is a totally anti-symmetric product of (unknown) single-particle wave functions. If these single-particle wave functions are labelled by ϕ_i, then the totally anti-symmetric wave function is given by the so-called Slater determinant

$$\begin{aligned}\Psi(\mathbf{r}_1 \ldots \mathbf{r}_A) &= \frac{1}{\sqrt{A!}}\begin{vmatrix} \phi_1(\mathbf{r}_1) & \ldots & \phi_A(\mathbf{r}_1) \\ \ldots & \ldots & \ldots \\ \phi_1(\mathbf{r}_A) & \ldots & \phi_A(\mathbf{r}_A) \end{vmatrix} \\ &= \frac{1}{\sqrt{A!}}\sum_{P}(-)^P \phi_{P(1)}(\mathbf{r}_1)\ldots\phi_{P(A)}(\mathbf{r}_A), \end{aligned} \tag{2.18}$$

where in the last line we have introduced the sum over all possible permutations P of the indices $1 \ldots A$, and $(-)^P$ is $+1$ (-1) if the number of exchanges with respect to the identical permutation is even (odd).

Consequently, the Hartree-Fock theory amounts to the minimisation of the total energy in the Hilbert space made up with Slater determinants; we need to calculate the expectation value $E = \langle\Psi|H|\Psi\rangle$, and to solve the equation

$$\delta E = 0. \tag{2.19}$$

We will actually add a Lagrange multiplier to ensure orthonormal single-particle wave functions, so that the latter equation will read

$$\delta\left(E - \sum_i \varepsilon_i \int d^3r\ \phi_i^*(\mathbf{r})\phi_i(\mathbf{r})\right). \tag{2.20}$$

We first calculate the expectation value of the kinetic energy and we obtain

$$\langle \Psi|T|\Psi\rangle = \sum_{i=1}^{A} -\frac{\hbar^2}{2m}\int d^3r\ \phi_i^*(\mathbf{r})\nabla^2\phi_i(\mathbf{r}). \tag{2.21}$$

The calculation of the expectation value of the potential can be developed along a similar line and one obtains

$$\begin{aligned}\langle \Psi|V|\Psi\rangle &= \frac{1}{2}\sum_{ij}\int d^3r\ d^3r'\ \phi_i^*(\mathbf{r})\phi_j^*(\mathbf{r}')v(\mathbf{r},\mathbf{r}')\phi_i(\mathbf{r})\phi_j(\mathbf{r}') + \\ &- \frac{1}{2}\sum_{ij}\int d^3r\ d^3r'\ \phi_i^*(\mathbf{r})\phi_j^*(\mathbf{r}')v(\mathbf{r},\mathbf{r}')\phi_i(\mathbf{r}')\phi_j(\mathbf{r}).\end{aligned} \tag{2.22}$$

If we perform the variation defined by Eq. (2.20), using ϕ_i^* as the quantity to be varied (the variation of ϕ_i would not produce a new independent equation), we arrive at the following set of equations:

$$\begin{aligned}&-\frac{\hbar^2}{2m}\nabla_i^2\phi_i(\mathbf{r}) + \sum_{j=1}^{A}\int d^3r'\ \phi_j^*(\mathbf{r}')v(\mathbf{r},\mathbf{r}')\phi_j(\mathbf{r}')\phi_i(\mathbf{r}) + \\ &-\sum_{j=1}^{A}\int d^3r'\ \phi_j^*(\mathbf{r}')v(\mathbf{r},\mathbf{r}')\phi_j(\mathbf{r})\phi_i(\mathbf{r}') = \varepsilon_i\phi_i(\mathbf{r}).\end{aligned} \tag{2.23}$$

One should note that the Lagrange multipliers introduced in Eq. (2.20) play the role of single-particle energies.

In fact, the set (2.23) has the form of a set of Schrödinger equations. Their specific feature is that the potential depends on the wave functions, and in this respect we call these a set of *self-consistent*[3] equations. The solution must be found in an iterative fashion. One starts with a guess for some initial potential, finds the corresponding initial wave functions, insert them in the HF equations and iterate the procedure until convergence.

Before we analyse in a slight more detail the potential terms of the HF equations, we remind that the one-body density or, in short, the density, is obtained from the total wave function (2.18) as

$$\rho(\vec{r}) = A\int d^3r_2\ldots d^3r_A\ \Psi(\mathbf{r},\mathbf{r}_2\ldots\mathbf{r}_A) = \sum_i \phi_i^*(\mathbf{r})\phi_i(\mathbf{r}). \tag{2.24}$$

[3]This wording is used, within nuclear theory, in different contexts. Here it means that potential and wave functions (or the associated density) must be consistent with one another.

The two terms that follow the kinetic energy, in the l.h.s. of Eq. (2.23), are called the Hartree and Fock terms. The Hartree term can be re-written as

$$\sum_{j=1}^{A} \int d^3r' \; \phi_j^*(\mathbf{r}')v(\mathbf{r},\mathbf{r}')\phi_j(\mathbf{r}')\phi_i(\mathbf{r}) = \int d^3r' \; v(\mathbf{r},\mathbf{r}')\rho(\mathbf{r}') \times \phi_i(\mathbf{r}). \quad (2.25)$$

This term has a simple interpretation, since it represents the interaction of a nucleon with an environment where other nucleons are distributed with a density ρ: it is, in other words, the classical mean field felt by nucleons. It also corresponds to a multiplicative potential. The Fock term cannot, instead, be written as a multiplicative potential times the wave function and it makes the whole equation an integro-differential one. It is due, of course, to the fermionic nature of the nucleons.

The total energy is the sum of (2.21) and (2.22), calculated with the wave functions that minimise these expressions. We will use the notation

$$\langle i|t|j\rangle = -\frac{\hbar^2}{2m} \int d^3r \; \phi_i^*(\mathbf{r})\nabla^2\phi_j(\mathbf{r}) \quad (2.26)$$

for the matrix elements of the kinetic energy, and

$$\langle ij|v|kl\rangle_{\rm AS} = \int d^3r \; d^3r' \; \phi_i^*(\mathbf{r})\phi_j^*(\mathbf{r}')v(\mathbf{r},\mathbf{r}') \left[\phi_i(\mathbf{r})\phi_j(\mathbf{r}') - \phi_i(\mathbf{r}')\phi_j(\mathbf{r})\right] \quad (2.27)$$

for the antisymmetrized matrix elements of the two-body potential. Then, the total energy can be written

$$E = \sum_i \langle i|t|i\rangle + \frac{1}{2}\sum_{ij} \langle ij|v|ij\rangle_{\rm AS}. \quad (2.28)$$

Sometimes one can use the notation $\langle ij|\bar{v}|kl\rangle$ instead of $\langle ij|v|kl\rangle_{\rm AS}$ for the sake of further brevity.

For atoms or molecules, one could solve the HF equations with the Coulomb interaction. Solving the HF equations with the realistic potentials that we have described in Chapter 1 is technically difficult but, even more importantly, may not be anything more than a starting point for a better approximation of the nuclear wave function than the Slater determinant (2.18). When the *ab initio* methods that we have mentioned in Chapter 1 were not yet available, but even today, one can grasp a lot of physics from the HF solution provided appropriate effective interactions are employed. A brief discussion of these effective interactions for HF, or mean-field, is provided in the next Section, but one can find many more details e.g. in Ref. [29].

2.3 Effective interactions for Hartree-Fock

One should, and can, build *ad hoc* effective interactions whose parameters are fitted on few data with the purpose of describing quite well the nuclear ground states of nuclei at the HF level. This has been extensively done in the last four decades. Popular effective interactions include the so-called Skyrme and Gogny forces, plus others. Skyrme-type interactions are zero-range forces while Gogny forces are of Gaussian type. These interactions contain, typically, about 10 free parameters that are fitted on data for 10-20 nuclei, and are the applied to calculate 10^2–10^3 nuclei throughout the isotope chart; they reproduce, on average, the binding energies of nuclei with a remarkable accuracy of $\approx$ 1-2 MeV and perform quite well for other observables, like charge radii.

We do not discuss many details here. We recall that the popularity of Skyrme forces stems from the fact that with a force that is proportional to a Dirac delta function, $\delta(\mathbf{r}-\mathbf{r}')$, the Fock term loses its non-locality and becomes proportional to the Hartree term. As we shall see in the next Section, Skyrme forces are now to some extent abandoned in favour of Skyrme *energy functionals*.

The standard Skyrme interaction reads

$$\begin{aligned} v(\mathbf{r},\mathbf{r}') &= t_0(1+x_0P_\sigma)\delta(\mathbf{r}) + \frac{1}{2}t_1(1+x_1P_\sigma)[\mathbf{P}'^2\delta(\mathbf{r}) + \delta(\mathbf{r})\mathbf{P}^2] \\ &+ t_2(1+x_2P_\sigma)\mathbf{P}'\cdot\delta(\mathbf{r})\mathbf{P} + \frac{1}{6}t_3(1+x_3P_\sigma)\rho^\alpha(\mathbf{R})\delta(\mathbf{r}) \\ &+ iW_0(\sigma_1+\sigma_2)\cdot[\mathbf{P}'\times\delta(\mathbf{r})\mathbf{P}]\ , \end{aligned} \tag{2.29}$$

where $\mathbf{r}=\mathbf{r}-\mathbf{r}'$, $\mathbf{R}=\frac{1}{2}(\mathbf{r}+\mathbf{r}')$, $\mathbf{P}=\frac{1}{2i}(\nabla-\nabla')$, $\mathbf{P}'$ is the hermitian conjugate of $\mathbf{P}$ (acting on the left), $P_\sigma=\frac{1}{2}(1+\sigma_1\cdot\sigma_2)$ is the spin-exchange operator and $\rho=\rho_n+\rho_p$ is the total nucleon density. The parameters t_i, x_i, α and W_0 are the free parameters that need to be fitted and characterise a specific interaction of the Skyrme family.

The terms in t_0 and t_3 are, respectively, attractive and repulsive. The former accounts for the overall attractive character that must characterise any sensible effective force. The equilibrium of the nuclear system must result from the balance with a repulsive term and the kinetic energy, albeit repulsive, is too weak. The term in t_3 becomes relevant when the density grows (if $\alpha>0$) and takes care of the short-range repulsion among nucleons. We shall see these terms in action in the simplified case of the next subsection.

The remaining terms are also relevent. The terms in t_1 and t_2 depend on the relative momentum and correspond to the lowest contributions in a Taylor expansion for low momenta. The last term of Eq. (2.29) can be shown to correspond to the zero-range limit of a spin-orbit force. This last statement needs some care to be proven. Discussing the details of the Skyrme force, or of other effective forces, goes beyond the scope of these lectures. The interested reader can consult the specialised literature. A computer code that solves the HF equations for a Skyrme standard force, in spherical symmetry, can be used as a tool to have a look at total energies, radii and single-particle states [30]. Here, in the next subsection, we discuss a simplified solution of the HF equations in the case of uniform, symmetric nuclear matter.

2.3.1 Symmetric nuclear matter with a simplified Skyrme force

As we have discussed at the start of this Chapter, electron scattering experiments, together with other direct and indirect evidences, suggest that the inner part of medium-heavy nuclei is characterised by an approximately constant density, $\rho_0 \approx 0.16$ fm^{-3}. In this radial region, the proton and neutron densities do not differ too much. This suggests that such inner part of nuclei can be thought as a portion of an hypothetic extended system of equal number of protons and neutrons. Such system, called "symmetric" nuclear matter, has, therefore, an equlibrium density ρ_0 and a corresponding energy E_0 that is given by the volume term of the mass formula, that is, $\approx$ -16 MeV.

The purpose of this subsection is to show that such equilibrium state can be obtained with a simplified Skyrme force. Before showing this, let us recall some features of symmetric nuclear matter that are often mentioned in the literature[4]. If we estimate the Fermi momentum k_F corresponding to the density ρ_0, we obtain

$$k_F = \left(\frac{3\pi^2\rho_0}{2}\right)^{1/3} \approx 1.33 \text{ fm}^{-1}. \tag{2.30}$$

[4]As implicit in the previous discussion, symmetric nuclear matter is an ideal system and not a real one. The numbers we discuss in this subsection are not true experimental data. Neverthless, they can be considered to be useful "pseudo-data" that shed light on the physics of real nuclei.

The corresponding Fermi energy is

$$\varepsilon_F = \frac{\hbar^2 k_F^2}{2m} \approx 37 \text{ MeV}, \tag{2.31}$$

and the velocity as a fraction of the light velocity is

$$\frac{v}{c} = \frac{\hbar k_F}{mc} \approx 0.28. \tag{2.32}$$

The typical time for a nucleon to cross a nucleus with mass around ≈ 100 is

$$\tau = \frac{r_0 A^{1/3}}{v_F} \approx 6.6\ 10^{-23} \text{ s}. \tag{2.33}$$

As we said, the typical mean free path of a nucleon is of the order, or larger, than the nuclear radius; then, the typical time between two NN collisions is often estimated as $\tau \approx 10^{-23} - 10^{-22}$ s.

The wave functions in a uniform system like symmetric nuclear matter are plane waves due to translational invariance. This simplifies the calculation of the total HF energy (2.28), in keeping with the well-known replacements

$$\begin{aligned} \phi_i &\rightarrow \phi_{\mathbf{k}} = \frac{1}{\sqrt{\Omega}} e^{i\mathbf{k}\cdot\mathbf{r}}, \\ \sum_i &\rightarrow \frac{g\Omega}{(2\pi)^3} \int d^3k\ , \end{aligned} \tag{2.34}$$

where g is the degeneracy equal to 4 and Ω is the quantisation volume. The kinetic energy is

$$\begin{aligned} \sum_i \langle i|t|i\rangle &= \frac{4\Omega}{8\pi^3}\frac{1}{\Omega} \int d^3k \int d^3r\ e^{-i\mathbf{k}\cdot\mathbf{r}} \left(-\frac{\hbar^2}{2m}\nabla^2\right) e^{i\mathbf{k}\cdot\mathbf{r}} \\ &= \frac{2}{\pi^2}\frac{\hbar^2}{2m}\frac{k_F^5}{5}\Omega. \end{aligned} \tag{2.35}$$

If we re-express this latter quantity in terms of the density through Eq. (2.30), we obtain

$$\frac{T}{A} = \frac{3}{5}\left(\frac{3\pi^2}{2}\right)^{2/3} \frac{\hbar^2}{2m}\rho^{2/3}. \tag{2.36}$$

We now evaluate the potential energy with the effective force

$$v(\mathbf{r},\mathbf{r}') = t_0(1 + x_0 P_\sigma)\delta(\mathbf{r}) + \frac{1}{6}t_3(1 + x_3 P_\sigma)\rho^\alpha(\mathbf{R})\delta(\mathbf{r}), \tag{2.37}$$

which is a simplified version of (2.29). For the antisymmetrized matrix elements of a zero-range force we can use the following simple trick,

$$\langle ij|v|kl\rangle_{\rm AS} = \langle ij|v(1-P_{12})|kl\rangle, \tag{2.38}$$

where P_{12} is the operator that exchanges particles 1 and 2, given by the product $P_r P_\sigma P_\tau$ (these three operators are defined as those exchanging position, spin and isospin, respectively). For a simple δ-force like (2.37) P_r is 1. Since P_σ is known to be $\frac{1+\sigma_1\sigma_2}{2}$ and P_τ has a similar form, we can write

$$\begin{aligned} v(1-P_{12}) &= t_0(1+x_0P_\sigma)(1-P_\sigma P_\tau)\delta(\mathbf{r}) \\ &+ \frac{1}{6}t_3(1+x_3P_\sigma)(1-P_\sigma P_\tau)\rho^\alpha(\mathbf{R})\delta(\mathbf{r}) \\ &= t_0\delta(\mathbf{r})\left(\frac{3}{4}+\frac{x_0}{2}\sigma_1\sigma_2-\frac{1}{2}\sigma_1\sigma_2-\frac{x_0}{2}\tau_1\tau_2-\frac{1}{2}\tau_1\tau_2-\frac{1}{4}\sigma_1\sigma_2\tau_1\tau_2\right) \\ &+ \text{analogous term in } t_3. \end{aligned} \tag{2.39}$$

It can be easily shown that the terms in $\sigma_1\sigma_2$ and $\tau_1\tau_2$ give a vanishing contribution in symmetric nuclear matter[5]. Thus,

$$\begin{aligned} \frac{1}{2}\sum_{ij}\langle ij|v|ij\rangle_{\rm AS} &= \frac{1}{2}\sum_{ij}\langle ij|\frac{3}{4}\left(t_0+\frac{t_3}{6}\rho^\alpha\right)\delta(\mathbf{r})|ij\rangle \\ &= \frac{1}{2}\frac{\Omega^2}{4\pi^6}\frac{1}{\Omega^2}\int d^3k\; d^3k' \int d^3r\; d^3r'\; e^{-i\mathbf{k}\cdot\mathbf{r}}e^{-i\mathbf{k}'\cdot\mathbf{r}'}\times \\ &\quad \times\left(t_0+\frac{t_3}{6}\rho^\alpha\right)\delta(\mathbf{r})e^{i\mathbf{k}\cdot\mathbf{r}}e^{i\mathbf{k}'\cdot\mathbf{r}'} \\ &= \frac{3}{8}t_0\Omega\rho^2+\frac{1}{16}t_3\Omega\rho^{\alpha+2}. \end{aligned} \tag{2.40}$$

Therefore, the total energy per particle reads

$$\frac{E}{A} = \frac{3}{5}\left(\frac{3\pi^2}{2}\right)^{2/3}\frac{\hbar^2}{2m}\rho^{2/3}+\frac{3}{8}t_0\rho+\frac{1}{16}t_3\rho^{\alpha+1}. \tag{2.41}$$

If t_0 is negative and t_3 is positive, as discussed below Eq. (2.29), it is clear that the energy per particle defined by (2.41) can have an absolute minumum.

[5]The formal proof is based on the properties of the Pauli matrices and it can be made available under request, but the basic idea is that the sum over ij in (2.28) involves, with the same weight and opposite sign, states with spin (isospin) up and down.

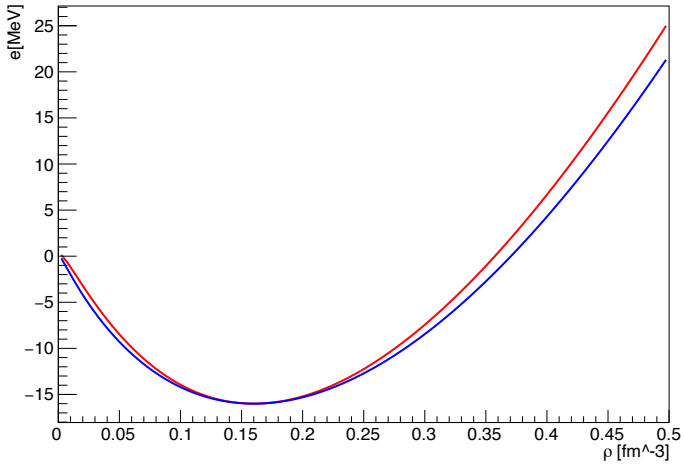

Figure 2.3: Energy per particle in symmetric nuclear matter, calculated with a simplified Skyrme force of the type (2.37) and parameters t_0 = -2552.84 MeV·fm^3, t_3 = 16694.7 MeV·fm$^{3(\alpha+1)}$, α = 0.20309 (red curve). The blue curve is a result from a simplified Gogny force, which is not discussed in these lectures. Figure taken from Ref. [31].

In fact, what is usually done is to make an ansatz for the exponent α and fix t_0 and t_3 by imposing that this minimum appears at $\rho_0 = 0.16$ fm^3 and that the corresponding E/A has the value -16 MeV. A typical result is shown in Fig. 2.3.

2.4 Nuclear Density Functional Theory (DFT)

The reader may be puzzled by the fact that the Skyrme interaction that we have introduced in Eq. (2.29) is density-dependent; definitely, this is the signature of an effective interaction. In fact, even if we extend our considerations to effective interactions that are not discussed in this text, like the Gogny force, we can see that most of them, if not all of them, are density-dependent. So far, it has been very hard, if not simply impossible, to design an effective interaction that provides a successful description both of bulk nuclear properties (nuclear saturation and properties of uniform matter around ρ_0, as well as masses and radii of finite nuclei) and of spectroscopic properties, without introducing some kind of density dependence. The underlying reasons have been discussed in Refs. [32, 33], but such analysis goes beyond

our scope here.

A density-dependent interaction $V[\rho]$, or a density-dependent Hamiltonian $H[\rho]$, pose, generally speaking, conceptual problems unless one considers them merely as a tool to generate an energy functional $E[\rho]$ through Eq. (2.28). In fact, we have seen by explicit calculation in subsection 2.3.1 that the total energy eventually depends on ρ. This explicit calculation has been performed in uniform matter and, thus, the density is a number; however, in a finite system the density is a function of the position, $\rho(\mathbf{r})$, and the total energy is actually a *functional* [6] of the density.

In the specialised literature one can find several proofs that, whatever the effective interaction is, the expectation value on a general Slater determinant $\langle\Psi|H|\Psi\rangle$ that we have introduced in Sec. 2.2 is a functional of the number density and/or other generalised densities:

$$E[\rho] = \langle\Psi|H|\Psi\rangle. \tag{2.42}$$

This why we currently believe that effective forces are nothing but tools to generate a functional $E[\rho]$, which is dubbed as Energy Density Functional (EDF). In other terms, nuclear mean-field is at present evolved into what we call nuclear Density Functional Theory (DFT).

DFT was born as a theory for electronic systems. It is based on the fundamental theorems that have been proposed by P. Hohenberg and W. Kohn back in Ref. [34]. The theorems assert that, for a system of fermions that are subject to an external potential $v_{\rm ext}$, the total energy can be written as a functional of the particle density $\rho(\mathbf{r})$. More precisely,

$$E_v[\rho] = F[\rho] + \int d^3r\ v_{\rm ext}(\mathbf{r})\rho(\mathbf{r}), \tag{2.43}$$

where the contribution of the external potential is singled out in the second term and the functional F should be universal, namely it is related to the kind of fermions and not to $v_{\rm ext}$. In fact, for self-bound systems like ordinary nuclei F would be the only term. Eq. (2.43) also implies that the total functional E_v displays a minimum at the exact ground-state density, and its value is the exact ground-state energy.

Unfotunately, the Hohenberg-Kohn theorems give no clue on how the exact functional F must look like. Given the relative success of effective

[6] We remind that a functional is, here, a scalar that depends on a function in 3D space.

forces like the Skyrme interaction, many practitioners have started from $E[\rho]$ generated through Eq. (2.42) and then progressively generalized them. As of today, many existing and successful EDFs are written directly as a given $E[\rho]$ and have lost the link with an underlying Hamiltonian or effective force. The successes and limitations of nuclear DFT have been already the subject of textbooks [35]. Refs. [10, 31, 36] are short introductions.

Chapter 3

Nuclear superfluidity

At the end of Sec. 2.2 we have stated that the HF theory, supplemented by a well calibrated effective interaction, is able to reproduce the experimental values of the total binding energies and charge radii, that are the main nuclear ground state properties [29]. However, this is true only for double-magic nuclei (or neighbouring ones). It is mandatory, for open shell nuclei, to take into account at least the so-called "pairing" residual interaction within the framework of the Bardeen-Cooper-Schrieffer (BCS) or Bogoliubov approximations.

There are many proofs of the existence of pairing in nuclei.

- One is the trend of the binding energies themselves. Even in the simplest formula, the semi-empirical one, it is known that there is a pairing term whose value is $+\Delta$ for even-even nuclei, zero for odd nuclei, and $-\Delta$ for odd-odd nuclei. Thus, we are led to introduce the idea that nuclei get extra binding if the nucleons of the same kind can form pairs. This fact is clearly illustrated in Fig. 3.1. A rough estimate of Δ is $12/\sqrt{A}$ (in MeV), but this is not so reliable for light systems while it works better for medium-heavy ones.

- Historically, however, the previous one has not been the main reason to introduce a special residual force that "pairs" nucleons. It has been noted by A. Bohr, B.R. Mottelson and D. Pines [37] that the first excited states of odd isotopes are quite low in energy, while those of even-even ones lie around 1 MeV (cf. Fig. 3.2). This "gap" in the excitation spectrum is reminiscent of the one that had been already noticed in the superconductors. Then, the same BCS theory that has

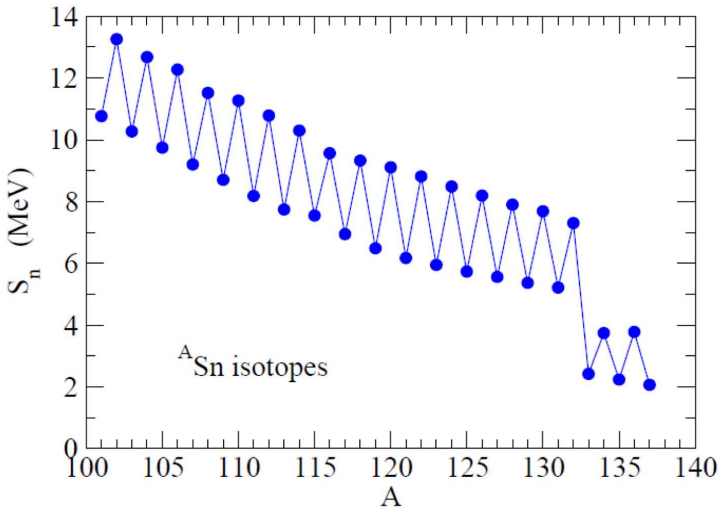

Figure 3.1: Separation energy of the Sn isotopes. We remind that $S_{\rm n} = BE(N+1) - BE(N)$. The so-called odd-even staggering, namely the difference between odd and even isotopes that we have mentioned in the text, is clearly evident.

successfully explained ordinary superconductivity has been extended to atomic nuclei. Since the nucleon pairs are made up either with protons or with neutrons, we better speak of nuclear superfluidity rather than superconductivity in the present context.

- There are other evidences for nuclear pairing: for instance, as we shall mention in Chapter 5, the moment of inertia of deformed nuclei is a strong one.

3.1 BCS theory

In the nuclear BCS theory for systems with an even number of particles, the ansatz is that the pairs are made by nucleons that are in the same orbital and can be coupled to total angular momentum $J = 0$. The state $|JM = 00\rangle$

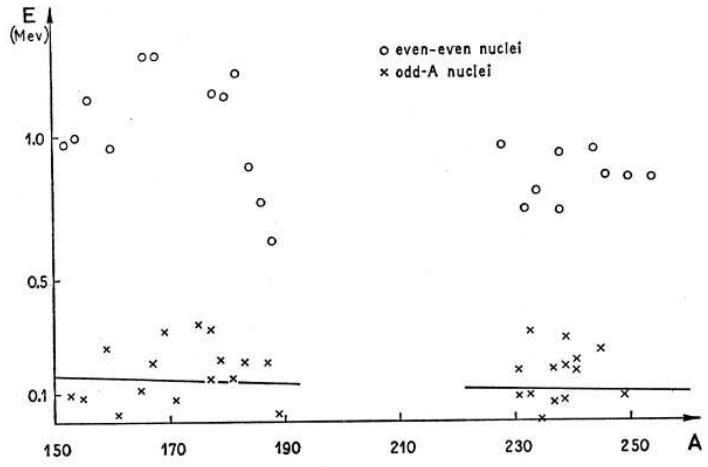

Figure 3.2: Energies of the first excited states in even-even (circles) and odd nuclei (crosses). The figure is taken from Ref. [37] and includes most of the data available at that time in the regions in which nuclei have nonspherical equilibrium shapes (cf. Chapter 5). Deformed nuclei have a larger density of states around the Fermi energy.

can be written as

$$\begin{aligned} |JM=00\rangle &= \sum_{m_1 m_2} \langle jm_1 jm_2|00\rangle |jm_1\rangle |jm_2\rangle \\ &= \sum_{m} \langle jmj-m|00\rangle |jm\rangle |j-m\rangle, \end{aligned} \tag{3.1}$$

where the first equality is the standard definition of a coupled state, and the second one stems from the fact that the Clebsch-Gordan coefficients vanish if $m_1 + m_2$ is not equal to the total M.

One could introduce again, at this stage, the time-reversal operator[1] T, that changes t into $-t$. We remind that for a particle without spin this operator coincides with the complex conjugation[2]. Spin introduces extra

[1] Although this operator has been discussed in Chapter 1, its explicit form was not introduced therein.

[2] This is easy to deduce since in the time-dependent Schrödinger equation,

$$i\hbar \frac{\partial}{\partial t}\phi = H\phi,$$

complications that are dealt with in standard textbooks. Here we just state without proof the result of the application of the time-reversal operator to a state $|jm\rangle$ of the form (2.7), that is,

$$T|jm\rangle \equiv |\widetilde{jm}\rangle = (-)^{j+m}|j-m\rangle. \tag{3.2}$$

Since

$$\langle jmj-m|00\rangle = \frac{(-)^{j-m}}{\sqrt{2j+1}},$$

then Eq. (3.1) becomes

$$|JM=00\rangle = -\frac{1}{\sqrt{2j+1}}\sum_m |jm\rangle|\widetilde{jm}\rangle. \tag{3.3}$$

In short, pairs of nucleons in time-reversal states correspond (aside from trivial factors) to pairs coupled to zero angular momentum. The BCS ansatz for the nuclear wave function is, accordingly,

$$|\mathrm{BCS}\rangle = \Pi_{k>0}\left(u_k + v_k a_k^\dagger a_{\tilde{k}}^\dagger\right)|-\rangle. \tag{3.4}$$

In this latter formula, k means jm, $k>0$ labels the states with positive projection of the total angular momentum, that is, $m>0$, u and v are variational parameters, and $a^\dagger$ labels the creation operators that act on the particle vacuum $|-\rangle$. The following comments are in order.

- The BCS wave function (3.4) generalises the HF one. In fact, for a nucleus with an even number of nucleons of each type, HF corresponds to filling orbitals with both m and $-m$ up to the Fermi energy. This is obtained from (3.4) if we set $v_k=1$ and $u_k=0$ when the state k lies below the Fermi energy, and we set $v_k=0$ and $u_k=1$ otherwise:

  $$|\mathrm{HF}\rangle = \Pi_{k<\text{Fermi level}} a_k^\dagger a_{\tilde{k}}^\dagger|-\rangle. \tag{3.5}$$

  In other words, if we use the variational wave function (3.4) we generalise the HF ansatz without excluding it *a priori*.

- The BCS wave functions contains many more terms, as compared to HF, in which pairs of nucleons can be scattered to unoccupied levels above the Fermi one. In the case in which the BCS state is not markedly different from the HF one, we can think of few particles scattered from just below to just above the Fermi level.

when $t\to -t$, then ϕ^* becomes the new solution.

- One of the main features of the BCS wave function is that, in principle, it mixes states with different number of particles.

In the BCS theory, the nuclear ground-state is obtained by minimising the energy in the Hilbert space of wave functions of the type (3.4).

3.2 Derivation of the BCS equations

The BCS equations can be derived using the variational principle, as in the HF case, but with the more general wave function (3.4). To this aim, we need to write the Hamiltonian in second quantization as

$$H = T + V = \sum_{k_1 k_2} \langle k_1|t|k_2\rangle a^\dagger_{k_1} a_{k_2} + \frac{1}{4} \sum_{k_1 k_2 k_3 k_4} \langle k_1 k_2|\bar{v}|k_3 k_4\rangle a^\dagger_{k_1} a^\dagger_{k_2} a_{k_4} a_{k_3}, \quad (3.6)$$

where the notation is the same as in Sec. 2.2 but we use $\langle ij|\bar{v}|kl\rangle$ instead of $\langle ij|v|kl\rangle_{\rm AS}$.

Since the BCS wave function mixes states with different particle number, and we would like that such number is conserved at least on average, we request it through a Lagragnge multiplier and we implement the variational principle as the search of the minimum of $\langle {\rm BCS}|H - \lambda N|{\rm BCS}\rangle$. The meaning of λ is provided by the equation

$$\lambda \equiv \frac{\partial}{\partial N} \langle {\rm BCS}|H|{\rm BCS}\rangle. \quad (3.7)$$

In other words, λ represents the energy which is needed to add or remove a particle, that is, the Fermi energy. In summary, we have several variational parameters, that are the single-particle states k with their energies ε_k, as well as u_k, v_k and the Fermi energy λ.

We first show that the state $|{\rm BCS}\rangle$ is normalized.

$$\langle {\rm BCS}|{\rm BCS}\rangle = \Pi_{k>0} \langle -|(u_k + v_k a_{\tilde{k}} a_k)(u_k + v_k a^\dagger_k a^\dagger_{\tilde{k}})|-\rangle. \quad (3.8)$$

The only non-vanishing terms in vacuum expectation values are those in which the number of creation and annihilation operators is the same, so that contractions of the type $\overbrace{aa^\dagger}$ can provide a finite number. This is why the terms in (3.8) having $k' \neq k$ in the two factors do not contribute. We are left with

$$\langle {\rm BCS}|{\rm BCS}\rangle = \Pi_{k>0} \langle -|u_k^2 + v_k^2 \overbrace{a_{\tilde{k}} a_k a^\dagger_k a^\dagger_{\tilde{k}}}|-\rangle = \Pi_{k>0}(u_k^2 + v_k^2). \quad (3.9)$$

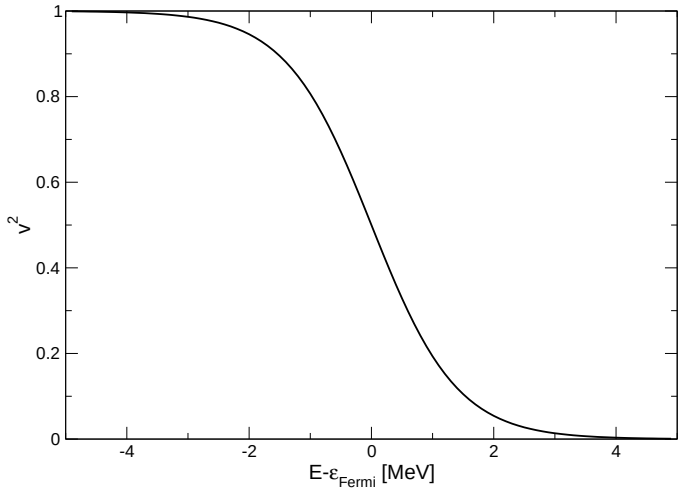

Figure 3.3: Schematic picture of the occupation factors v^2 as a function of $\varepsilon - \lambda$ [see also Eq. (3.25)].

This shows that we have to request that

$$u_k^2 + v_k^2 = 1, \tag{3.10}$$

and this latter equation, valid for each k, supports the interpretation that u_k is the probability amplitude that the state k is empty, while v_k is the probability apmplitude that the state k is occupied. In other words, v_k^2 is the BCS occupation factor of the state k. A schematic picture of these occupation factors is shown in Fig. 3.3. The HF occupation factors have the form of a step, while in BCS they are smoothed out over an interval of the order of $\approx \Delta$.

We now calculate the quantity that will be minimised, namely

$$\langle \mathrm{BCS}|H - \lambda N|\mathrm{BCS}\rangle = \langle \mathrm{BCS}|T - \lambda N|\mathrm{BCS}\rangle + \langle \mathrm{BCS}|V|\mathrm{BCS}\rangle. \tag{3.11}$$

The first quantity at the r.h.s. includes one-body operators and the second is associated with the two-body operator V. The former is straightforward to evaluate. We use the standard definition of the number operator,

$$N = \sum_k a_k^\dagger a_k, \tag{3.12}$$

as well as the result provided by Eq. (3.38), to obtain

$$\begin{aligned}\langle \mathrm{BCS}|T-\lambda N|\mathrm{BCS}\rangle &= \sum_{k_1k_2}\left(\langle k_1|t|k_2\rangle-\lambda\delta(k_1,k_2)\right)\langle \mathrm{BCS}|a^\dagger_{k_1}a_{k_2}|\mathrm{BCS}\rangle \\ &= \sum_k\left(\langle k|t|k\rangle-\lambda\right)v_k^2. \end{aligned} \tag{3.13}$$

The detail is given in Appendix.

Before we move to the expectation value of V, we must notice that the previous formula also provides the expectation value of the number operator. One of the requirements of the BCS theory, as we have already mentioned, is that this expectation value is equal to the actual number of particles[3]. This amounts to

$$\boxed{N=\sum_k v_k^2 = 2\sum_{k>0}v_k^2.} \tag{3.14}$$

The expectation value of V is calculated in the Appendix. If we sum the result of Eq. (3.40) to the one of (3.13), we obtain

$$\begin{aligned}\langle \mathrm{BCS}|H-\lambda N|\mathrm{BCS}\rangle &= \sum_k\left[\left(t_{kk}-\lambda\right)v_k^2+\frac{1}{2}\sum_{k'}\bar{v}_{kk'kk'}v_k^2v_{k'}^2\right] \\ &+ \sum_{kk'>0}\bar{v}_{k\tilde{k}k'\tilde{k}'}u_kv_ku_{k'}v_{k'}. \end{aligned} \tag{3.15}$$

We now calculate

$$\delta\langle \mathrm{BCS}|H-\lambda N|\mathrm{BCS}\rangle = 0. \tag{3.16}$$

We use v_k as a variational parameter, that is, we equate the total derivative with respect to v_k to zero. Since $u_k=\sqrt{1-v_k^2}$, then

$$\frac{d}{dv_k}=\frac{\partial}{\partial v_k}-\frac{v_k}{u_k}\frac{\partial}{\partial u_k}.$$

[3]Note that we use, for the sake of simplicity, the same symbol for the particle number operator and the number of particles in the system. The context should make it clear what we precisely refer to.

We apply this operator to (3.15) and, by multiplying by $\frac{u_k}{2}$ we obtain

$$\begin{aligned} 0 &= u_k v_k \left[(t_{kk} + t_{\tilde{k}\tilde{k}} - 2\lambda) + \sum_{k'} \left(\bar{v}_{kk'kk'} + \bar{v}_{\tilde{k}k'\tilde{k}k'} \right) v_{k'}^2 \right] \\ &+ \sum_{k'>0} \bar{v}_{k\tilde{k}k'\tilde{k}'} \left(u_k^2 - v_k^2 \right) u_{k'} v_{k'}. \end{aligned} \tag{3.17}$$

We introduce the quantity

$$\boxed{\tilde{\varepsilon}_k = \frac{1}{2} \left[(t_{kk} + t_{\tilde{k}\tilde{k}} - 2\lambda) + \sum_{k'} \left(\bar{v}_{kk'kk'} + \bar{v}_{\tilde{k}k'\tilde{k}k'} \right) v_{k'}^2 \right].} \tag{3.18}$$

Another important definition is that of the pairing gap,

$$\Delta_k = -\sum_{k'>0} \bar{v}_{k\tilde{k}k'\tilde{k}'} u_{k'} v_{k'}. \tag{3.19}$$

With these definitions, Eq. (3.17) becomes

$$\begin{aligned} 0 &= 2u_k v_k \tilde{\varepsilon}_k + \Delta_k \left(v_k^2 - u_k^2 \right), \\ 4\tilde{\varepsilon}_k^2 u_k^2 v_k^2 &= \Delta_k^2 \left(u_k^2 - v_k^2 \right)^2. \end{aligned} \tag{3.20}$$

By using Eq. (3.10),

$$\begin{aligned} (u_k^2 + v_k^2)^2 &= 1 = u_k^4 + v_k^4 + 2u_k^2 v_k^2, \\ u_k^4 + v_k^4 &= 1 - 2u_k^2 v_k^2, \\ (u_k^2 - v_k^2)^2 &= 1 - 4u_k^2 v_k^2, \end{aligned} \tag{3.21}$$

and one arrives at

$$4\tilde{\varepsilon}_k^2 u_k^2 v_k^2 = \Delta_k^2 - \Delta_k^2 u_k^2 v_k^2. \tag{3.22}$$

We introduce at this stage the quasi-particle energy:

$$\boxed{E_k = \sqrt{\tilde{\varepsilon}_k^2 + \Delta_k^2}.} \tag{3.23}$$

If this definition, together with the condition (3.10), is inserted into Eq. (3.22), an equation for v_k^2 is obtained, whose solution is straightforward and reads

$$v_k^2 = \frac{1}{2} \pm \frac{|\tilde{\varepsilon}_k|}{2E_k}. \tag{3.24}$$

It is easy to check that the solution that leads to the correct HF limit, in which v_k^2 should be 0 (1) above (below) the Fermi energy λ, is

$$v_k^2 = \frac{1}{2} - \frac{\tilde{\varepsilon}_k}{2E_k}. \tag{3.25}$$

The corresponding solution for u_k^2 that has the correct HF limit as well, that is, 0 (1) below (above) the Fermi energy λ, reads

$$u_k^2 = \frac{1}{2} + \frac{\tilde{\varepsilon}_k}{2E_k}. \tag{3.26}$$

If we now write the product $u_{k'}v_{k'}$ from the two latter equations (3.25) and (3.26), we insert this in the definition (3.19), and we also use the other definiton (3.23), we arrive at the gap equation

$$\Delta_k = -\sum_{k'>0} \frac{\Delta_{k'}}{2E_{k'}} v_{k\tilde{k}k'\tilde{k}'}. \tag{3.27}$$

The system made up with Eqs. (3.14, 3.18, 3.23, 3.25, 3.26, 3.27) is closed. The equations are displayed within a box for the reader's convenience.

Before we attempt some schematic solutions of this system, we should give a tentative interpretation of the quantities that we have introduced.

- The number equation (3.14) expresses the fact that, on average, the particle number is conserved. In fact, as we have already remarked, we ought to consider v_k^2 as the probability the the level k is occupied or, equivalently, the average number of particles on the level k.

- The quantity $\tilde{\varepsilon}_k$ that has been introduced through Eq. (3.18) generalises the single-particle energy that has been introduced in the HF theory. In fact, it represents the difference between the single-particle energy and the Fermi energy λ. This can be shown in the following way. If we assume that the nucleus at hand is invariant under time-reversal, and we set ourselves in the HF limit in which $v_{k'}$ is 1 below the Fermi energy and vanishes above it, then Eq. (3.18) becomes

$$\tilde{\varepsilon}_k = t_{kk} - \lambda + \sum_{k'} \bar{v}_{kk'kk'}. \tag{3.28}$$

The same equation can be derived if one subtracts λ from the single-particle energy ε_i deduced from Eq. (2.23). This is achieved by multiplying Eq. (2.23) at left by $\varphi_i^*(\mathbf{r})$, and integrating over $\mathbf{r}$.

- The quasi-particle energy definition (3.23) again reduces to a single-particle energy measured with respect to the Fermi energy λ in the HF limit, namely if Δ_k vanishes. In the non-trivial case of a finite gap Δ_k, however, we notice that the energy needed to add a nucleon to the system cannot be smaller than Δ_k. This holds if we have a system with an even number of particles, and does explain the gap in the spectrum that has been mentioned at the start of the Chapter. If the system has an odd number of nucleons, the odd nucleon is added on top of the BCS wave function without belonging to any Cooper pair, so that its energy can be arbitrarily small with respect to the Fermi energy and the odd system does not display any gap. We have also explained, in this way, the pairing term $\approx 12/\sqrt{A}$ in the semi-empirical mass formula.

- The equation that determines whether the system has the simple HF solution or the non-trivial solution (that we shall call superfluid from now on) is the gap equation (3.27). This is the most important equation within the BCS theory. Intuitively, one can understand that if the density of levels is not extremely large, so that $\varepsilon_k - \lambda$ must remain finite, and $v_{k\tilde{k}k'\tilde{k}'}$ is small, the HF solution will be the correct one. Otherwise, a supefluid solution will be preferred. We shall discuss this on the explicit examples that follows.

3.3 Solution of the BCS equations in schematic cases

In both the toy models that we discuss below, we assume that the matrix elements that enter the gap equation are constant, namely we approximate $\bar{v}_{k\tilde{k}k'\tilde{k}'}$ with $-G$. In this case, it is convenient to start from the gap equation in the form (3.19), and we can write

$$\Delta_k = G \sum_{k'} u_{k'} v_{k'} = \Delta, \tag{3.29}$$

since, clearly, the pairing gap becomes state-independent.

3.3.1 Solution for equally spaced levels

We consider two-fold degenerate levels having a constant spacing d, in an energy window which is symmetric with respect to the Fermi energy λ, so that the lowest level is at $\lambda - \Lambda$ and the upper level at $\lambda + \Lambda$. The density of levels if $g = 2/d$, and the density of levels with positive projection of the angular momentum is $g/2 = 1/d$. By approximating the sum in the gap equation (3.27) with an integral, we obtain

$$\begin{aligned} \Delta &= \frac{G}{2}\Delta \sum_{k'>0,\ \lambda-\Lambda<\varepsilon_{k'}<\lambda+\Lambda} \frac{1}{\sqrt{(\varepsilon_{k'}-\lambda)^2+\Delta^2}}, \\ 1 &= \frac{G}{2}\frac{1}{d}\int_{-\Lambda}^{+\Lambda} d\varepsilon\ \frac{1}{\sqrt{\varepsilon^2+\Delta^2}}. \end{aligned} \tag{3.30}$$

The integral can be solved and it turns out to be $2\sinh^{-1}\left(\frac{\Lambda}{\Delta}\right)$. The solution of the model is therefore

$$\Delta = \frac{\Lambda}{\sinh\frac{d}{G}} \approx 2\Lambda \mathrm{e}^{-d/G}. \tag{3.31}$$

In this solvable model one can see, in a transparent manner, that the parameter that plays a role is the ratio between the level spacing and the value of the typical pairing matrix elements G. If this parameter is large, the gap essentially vanishes; this is what happens in magic nuclei. The gap is finite if the pairing matrix elements are comparable with, or larger than, the level spacing. This is what happens, instead, in the case of open-shell nuclei that are characterised by superfluid solutions.

3.3.2 Solution for a single j-shell

Let us now make the further assumption that we restrict to a single level, with degeneracy $2j + 1 \equiv 2\Omega$ (Ω is the number of states with positive projection of the angular momentum). The number equation becomes simply

$$N = 2\sum_{k>0} v_k^2 = 2\Omega v^2, \tag{3.32}$$

so that

$$v = \sqrt{\frac{N}{2\Omega}} \qquad u = \sqrt{1 - \frac{N}{2\Omega}}, \tag{3.33}$$

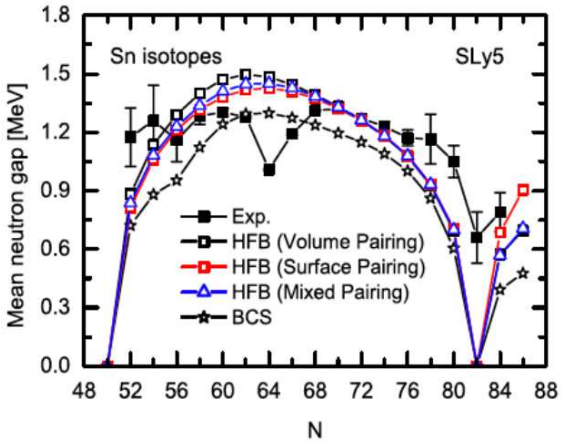

Figure 3.4: Mean pairing gap of the states k around the Fermi energy, for the Sn isotopes. The figure is taken from [38], and is displayed here to remark the qualitative validity of Eq. (3.34). Details about the specific BCS implementation, or about the Hartree-Fock-Bogoliubov (HFB) theory and the way to extract a pairing gap from experimental data, go beyond the scope here.

and the pairing gap extracted from Eq. (3.29) becomes

$$\Delta = G\Omega\sqrt{\frac{N}{2\Omega}\left(1-\frac{N}{2\Omega}\right)} = G\sqrt{\frac{N}{2}\left(\Omega-\frac{N}{2}\right)}. \tag{3.34}$$

This kind of trend like a hat, with a maximum when the shell is half-occupied ($N = \Omega$) and minima at zero in correspondence of the completely empty or filled shell, is typical also of microscopic calculations. It shows up, for instance, in the isotopes $^{120-132}$Sn, where the single $h_{11/2}$ level plays indeed a major role. Actually, microscopically calculated gaps throughout the whole shell $N = 50 - 82$ often display such simple behaviour as in the example of Fig. 3.4.

3.A Appendices

3.A.1 Matrix elements of use for the BCS theory

First, we wish to calculate

$$\langle \mathrm{BCS}|a^\dagger_{k_1}a_{k_2}|\mathrm{BCS}\rangle. \tag{3.35}$$

A useful consideration to be made is that the BCS wave functions at the left and at the right will bring in, respectively, pairs of operators like $a_{\tilde{k}_1}a_{k_1}$ and $a^\dagger_{k_2}a^\dagger_{\tilde{k}_2}$. There is no way to obtain an even number of creation and annihilation operators with the same label, unless $k_1 = k_2$. Thus, we are left with

$$\begin{aligned}&\langle \mathrm{BCS}|a^\dagger_k a_k|\mathrm{BCS}\rangle = \\ &= \Pi_{l>0,l\neq k}\langle -|(u_l + v_l a_{\tilde{l}}a_l)(u_k + v_k a_{\tilde{k}}a_k)a^\dagger_k a_k(u_k + v_k a^\dagger_k a^\dagger_{\tilde{k}})(u_l + v_l a^\dagger_l a^\dagger_{\tilde{l}})|-\rangle.\end{aligned} \tag{3.36}$$

We can move the operators carrying l and $\tilde{l}$ as labels on the left side by exploiting the anticommutation relations. If $k \neq l$, all operators anticommute and exchanging two of them produces a minus sign, so that an even number of exchanges leaves the product of operators invariant.

$$\begin{aligned}&\langle \mathrm{BCS}|a^\dagger_k a_k|\mathrm{BCS}\rangle = \\ &= \Pi_{l>0,l\neq k}\langle -|(u_l + v_l a_{\tilde{l}}a_l)(u_l + v_l a^\dagger_l a^\dagger_{\tilde{l}})(u_k + v_k a_{\tilde{k}}a_k)a^\dagger_k a_k(u_k + v_k a^\dagger_k a^\dagger_{\tilde{k}})|-\rangle = \\ &= \Pi_{l>0,l\neq k}(u_l^2 + v_l^2)\langle -|(u_k + v_k a_{\tilde{k}}a_k)a^\dagger_k a_k(u_k + v_k a^\dagger_k a^\dagger_{\tilde{k}})|-\rangle = \\ &= v_k^2\langle -|\overbrace{a_{\tilde{k}}a_k a^\dagger_k a_k a^\dagger_k a^\dagger_{\tilde{k}}}|-\rangle = v_k^2.\end{aligned} \tag{3.37}$$

In conclusion,

$$\langle \mathrm{BCS}|a^\dagger_{k_1}a_{k_2}|\mathrm{BCS}\rangle = \delta(k_1,k_2)v^2_{k_1}. \tag{3.38}$$

In order to calculate the expectation value of V, we fix two indices k and k' and define for the sake of brevity

$$|\psi\rangle \equiv \Pi_{k''\neq k,k'}(u_{k''} + v_{k''}a^\dagger_{k''}a^\dagger_{\tilde{k}''})|-\rangle.$$

Then,

$$\begin{aligned}\langle \mathrm{BCS}|V|\mathrm{BCS}\rangle = \frac{1}{4}\sum_{k_1k_2k_3k_4}&\langle\psi|(u_k + v_k a_{\tilde{k}}a_k)(u_{k'} + v_{k'}a_{\tilde{k}'}a_{k'})\times \\ \times a^\dagger_{k_1}a^\dagger_{k_2}a_{k_4}a_{k_3}&(u_{k'} + v_{k'}a^\dagger_{k'}a^\dagger_{\tilde{k}'})(u_k + v_k a^\dagger_k a^\dagger_{\tilde{k}})|\psi\rangle.\end{aligned} \tag{3.39}$$

Note that $|\psi\rangle$ is equivalent to the vacuum for operators that carry the labels k and k'. There are potentially many terms but one must exclude those that do not give any contribution because the creation and annihilation operators cannot be matched. After a tedious enumeration one arrives at

$$\langle \mathrm{BCS}|V|\mathrm{BCS}\rangle = \frac{1}{2}\sum_{kk'} \bar{v}_{kk'kk'} v_k^2 v_{k'}^2 + \sum_{kk'>0} \bar{v}_{k\tilde{k}k'\tilde{k}'} u_k v_k u_{k'} v_{k'}. \tag{3.40}$$

Chapter 4

Spectroscopy of even-even nuclei and collective vibrations

It is well known that the excitation spectra of atomic nuclei display an extremely rich variety of phenomena. The lowest nuclear excitations can be as low as 11 keV (the first excited state in ^{237}U) or as large as 6 MeV (the first excited state in ^{16}O). A comprehensive database for nuclear excited states can be found at `http://www.nndc.bnl.gov/`. Besides their energy, these states are characterised by the good quantum numbers associated with the nuclear Hamiltonian, namely the total angular momentum and parity, J^π.

Many different effects contribute to create the huge diversity in the pattern of nuclear excited states. Nuclear spectroscopy is, as a consequence, a complicated subject. Shell effects are of paramount importance: intuitively, one can understand that in closed-shell systems the nucleons need to jump across a major shell to create an excited state of the whole nucleus, whereas in open-shell systems one can have low-energy states. When the trend of the excititation energy of a given state with J^π is considered, along an isotopic or isotonic chain, a sudden increase of the energy is often a signature of a shell closure. In addition to this, pairing and deformation do play a special role. Deformation splits the spherical levels and gives rise to a higher level density; pairing makes a difference between even and odd systems. Thinking about all this, the fact that the first excited state in ^{237}U is so much lower than the one in ^{16}O makes some sense.

We have seen the effects produced by pairing in the last Chapter. In the next Section, we shall discuss how the nuclear shape (either spherical or deformed) is responsible for creating two different kinds of pattern in

the excitation spectra. In fact, collective vibrations around the equilibrium shape are among the typical excited states of spherical nuclei. We shall introduce the main features of these collective vibrations in the present Chapter, together with a theory that can explain them, that is, the linear response theory. Spherical nuclei cannot rotate. Non-spherical nuclei, in particular those characterised by a quadrupole deformation, display instead spectra in which collective rotations show up. This will be the subject of the next Chapter.

Before starting our treatment of all these topics, we provide some useful reminder about discrete levels and levels in the continuum. The patterns of the excitation spectra that we have just introduced are evident in the low-energy region. As is well known, nuclei have separation energies of the order of $\approx$ 7-8 MeV, if we stay within the stability valley. Below this energy the excitation spectrum is discrete, and γ-transitions provide additional information about the specific character of the excited states. Accordingly, we will review some main characteristics of electromagnetic transitions between nuclear states in Chapter 6. The energy region below the separation energy is normally referred to, sometimes implicitly, when one talks about nuclear spectroscopy. Above the separation energy, the excitation spectra are not discrete any longer and only in very specific cases one identifies narrow structures. In this region, for each J^π, there is a continuum of states which, whenever featureless, does not bring very useful information. One can seek prominent states that emerge from the featureless background. The main example of these prominent states is constituted by the so-called giant resonances, that show up at energies around 10-30 MeV and carry interesting information about the nuclear properties, as we will briefy discuss below.

In what follows, we restrict ourselves to the case of even-even nuclei where the ground state is always $J^\pi = 0^+$. Excited states have integer angular momentum. Often, but not always, the first excited states has $J^\pi = 2^+$.

4.1 Spectra of vibrational and rotational nuclei

In Fig. 4.1, the quantity which is shown is

$$R = \frac{E(4_1^+)}{E(2_1^+)}, \tag{4.1}$$

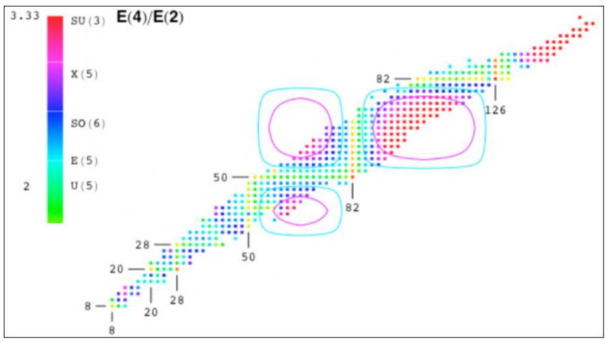

Figure 4.1: The ratio R between the energies of the first excited 4^+ and 2^+ states [Eq. (4.1)] is displayed along the whole nuclear chart, in the case of even-even nuclei. The labels close to the color code legend correspond to group symmetries that are not discussed in the present text. The figure has been prepared by P. Van Isacker.

which is the ratio between the energies of the first excited 4^+ and 2^+ states, respectively, in even-even nuclei. Although such values tend to vary, there are certainly regions in which they are close either to 2 or 3.33. These values are associated with some paradigmatic nuclei whose excitation spectrum can be to a large extent interpreted in simple terms: we mean the spherical nuclei that vibrate and the non-spherical ones that display collective rotations, as we now clarify.

We first note that the nuclei associated with $R = 2$ tend to lie on lines having constant Z or constant N, where at least one of them is a magic number. In the regions where neither of them is a magic number there are clear "islands" where nuclei associated with $R = 3.33$ tend to cluster.

A simple paradigm for a spherical system that undergoes small oscillations around the equilibrium shape is that of the harmonic oscillator spectrum. If the ground state is 0^+, we can imagine that the excited states are associated with "phonons", or vibrational quanta, having a given angular momentum and parity. As we said above, in many cases the lowest among such states

turns out to be a 2^+ state. Consequently, within the harmonic picture, we expect a two-phonon state at twice the 2^+ energy. The two-phonon state results from the coupling of the 2^+ with itself, so that we should actually expect a triplet of 0^+, 2^+ and 4^+ states which are degenerate[1]. This type of spectrum is displayed in the left part of Fig. 4.2. Thus, nuclei having R equal, or close, to 2, are spherical nuclei that can vibrate and are often called "vibrational nuclei".

Nuclei with a non-spherical shape can instead rotate. A classical rotor will display a spectrum in which excitation energies scale like $J^2/2\mathcal{I}$, where J is the angular momentum and $\mathcal{I}$ is the moment of inertia. If we discard for the moment the question whether all values, even or odd, of the quantized angular momentum J are allowed, we find that for energies that scale like

$$E_{\text{rotational}} = \frac{\hbar^2}{2\mathcal{I}} J(J+1) \tag{4.2}$$

the ratio R is exactly 3.33. Such nuclei can be called "rotational nuclei" and the spectrum associated with the latter formula (4.2) is depicted in the right part of Fig. 4.2. The regions that are circled in Fig. 4.1 are usually referred to as "islands of deformation". They correspond to regions in which both neutrons and protons have open shells.

Our discussion leaves out the intermediate values of R. Of course, the transition between spherical and deformed nuclei does not take place all of a sudden. This is clear from Fig. 4.1, where one can spot intermediate regions between the two patterns that we have described, in which R takes values between 2 and 3.33. These "transitional nuclei" will not be treated. In the next Chapter we shall deal with nuclear deformation and collective rotation. We stick to spherical nuclei that vibrate in the rest of this Chapter.

4.2 Phenomenology of nuclear vibrations

There are vibrations characterised by different quantum numbers, as we already alluded to. In addition to the exact quantum numbers J^π, approximate quantum numbers are L (orbital angular momentum) and S (spin angular momentum). We remind that $\vec{J} = \vec{L} + \vec{S}$. One more approximate quantum number is T (isospin). Generally speaking, spin excitations are higher in

[1]Experimental spectra can inform us about the relevance of anharmonicities, that is, deviations from the pure harmonic picture. These anharmonicities turn out to be small.

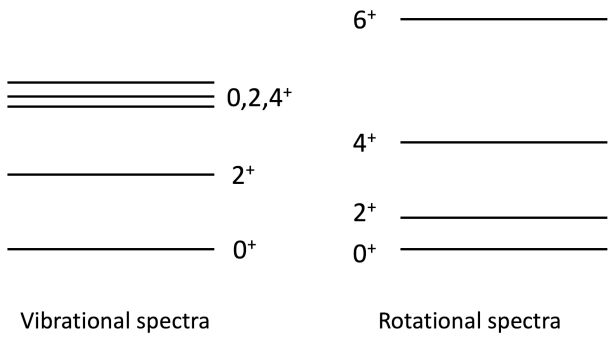

Figure 4.2: The vibrational and rotational patterns in the nuclear excitation spectra as described in the main text.

energy than non-spin ones, and $T = 1$ (isovector) excitations are higher than $T = 0$ (isoscalar) ones. In the discrete part of the spectrum, states with $S = T = 0$ are prevalent.

If we have to single out paradigmatic states among the vibrational ones, we should definitely point to the so-called Giant Resonances. There exist monographs on this subject, like Ref. [39]. They lie above the particle threshold, that is, around $\approx$ 10-30 MeV. They have the shape or a resonance, with a peak energy and a width Γ, and clearly emerge on top of the background of other excited states; in other words, they have large cross section associated with inelastic processes (we shall return to this point when discussing inelastic reactions in Chapter 7).

The first evidence of such resonances has been found in experiments in which a photon beam impinges on a nucleus. A large resonance has been found systematically in all nuclei, at an energy of the order of

$$E_{\rm IVGDR} \approx 80 \ {\rm A}^{-1/3} \ [{\rm MeV}]. \tag{4.3}$$

At such energies, it is easy to verify that the wavelength associated with the photons, $\lambda = \frac{2\pi\hbar c}{E} \approx 15 \ {\rm A}^{1/3}$ fm, is much larger than the nuclear size. The protons feel the electric field that oscillates rapidly in time but is essentially uniform in space. These conditions correspond to the well-known dipole approximation. Protons are pulled apart from neutrons, but the strong proton-neutron attraction provides the restoring force. In the limit of a small

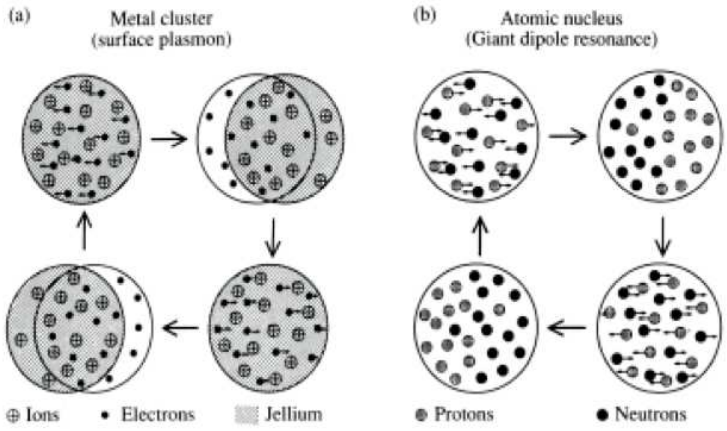

Figure 4.3: Schematic picture associated with the Giant Dipole Resonance (GDR) as discussed in the main text (b). The case of plasmon excitations is shown in (a) for the sake of comparison. Figure taken from [40].

external perturbation, we can model such situation as a forced harmonic motion (cf. Fig. 4.3, where the case of plasmon excitations in metallic clusters is also displayed). We expect a resonance when the external frequency matches the eigenmode of the system. We can describe this resonance in a classical framework, but our aim is to relate its existence to the mean-field description of the previous Chapter, and this will be discussed in the next Section. The resonance is called Isovector Giant Dipole Resonance (IVGDR) because protons and neutrons move against each other.

We use this example to introduce some general tools that are very useful for the study of states like the Giant Resonances. If the external field (i.e. the electromagnetic field in the above case) is written as $\hat{F}$, the probability amplitude to excite a state $|n\rangle$ is proportional to

$$\langle n|\hat{F}|0\rangle, \tag{4.4}$$

where $|0\rangle$ is the ground state (this can be seen, for instance, via the Fermi golden rule). We, then, define the "strength function" associated with the

operator $\hat{F}$ in the following way:

$$S(E) = \sum_n |\langle n|\hat{F}|0\rangle|^2 \delta(E - E_n). \tag{4.5}$$

Here, the sum is over a complete set of states that have energies E_n. We stress again that this function is not dimensionless and still the square of the matrix element of $\hat{F}$ is associated with the probability of exciting the specific state $|n\rangle$.

A state is dominant in the response to the external operator $\hat{F}$ if its contribution to the strength function, $|\langle n|\hat{F}|0\rangle|^2$, is a large fraction of the total integral. The total integral is called "non-energy weighted sum rule" and is the zero-th moment, m_0, of S:

$$m_0 = \int dE\ S(E) = \sum_n |\langle n|\hat{F}|0\rangle|^2. \tag{4.6}$$

Other moments characterise the strength function, like the first or "energy-weighted" moment m_1, that reads

$$m_1 = \int dE\ E\ S(E) = \sum_n E_n |\langle n|\hat{F}|0\rangle|^2. \tag{4.7}$$

A reasonable definition of the average energy that is transferred to the nucleus through the action of the operator $\hat{F}$ is

$$\bar{E} \equiv \frac{m_1}{m_0}. \tag{4.8}$$

In other terms, if in the strength function a single state is dominant, that state absorbs most of the energy: this is the case of Giant Resonances.

The appearance of δ-functions in the strength function (4.5) is related to the assumption that the states are discrete. This is usually not the case, as we mentioned, because the excited states can have a finite lifetime due to decay to other states, or particle emission (γ-decay contributes only to a tiny fraction of the width). In this case, the matrix elements squared, $|\langle n|\hat{F}|0\rangle|^2$, should be multiplied by functions having a width Γ, like gaussians or lorentzians. The width is related to the lifetime τ by

$$\Gamma = \frac{\hbar}{\tau}. \tag{4.9}$$

Giant resonances have, as a rule, widths of the order of few MeV, that is, lifetimes of the order of few 10^{-22} s.

An external electromagnetic field excites the IVGDR in a practically exhaustive way. If one wishes to study other kinds of excitations one needs to resort to a strong, i.e. hadronic, field. The problem is then how to find a probe that excites the state of interest in a reasonably "exclusive" way. Most of the hadronic probes excite several states and disentangling them can be rather troublesome. Another issue is that we cannot avoid treating the reaction process that leads to the excitation.

We will discuss inelastic scattering in Chapter 7, and we will touch upon the problem of how to relate the inelastic cross section to the strength function (4.5). Here we just mention that some types of experiments have been proven to be rather selective and very instrumental to identify specific giant resonances. α-particle inelastic scattering excites only $S = T = 0$ states. In the last decades, such experiments have been provided evidence of a $L = 2$, i.e. quadrupole, resonance at an energy

$$E_{\mathrm{ISGQR}} \approx 65 \ \mathrm{A}^{-1/3}, \tag{4.10}$$

and of a $L = 0$, i.e. monopole, resonance at an energy

$$E_{\mathrm{ISGMR}} \approx 80 \ \mathrm{A}^{-1/3}, \tag{4.11}$$

in medium-heavy nuclei.

We now move to the theoretical description of the vibrational spectrum. The reader who wishes to deepen her/his knowledge in the field of Giant Resonances can consult the specialized literature: we have already mentioned the excellent monograph [39].

4.3 Linear response theory for nuclear vibrations

We work under the assumption that the external electromagnetic or hadronic field $\hat{F}$ is weak enough, so that all equations can be computed at lowest order in such field (and in the quantities that characterise the nuclear response). In particular, we want to derive the response of a magic nucleus whose ground-state can be described within the HF approximation as discussed in Sec. 2.2.

Accordingly, we derive the linear response equations from the small amplitude limit of the *time-dependent* Hartree-Fock equations. The static HF equations (2.23) read

$$h\phi_i = \varepsilon_i \phi_i, \tag{4.12}$$

and the single-particle HF Hamiltonian (sum of kinetic energy, Hartree and Fock potentials) depends obviously on the density. An external harmonic perturbation F is supposed to act and to give a boost[2]

$$F(t) = f e^{-i\omega t} + f^\dagger e^{+i\omega t}. \tag{4.13}$$

Then, the corresponding variations of ρ and h have the same form:

$$\delta\rho(t) = \delta\rho\ e^{-i\omega t} + \delta\rho^\dagger e^{+i\omega t}, \tag{4.14}$$

$$\delta h(t) = \delta h\ e^{-i\omega t} + \delta h^\dagger e^{+i\omega t}. \tag{4.15}$$

We write the equation of motion

$$i\hbar\dot{\rho} = [h, \rho]\,, \tag{4.16}$$

and we solve it by assuming that $h = h^{(0)} + \delta h + f$, and that we can stop at linear terms either in $\delta\rho$, δh, or f:

$$i\hbar\delta\dot{\rho} = [h^{(0)}, \delta\rho] + [\frac{\delta h}{\delta\rho}\delta\rho, \rho^{(0)}] + [f, \delta\rho]. \tag{4.17}$$

Note that in this latter equation we have used the fact that in the HF basis the Hamiltonian and the density are simultaneously diagonal, that is, $\left[\rho^{(0)}, h^{(0)}\right] = 0$.

We express now Eq. (4.17) on a basis made up with particle -hole (p-h) excitations $|ph^{-1}\rangle$, by assuming that it is a complete basis. This is called Tamm-Dancoff approximation (TDA). Thus, we take the matrix elements of Eq. (4.17) between $\langle ph^{-1}|$ and the ground state $|0\rangle$ and we obtain, for the terms that go like $e^{-i\omega t}$,

$$\hbar\omega\ \delta\rho_{ph} = \langle p|h^{(0)}\ \delta\rho - \delta\rho\ h^{(0)}|h\rangle + \langle p|\frac{\delta h}{\delta\rho}\delta\rho\ \rho^{(0)} - \rho^{(0)}\frac{\delta h}{\delta\rho}\delta\rho|h\rangle, \tag{4.18}$$

[2]At the moment we do not specify anything about the nature of the perturbation F. In Chapter 6 we will study the form of F in the case of an electromagnetic field. In Sec. 7.4.4, we will see that, within a simple approximation for the inelastic scattering cross section, this latter turns out to be proportional to matrix elements of operators F of the type $r^L Y_{LM}$.

where $\delta\rho_{ph} = \langle ph^{-1}|\delta\rho|0\rangle$ and will be denoted by X_{ph} in the following. Note also that, since we need to perform anyway the limit $f \to 0$ at the end, we have already neglected the commutator including the external field. We have also used the freedom to exchange the state $\langle h^{-1}|$ in the bra with the state $|h\rangle$ in the ket, and we shall use the equations $h^{(0)}|p\rangle = \varepsilon_p|p\rangle$, $h^{(0)}|h\rangle = \varepsilon_h|h\rangle$, whereas $\rho^{(0)}|p\rangle = 0$ and $\rho^{(0)}|h\rangle = |h\rangle$, in the HF basis.

The last ingredient that we need to use is the completeness relation

$$|0\rangle\langle 0| + \sum_{p'h'} |p'h'^{-1}\rangle\langle p'h'^{-1}| = 1, \tag{4.19}$$

that we insert between the operators in the last matrix element at the r.h.s. of (4.18). We obtain

$$\hbar\omega\ \delta\rho_{ph} = (\varepsilon_p - \varepsilon_h)\,\delta\rho_{ph} + \sum_{p'h'} \langle ph^{-1}|\frac{\delta h}{\delta\rho}|p'h'^{-1}\rangle\delta\rho_{p'h'}. \tag{4.20}$$

By defining

$$A_{ph,p'h'} = \delta_{pp'}\delta_{hh'}(\varepsilon_p - \varepsilon_h) + \langle ph^{-1}|\frac{\delta h}{\delta\rho}|p'h'^{-1}\rangle, \tag{4.21}$$

and introducing the notation X_{ph} for the matrix elements $\langle ph^{-1}|\delta\rho|0\rangle$, we can write the set of TDA equations (4.20) in a matrix form:

$$AX = \hbar\omega X. \tag{4.22}$$

The meaning of the TDA equations is quite straightforward. $\hbar\omega$ is the eigenvalue associated with a given vibrational mode. The first term of the matrix element A in (4.21) is diagonal, and just expresses the fact that such eigenvalues would correspond to the unperturbed p-h energy differences $\varepsilon_p - \varepsilon_h$ in absence of any interaction. The second term of the matrix elements A couples such p-h excitations with one another, and provides eigenstates that are mixed. It is easy to demonstrate that in simple cases (interactions V without density dependence) the matrix element of $\frac{\delta h}{\delta\rho}$ is just the antisymmetrized matrix element of the potential V. X_{ph} represents the amplitude, in the eigenmode, that is associated with the specific configuration $|ph^{-1}\rangle$. We may like to call collective those states in which several, or many, amplitudes X_{ph} are non negligible. However, the schematic model discussed in the following Section will be quite instrumental in showing that the relative phase

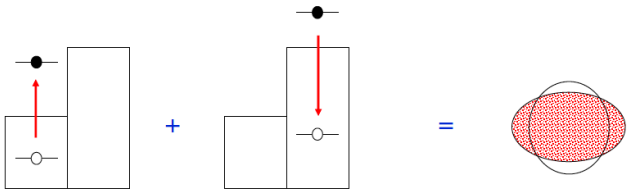

Figure 4.4: Schematic representation of the linear response equation.

of such amplitudes also matters. Fig. 4.4 is a cartoon of the TDA equations if the second term in the sum of the l.h.s. is neglected.

A more sophisticated theory considers the possibility that the ground-state is more general that the HF one. In other words, p-h pairs may be present in a more exact ground-state. Then, the linear response formalism can include the possibility that the p-h pairs are annihilated. In this case, the completeness relation becomes:

$$|0\rangle\langle 0| + \sum_{p'h'} |p'h'^{-1}\rangle\langle p'h'^{-1}| + |h'p'^{-1}\rangle\langle h'p'^{-1}| = 1. \tag{4.23}$$

If we include the states of the type $|hp^{-1}\rangle$ in the basis, the derivation becomes less straighforward and will be omitted here. We just quote the final result, which is, in matrix form,

$$\begin{pmatrix} A & B \\ -B^* & -A^* \end{pmatrix} \begin{pmatrix} X \\ Y \end{pmatrix} = \hbar\omega \begin{pmatrix} X \\ Y \end{pmatrix}. \tag{4.24}$$

This is called Random Phase Approximation (RPA) equation. In it,

$$B_{ph,p'h'} = \langle ph^{-1}|\frac{\delta h}{\delta \rho}|h'p'^{-1}\rangle, \tag{4.25}$$

while Y_{ph} is the amplitude of $|hp^{-1}\rangle$ in the eigenmode, that is, $\langle hp^{-1}|\delta\rho|0\rangle$. In Fig. 4.4, the complete linear response, namely the RPA equation, is schematically depicted. The second term in the sum at the l.h.s. corresponds precisely to the annihilation of virtual p-h pairs that are present in the ground-state.

4.4 Solution of the TDA equations in a schematic model

We consider, as a simple model for e.g. the IVGDR, a schematic form for the TDA matrix. We assume that we have N degenerate p-h excitations: in the IVGDR case for a magic nucleus, this corresponds to consider holes in the highest occupied shell, particles in the lowest unoccupied shell, and p-h energy differences all degenerate and equal to ε [according to Eq. (2.14), ε will be $1\hbar\omega \approx 41\ \mathrm{A}^{-1/3}$; the left side of Fig. 4.5 may be considered for the sake of better clarity]. We also take the matrix elements that appear in A all constant and equal to v, so that the TDA matrix becomes:

$$\begin{pmatrix} \varepsilon+v & v & \dots & v \\ v & \varepsilon+v & \dots & v \\ \dots & & & \dots \\ v & v & \dots & \varepsilon+v \end{pmatrix}. \tag{4.26}$$

Such simple model is exactly solvable.

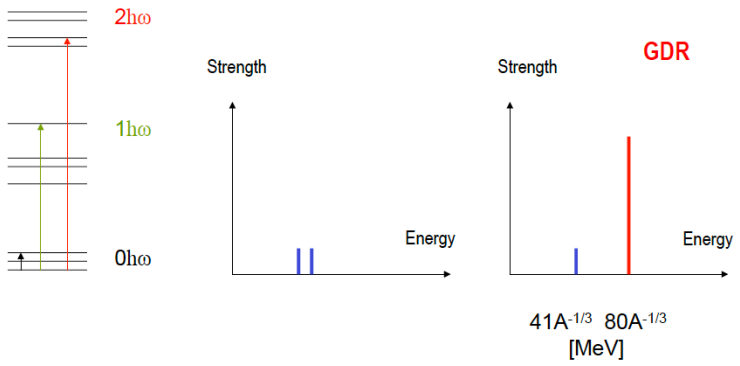

Figure 4.5: The emergence of the IVGDR in the schematic TDA model. See the text for the discussion.

In the two by two case the matrix reads

$$\begin{pmatrix} \varepsilon+v & v \\ v & \varepsilon+v \end{pmatrix}, \tag{4.27}$$

and the eigenvalues and eigenvectors are

$$\begin{aligned} \hbar\omega &= \varepsilon, \qquad X = \frac{1}{\sqrt{2}} \begin{pmatrix} 1 \\ -1 \end{pmatrix}, \\ \hbar\omega &= \varepsilon + v \qquad X = \frac{1}{\sqrt{2}} \begin{pmatrix} 1 \\ 1 \end{pmatrix}. \end{aligned} \tag{4.28}$$

We may call the first state as "incoherent" because the two amplitudes are in opposition of phase while the second state may be said to be "coherent". The meaning of this label becomes more transparent if we calculate the the matrix element associated with the operator $\hat{F}$ as defined in Eq. (4.4), by assuming that the X amplitudes are real:

$$\langle n|\hat{F}|0\rangle = \sum_{ph} X_{ph} \langle ph^{-1}|\hat{F}|0\rangle. \tag{4.29}$$

Around the Fermi surface, we expect that the matrix elements $\langle p|\hat{F}|h\rangle$ of a one-body operator are quite similar and can be approximated by a constant number M. This depends of course on the choice of the operator. For an electric or magnetic operator one expects to find these matrix elements are of the order of one Weisskopf, or single-particle, unit: we will discuss this in Chapter 6. Then, if one considers the "incoherent" state, the transition amplitude associated with $\hat{F}$ vanishes. Its value is instead increased by a factor $\sqrt{2}$ with respect to the single-particle value M in the "coherent" case.

The matrix equation (4.26) can be solved in the general case with N p-h transitions. In that case, one finds there is only one coherent mode, having eigenvalue $\varepsilon + Nv$ and the corresponding eigenvector of the type

$$\frac{1}{\sqrt{N}} \begin{pmatrix} 1 \\ 1 \\ \cdots \\ 1 \end{pmatrix}. \tag{4.30}$$

The transition amplitude associated with this state reads

$$\langle n|\hat{F}|0\rangle = \sum_{ph} X_{ph} \langle p|\hat{F}|h\rangle \approx N \frac{1}{\sqrt{N}} M = \sqrt{N}\ M. \tag{4.31}$$

Then, the quantity associated to the transition probability is the square of the latter equation, as we have discussed already in the previous Section:

$$|\langle n|\hat{F}|0\rangle|^2 = N\ M^2. \tag{4.32}$$

In the case of the IVGDR, we can imagine that the term Nv in the eigenvalue brings the excitation energy from the "unperturbed" value around 41 $A^{-1/3}$ to the value 80 $A^{-1/3}$ already mentioned in Eq. (4.3). The fact that this is a "giant" state stems from the last Eq. (4.32): its probability to be excited is N times larger the probability of a single-particle state. The situation is depicted in Fig. 4.5.

Chapter 5

Nuclear deformation and collective rotations

5.1 Introduction to nuclear shapes

The usual way to parametrize the nuclear shapes, when they deviate from sphericity, is to define the radius as

$$R(\theta,\phi) = R_0 \left[1 + \sum_{\lambda\mu} \alpha_{\lambda\mu} Y^*_{\lambda\mu}(\theta,\phi) \right], \tag{5.1}$$

in keeping with the fact that the spherical harmonics form a complete set of scalar functions on a spherical surface. The parameters $\alpha_{\lambda\mu}$ are complex numbers, and they will be taken as small in what follows, in the sense that $|\alpha_{\lambda\mu}|^2 \ll |\alpha_{\lambda\mu}|$. The radius must be obviously a real quantity, and since $Y^*_{\lambda\mu} = (-1)^\mu Y_{\lambda\ -\mu}$ the same relation must hold for the coefficients α.

In keeping with Eq. (5.1), one can easily imagine a nucleus characterised by a deformed mean-field that generalises, for instance, the Woods-Saxon potential of Eq. (2.3):

$$U(\mathbf{r}) = \frac{-U_0}{1 + e^{\frac{r - R(\theta,\phi)}{a}}} \tag{5.2}$$

[the diffuseness a may also have a mild dependence on angles, and be actually $a(\theta,\phi)$].

We shall describe deformations that do not change the nuclear volume. We exclude the term $\lambda = 0$ from the sum in Eq. (5.1) to this aim, because

$Y_{00}^* = \frac{1}{\sqrt{4\pi}}$ is a constant and the volume changes unless α_{00} vanishes. We actually need to exclude the terms with $\lambda = 1$ as well, the reason being that such terms describe a mere translation of the system[1].

Then, the sum starts from $\lambda = 2$ in Eq. (5.1). The volume of the system is

$$\begin{aligned}
&\int d\Omega \int_0^{R(\theta,\phi)} dR\ R^2 = \int d\Omega\ \frac{R_0^3}{3}\left(1 + \sum_{\lambda\geq 2,\mu} \alpha_{\lambda\mu} Y_{\lambda\mu}^*(\theta,\phi)\right)^3 = \\
&\approx \int d\Omega\ \frac{R_0^3}{3}\left(1 + 3\sum_{\lambda,\mu,\lambda',\mu'} \alpha_{\lambda\mu} Y_{\lambda\mu}^*(\theta,\phi)\alpha_{\lambda'\mu'} Y_{\lambda'\mu'}^*(\theta,\phi)\right) = \\
&= \int d\Omega\ \frac{R_0^3}{3}\left(1 + 3\sum_{\lambda,\mu,\lambda',\mu'} \alpha_{\lambda\mu} Y_{\lambda\mu}^*(\theta,\phi)\alpha_{\lambda'\mu'}^* Y_{\lambda'\mu'}(\theta,\phi)\right) = \\
&= \frac{4}{3}\pi R_0^3\left(1 + \frac{3}{4\pi}\sum_{\lambda\mu} |\alpha_{\lambda\mu}|^2\right). \qquad (5.3)
\end{aligned}$$

Ω is here a shorthand notation for the solid angle defined by θ and ϕ. In the second equality we have stopped at the lowest order in the parameters α. We have then used the relationship of α and Y with the complex conjugate quantities, and also the orthonormality of the spherical harmonics,

$$\int d\Omega\ Y_{\lambda\mu}^*(\theta,\phi) Y_{\lambda'\mu'}(\theta,\phi) = \delta(\lambda,\lambda')\delta(\mu,\mu').$$

The result of Eq. (5.3) shows that if we neglect the square of the parameters $\alpha_{\lambda\mu}$ the volume is unchanged.

Although there is active research and evidence of octupole deformation [41], static quadrupole deformation is more widespread in the isotope chart and more well established. We shall limit ourselves to the treatment of quadrupole, and consider

$$R(\theta,\phi) = R_0\left[1 + \sum_{\mu=-2}^{2} \alpha_{2\mu} Y_{2\mu}^*(\theta,\phi)\right]. \qquad (5.4)$$

[1] One can show this with elementary geometry, in the case at hand in which $|\alpha_{\lambda\mu}|^2 \ll |\alpha_{\lambda\mu}|$.

5.2 Intrinsic shape and orientation

The goal of this Section is to introduce some concepts that are widely used when discussing quadrupole deformation, and in particular the difference between a given shape and a given orientation of the nucleus.

We define two coordinate systems, the intrinisic one O' and the laboratory one O. The intrinisic system or intrinsic frame is defined in the following way: given a matter distribution that is approximately constant within the volume defined by the radius (5.4), we can diagonalize the associated tensor of inertia, and identify the intrinsic system as the one in which the tensor of inertia is diagonal. The tensor of inertia is proportional to α_{ij} (the indices assume the values x, y, z). α_{ij} are the weights in front of the terms $x_i x_j$ in the expansion (5.4), when this latter is written in cartesian coordinates. We avoid the straightforward steps associated with this transformation and we just give the main idea.

It is possible to write Eq. (5.4) in cartesian coordinates as

$$R = R_0 \left(1 + \alpha_{xx}\frac{x^2}{r^2} + \ldots + \alpha_{xy}\frac{xy}{r^2} + \ldots\right). \tag{5.5}$$

To accomplish this, one uses the well known coordinate transformations that allow expressing the spherical harmonics in cartesian coordinates, like

$$Y_{20} = \frac{1}{4}\sqrt{\frac{5}{\pi}}(3cos^2\theta - 1) = \frac{1}{4}\sqrt{\frac{5}{\pi}}\frac{2z^2 - x^2 - y^2}{r^2},$$

and similar ones that can be found in standard textbooks. Once Eq. (5.4) is written in cartesian coordinates, one can identify the coefficients that appear in Eq. (5.5). The result reads

$$\begin{aligned}
\alpha_{\pm 2} &= \sqrt{\frac{2\pi}{15}}(\alpha_{xx} - \alpha_{yy} \pm 2i\alpha_{xy}), \\
\alpha_{\pm 1} &= \mp 2\sqrt{\frac{2\pi}{15}}(\alpha_{xz} \pm i\alpha_{yz}), \\
\alpha_0 &= \sqrt{\frac{\pi}{5}}\frac{2}{3}(\alpha_{zz} - \alpha_{xx} - \alpha_{yy}).
\end{aligned} \tag{5.6}$$

We will label as a instead of α the coefficients in the intrinisic frame. In the intrinsic frame $a_{xy} = a_{xz} = a_{yz} = 0$, and from the latter equation:

$$a_{\pm 1} = 0, \qquad a_{-2} = a_2. \tag{5.7}$$

Theferore, in the intrinsic frame there are only two independent parameters that define the shape. These are usually expressed in terms of β and γ defined by

$$a_0 = \beta cos\gamma, \qquad a_2 = \frac{\beta}{\sqrt{2}} sin\gamma. \tag{5.8}$$

The laboratory system O is rotated with respect to O'. The rotation that brings O into O', as any rotation in three dimensions, can be written in terms of the three Euler angles[2] $\{\phi, \theta, \psi\}$ that are denoted collectively as Ω (although we use the same notation, one should not mix up the Euler angles with the polar angles θ, ϕ in the frame O). The relationship between the spherical harmonics in the two systems read

$$Y_{\lambda\mu}(\theta', \phi') = \sum_{\mu'} \mathcal{D}^{(\lambda)}_{\mu'\mu}(\Omega) Y_{\lambda\mu'}(\theta, \phi), \tag{5.9}$$

where $\mathcal{D}$ are the Wigner D-functions. Note that we do not need the explicit expression of these functions for what follows. The three Euler angles and the parameters β and γ are equivalent to the five parameters $\alpha_{2\mu}$: there are five degrees of freedom associated with the quadrupole deformation but in the intrinsic frame we better understand that two of them are actually related to the nuclear shape, while the remaining three depend only on the orientation.

In summary, in the intrinsic frame we can write

$$R(\theta', \phi') = R_0 \left[1 + a_0 Y_{20}(\theta', \phi') + 2a_2 Y_{22}(\theta', \phi')\right], \tag{5.10}$$

in keeping with the fact that Y_{20} and $Y_{2-2} = Y_{22}$ are real. We shall drop the prime superscript on the angles, in what follows, for the sake of simplicity. It is now easy to plug both the definition (5.8) and the explicit form of the spherical harmonics into Eq. (5.10). The explicit result reads

$$R(\theta, \phi) = R_0 \left\{ 1 + \sqrt{\frac{5}{16\pi}} \beta \left[cos\gamma \ (3cos^2\theta - 1) + \sqrt{3} sin\gamma \ sin^2\theta \ (cos^2\phi - sin^2\phi) \right] \right\}. \tag{5.11}$$

Specific expressions can be easily found that define the variation $\delta R \equiv R - R_0$

[2]The definition of Euler angles can be found in standard textbooks.

along the three principal axes,

$$\begin{aligned}
\delta R_x &= \sqrt{\frac{5}{4\pi}}\beta R_0 cos(\gamma - \frac{2\pi}{3}), \\
\delta R_y &= \sqrt{\frac{5}{4\pi}}\beta R_0 cos(\gamma + \frac{2\pi}{3}), \\
\delta R_z &= \sqrt{\frac{5}{4\pi}}\beta R_0 cos\gamma. \qquad (5.12)
\end{aligned}$$

In the case $\gamma = 0$, one finds that $\delta R_x = \delta R_y < 0$ while $\delta R_z > 0$, if $\beta > 0$. The nucleus is *axially symmetric* (z is the symmetry axis) and *prolate* (it is elongated along the symmetry axis and shrinked on the perpendicular plane). One can easily see that when γ deviates from 0 one has *triaxial shapes*, that is, shapes that are not characterised by a symmetry axis. When γ reaches the value $\pi/3$, and still $\beta > 0$, one can deduce again from Eq. (5.12) that $\delta R_x = \delta R_z > 0$ and $\delta R_y < 0$. This shape is still axially symmetric (this time, y is the symmetry axis) but it is shrinked around this symmetry axis and enlarged on the perpendicular plane. Such form is said to be *oblate*. Values of γ outside the interval $(0, \pi/3)$ can be shown to produce the same shapes.

In short, based on Eq. (5.12) and simple trigonometry, the interval $\beta > 0$ and $0 < \gamma < \pi/3$ can be shown to be sufficient to describe all intrinsic quadrupole shapes. The situation is schematically depicted in Fig. 5.1.

5.3 Rotational bands of an axial even-even nucleus

Deformed nuclei can rotate. We can start by making the adiabatic hypothesis, in which the rotational motion and the intrinsic motion of the nucleons within the range of the deformed potential take place on different time scales and are decoupled. This hypohesis is well fulfilled in the case of many medium-heavy nuclei, where the low-lying rotational states are in the ≈10-100 keV range while the nucleon motion, as we have seen, is characterised by energies which are about two orders of magnitude larger (that is, associated time scales are two orders or magnitude smaller).

Within the adiabatic hypothesis, the Hamiltonian can thus be written as a sum

$$H = H_{\rm coll} + H_{\rm intr}. \qquad (5.13)$$

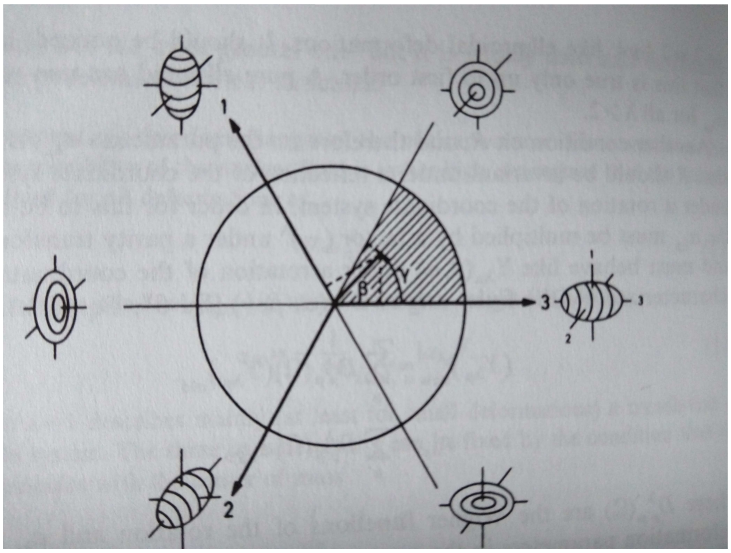

Figure 5.1: Schematic view of the nuclear shapes, taken from P. Ring and P. Schuck [42].

The collective Hamiltonian depends only on the coordinates of the rotation of the nucleus as a whole, that is, the three Euler angles Ω that describe the orientation of the intrinsic system with respect to the laboratory system. The intrinisic Hamiltonian depends instead on the coordinates of the nucleons in the intrinsic system, $\mathbf{r'_1} \ldots \mathbf{r'_A}$. In the adiabatic hypothesis, the wave function factorizes

$$\Psi = \mathcal{D}^I_{KM}(\Omega)\chi_K(\mathbf{r'_1} \ldots \mathbf{r'_A}). \tag{5.14}$$

We now discuss the meaning of the labels we have put, that ought to correspond to the good quantum numbers of the system. We shall call $\vec{J}$ the angular momentum associated with the intrinsic degrees of freedom. If the system is not spherical but has a rotational symmetry around z', the component of the angular momentum around z' is conserved: its eigenvalue is a good quantum number and we shall label it as Ω. We call $\vec{R}$ the angular momentum associated with the collective rotation, and $\vec{I}$ the total angular momentum, $\vec{I} = \vec{J} + \vec{R}$. The projections of this total angular momentum are also conserved. They are called respectively M (projection on z) and K (projection on z')[3]. In the specific case of an axially symmetric nucleus

[3]This statement follows from the fact that the square of the total angular momentum I^2 commutes both with its z and z' projections. We omit here the formal proof of this

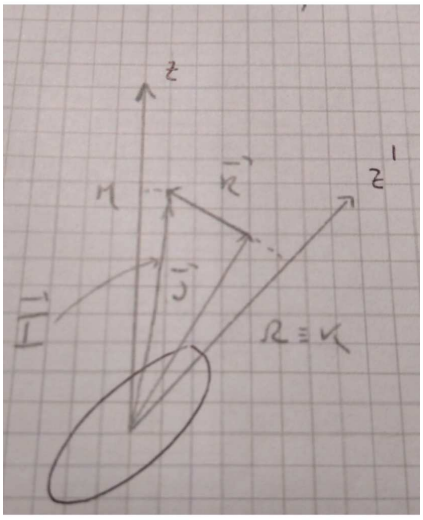

Figure 5.2: Schematic view of an axially deformed nucleus that rotates around an axis which is perpendicular to the intrinsic symmetry axis z'.

the rotation must take place around an axis whih is perpendicular to the symmetry axis z'. Therefore, $R_{z'} = 0$ and K coincides with Ω. We shall restrict to this case and use K from now on. Fig. 5.2 depicts the quantities we have just defined.

The intrinisc wave function can, of course, only depend on K. The collective wave function $\mathcal{D}$ must be a Wigner function because mathematically it can be proven that, if O' is rotated by an angle Ω with respect to O, then

$$\begin{aligned} \hat{I}^2\ \mathcal{D}^I_{KM}(\Omega) &= I(I+1)\mathcal{D}^I_{KM}, \\ \hat{I}_z\ \mathcal{D}^I_{KM}(\Omega) &= M\mathcal{D}^I_{KM}, \\ \hat{I}_{z'}\ \mathcal{D}^I_{KM}(\Omega) &= K\mathcal{D}^I_{KM}. \end{aligned}$$

In other words, these functions are eigenfunctions of the total angular momentum and of its z and z' components. If we consider another mathematical property of the Wigner functions,

$$\int d\Omega\ \mathcal{D}^{j_1 *}_{m'_1 m_1}(\Omega)\mathcal{D}^{j_2}_{m'_2 m_2}(\Omega) = \frac{8\pi^2}{2j_1+1}\delta(j_1,j_2)\delta(m_1,m_2)\delta(m'_1,m'_2),$$

we can easily infer that, if χ_K is normalized, the normalization factor of the wave function (5.14) is $\sqrt{\frac{2I+1}{8\pi^2}}$.

statement (the interested reader can consult e.g. Appendix A of [42]).

Let us now assume that the nucleus has one more symmetry, that is, it is unchanged under a rotation of π around an axis perpendicular to z', say y'. Since it can be shown that

$$\hat{R}_{y'}(\pi)\left[\mathcal{D}^I_{KM}(\Omega)\chi_K(\mathbf{r_1}'\ldots\mathbf{r_A}')\right] = (-)^{I+K}D^I_{-KM}(\Omega)\chi_{-K}(\mathbf{r_1}'\ldots\mathbf{r_A}'),$$

then the proper way to generalise Eq. (5.14) so that this symmetry is preserved reads

$$\psi_{IKM} = \sqrt{\frac{2I+1}{16\pi^2}(1+\delta_{K0})}\left[\mathcal{D}^I_{KM}(\Omega)\chi_K(\mathbf{r_1}'\ldots\mathbf{r_A}') + (-)^{I+K}\mathcal{D}^I_{-KM}\chi_{-K}(\mathbf{r_1}'\ldots\mathbf{r_A}')\right]. \tag{5.15}$$

If $K=0$ in the ground-state configuration, Eq. (5.15) shows that I must be even. Then, we expect that the *ground-state* rotational band is composed by states having $I^\pi = 0^+, 2^+, 4^+\ldots$ These states have energies

$$E_I = \frac{\hbar^2}{2\mathcal{I}}I(I+1), \tag{5.16}$$

that is, they form the typical rotational spectrum that has been introduced in the last Chapter. From the measurements of the energies of the γ transitions, we can reconstruct such spectrum and (i) verify if it respects the scaling as in (5.16), but also (ii) extract values of the moments of inertia. In most of the nuclei with mass between ≈ 150 and ≈ 190, and mass larger than ≈ 220 we find very regular rotational bands extending to high values of the angular momentum I. An example is shown in Fig. 5.3.

5.4 Electromagnetic transitions and exctraction of the intrinisic β

Not only the energies, but the electromagnetic transition probabilities among members of a rotational band can be measured. In the case that we have discussed in some detail, when the states have $I^\pi = 0^+, 2^+, 4^+\ldots$, the transitions[4] are electric quadrupole ones, E2.

[4]We assume some familiarity with the definition of electromagnetic multipole moments and transitions, the associated reduced transition probability B and, possibly, the values of the single-particle units (at least for the electric transitions). If the reader does not feel confident at least about the basics of the subject, reading of the next Chapter before this one is recommended.

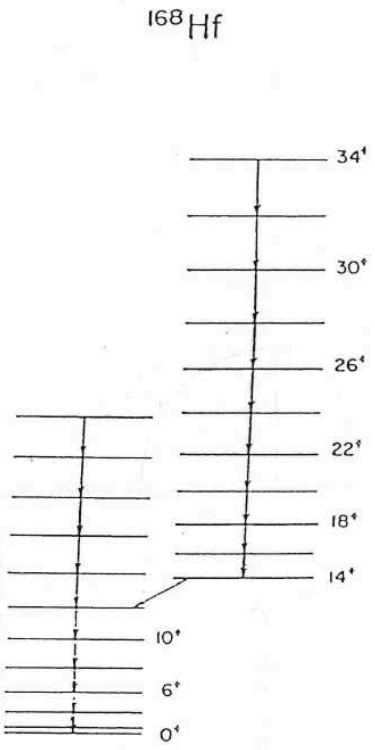

Figure 5.3: Rotational spectrum of the nucleus ^{168}Hf. The ground-state band that we have discussed in the text is evident, and extends to high values of the angumar momentum I. A rotational band based on a different intrinsic configuration χ_K appears as a "side band".

The reduced transition probability $B(E2)$ beween a state with initial (final) angular momentum I_i (I_f) reads

$$B(E2, I_i \rightarrow I_f) = \frac{1}{2I_i + 1} \sum_{M_i M_f} |\langle I_f M_f | \hat{Q}_{2\mu} | I_i M_i \rangle|^2, \tag{5.17}$$

where the quadrupole operator can be written explicity as $\sum_i e_i r_i^2 Y_{2\mu}(\hat{r}_i)$, and the sum runs over nucleons. This operator is obviously defined in the laboratory frame O where the photon is detected but can be transformed in the intrinsic frame. We have learnt in this Chapter that the spherical harmonics, as any tensor carrying good angular momentum, can be transformed from one frame to another by using the Wigner functions. Then,

$$\hat{Q}_{2\mu} = \sum_{\nu} \mathcal{D}^2_{\nu\mu}(\Omega) \hat{Q}^{\rm intr}_{2\nu}, \tag{5.18}$$

and, by sticking to the case $K = 0$ and reading the wave functions from

(5.15),

$$\langle I_f M_f|\hat{Q}_{2\mu}|I_i M_i\rangle = \frac{\sqrt{(2I_i+1)(2I_f+1)}}{8\pi^2}\sum_\nu \int d\Omega\, \mathcal{D}^{I_f *}_{0M_f}(\Omega)\mathcal{D}^2_{\nu\mu}(\Omega)\mathcal{D}^{I_i}_{0M_i}(\Omega)\,\langle\chi_0|\hat{Q}^{\rm intr}_{2\nu}|\chi_0\rangle, \tag{5.19}$$

where the bra and ket notation refers to the integral on the intrinsic coordinates $\vec{r}'_1 \ldots \vec{r}'_A$ (on which the intrinsic wave functions χ and the intrinisic operator $\hat{Q}^{\rm intr}$ depend). The integral over the Wigner functions that appear in the latter equation is known, since

$$\int d\Omega\, \mathcal{D}^{j_3 *}_{\mu_3 m_3}\mathcal{D}^{j_2}_{\mu_2 m_2}\mathcal{D}^{j_1}_{\mu_1 m_1} = \frac{8\pi^2}{2j_3+1}\langle j_1 m_1 j_2 m_2|j_3 m_3\rangle\langle j_1\mu_1 j_2\mu_2|j_3\mu_3\rangle.$$

Thus, the matrix elements (5.19) becomes

$$\langle I_f M_f|\hat{Q}_{2\mu}|I_i M_i\rangle = \sqrt{\frac{2I_1+1}{2I_f+1}}\langle I_i M_i 2\mu|I_f M_f\rangle\langle I_i 020|I_f 0\rangle\langle\chi_0|\hat{Q}^{\rm intr}_{\nu=0}|\chi_0\rangle. \tag{5.20}$$

The second Clebsch-Gordan coefficients in this equation implies that ν must vanish[5]. Then, the value of the reduced transition probability reads

$$\begin{aligned} B(E2, I_i \rightarrow I_f) &= \frac{1}{2I_i+1}|\langle\chi_0|\hat{Q}^{\rm intr}_{20}|\chi_0\rangle|^2\frac{(2I_i+1)\langle I_i 020|I_f 0\rangle^2}{(2I_f+1)}\sum_{M_i M_f}\langle I_i M_i 2\mu|I_f M_f\rangle^2 \\ &= \langle I_i 020|I_f 0\rangle^2|\langle\chi_0|\hat{Q}^{\rm intr}_{20}|\chi_0\rangle|^2. \end{aligned} \tag{5.21}$$

This equation expresses the very remarkable result that in a rotational band all transitions depend on a quantity which is related to the square of the intrinsic quadrupole moment, and the dependence on the specific initial and final states is a geometric, universal one - i.e. associated with the square of a Clebsch-Gordan coefficient.

We now show how the common quantity appearing in all reduced transition probability, the aforementioned intrinsic quadrupole moment, is related to β. We start from Eq. (5.11) restricted to $\gamma = 0$:

$$R(\theta) = R_0\left[1 + \sqrt{\frac{5}{16\pi}}\beta\left(3cos^2\theta - 1\right)\right]. \tag{5.22}$$

[5]We remind that for every non-zero coefficient $\langle j_1 m_1 j_2 m_2|j_3 m_3\rangle$, the equality $m_1 + m_2 = m_3$ must hold.

We assume that this is the radius associated both with the mass and charge distribution. The charge can be assumed to be uniform within the volume defined by $R(\theta)$. We have shown in the first part of this Chapter [cf. Eq. (5.3)] that at the lowest order in β the volume is conserved, so that

$$\rho_{\rm charge} = \frac{Z}{\frac{4}{3}\pi R_0^3}. \tag{5.23}$$

If we replace the square of the intrinsic wave function $|\chi|^2$ with the intrinisic density distribution, we obtain

$$\begin{aligned}
\langle\chi_0|\hat{Q}_{20}^{\rm intr}|\chi_0\rangle &= \int d^3r\ e\rho_{\rm charge} r^2 Y_{20} = \frac{3Ze}{16\pi R_0^3} 2\pi\sqrt{\frac{5}{\pi}} \int_{-1}^{+1} d\mu\ (3\mu^2-1) \int_0^{R(\theta)} dr\ r^4 \\
&= \frac{3Ze}{8R_0^3}\sqrt{\frac{5}{\pi}}\ \int_{-1}^{+1} d\mu\ (3\mu^2-1)\frac{R_0^5}{5}\left[1+\frac{5}{4}\sqrt{\frac{5}{\pi}}\beta(3\mu^2-1)+\dots\right] = \\
&= \frac{3ZeR_0^2}{4\pi}\beta+\dots\ ,
\end{aligned} \tag{5.24}$$

where in the second step we have used the definition of

$$Y_{20} = \frac{1}{4}\sqrt{\frac{5}{\pi}}(3cos^2\theta - 1)$$

that has been given previously, and we have defined $\mu = cos\theta$. In the following steps we have kept only the term at lowest order in β by marking the missing ones with dots. If β is small, and the approximation is meaningful, we find, by replacing the latter result (5.24) in Eq. (5.21):

$$B(E2, I_i\ \rightarrow\ I_f) = \langle I_i 020|I_f 0\rangle^2 \left(\frac{3ZeR_0^2}{4\pi}\right)^2 \beta^2. \tag{5.25}$$

In conclusion, the measurement of the reduced transition probability gives access to β^2.

It should be noted that other experimental techniques can provide values of β like, for instance, laser atomic spectroscopy. In this case, the measurement of hyperfine atomic transitions provide an indication of how the nuclear Coulomb field felt by the atomic electrons is different from a spherical one.

5.5 Moments of inertia

If the value of β can be extracted from Eq. (5.25), and the value of the moment of inertia is known from the energies of the rotational spectrum, one can ask oneself the question whether the rotation has a rigid-body character. By assuming a mass distribution which is again uniform within the radius defined by Eq. (5.22), namely $\rho_{\rm mass} = 3mA/4\pi R_0^3$, we can calculate the so-called rigid-body moment of inertia. In the case of an axially symmetric nucleus the rotation is around an axis perpendicular to the symmetry axis z', like x' or y'. Of course, $\mathcal{I}_{x'} = \mathcal{I}_{y'} = \mathcal{I}$. The moment of inertia can be evaluated with a similar calculation as the one which led us to the intrinsic quadrupole moment in Eq. (5.24), and the result is

$$\mathcal{I} = \frac{2}{5} mAR_0^2 \left(1 + \frac{1}{2}\sqrt{\frac{5}{4\pi}}\beta\right). \tag{5.26}$$

With the values of β extracted as discussed in the last Section, one obtains moment of inertia that are about a factor 2 larger than experiment.

Superfluidity makes this value smaller than the rigid-body value. This can be intuitively understood, as a superfluid portion can translate and rotate without contributing to the overall inertia of the system. Detailed microscopic calculations confirm this intuition.

5.6 Motion of a particle in a deformed potential: simple features

A simple model that describes the changes that the single-particle states undergo, when changing a spherical into a deformed shape, is that of the deformed harmonic oscillator. If ω_0 is the typical frequency that mimics the nuclear case, namely $\hbar\omega_0 \approx 41 \mathrm{A}^{-1/3}$ [cf. Eq. (2.14)], in an axially deformed nucleus we can assume that we have different frequencies along the symmetry axis z' (ω_z) and along the two perpendicular axes x' and y' ($\omega_\perp$). Thus, we can write

$$H = -\frac{\hbar^2}{2m}\nabla^2 + \frac{1}{2}m\left[\omega_\perp^2\left(x^2+y^2\right) + \omega_z^2 z^2\right]. \tag{5.27}$$

The conservation of the volume can be expressed by the condition

$$\omega_\perp^2 \omega_z = \omega_0^3, \tag{5.28}$$

and one can easily verify that this condition is fulfilled by

$$\omega_z = \omega_0 \left(1 - \frac{2}{3}\epsilon\right), \qquad \omega_\perp = \omega_0 \left(1 + \frac{1}{3}\epsilon\right) \tag{5.29}$$

at lowest order in ϵ, that is, by neglecting terms of the order ϵ^2. The simple model of Eq. (5.27) can be improved by adding a spin-orbit term, and empirical terms that make it more similar to the Woods-Saxon shape. When these terms are added, one has the so-called Nilsson model.

We can rewrite Eq. (5.27) as

$$\begin{aligned} H &= H_0 + \epsilon H_1 \\ H_0 &= -\frac{\hbar^2}{2m}\nabla^2 + \frac{1}{2}m\omega_0^2 r^2 \\ \epsilon H_1 &= \frac{1}{3}m\omega_0^2\epsilon\left(x^2 + y^2 - 2z^2\right) = -\frac{1}{3}\sqrt{\frac{16\pi}{5}}m\omega_0^2\epsilon r^2 Y_{20}, \end{aligned} \tag{5.30}$$

where in the last step we have used the definition of Y_{20} that has been often employed in this Chapter. If the deformation is small, and ϵ is a small parameter, the effect of H_1 can be treated within first-order perturbation theory. The levels that are degenerate under the spherical assumption undergo a splitting that can be calculated in the usual way:

$$\begin{aligned} \Delta\varepsilon_{nljm} &\equiv \langle nljm|\epsilon H_1|nljm\rangle \\ &= -\frac{1}{3}\sqrt{\frac{16\pi}{5}}\epsilon m\omega_0^2 \int dr\ r^2 u_{nlj}^2(r)\langle ljm|Y_{20}|ljm\rangle \\ &= \frac{1}{3}\frac{\epsilon}{2}m\omega_0^2 \int dr\ r^2 u_{nlj}^2(r)\frac{3m^2 - j(j+1)}{j(j+1)}, \end{aligned} \tag{5.31}$$

where in the last step we have used some standard formula[6] to calculate the expectation value of Y_{20} over a wave function of the type (2.7).

The latter expression (5.31) predicts that states with $\pm m$ remain degenerate, as it can be expected in the case of the symmetry at hand where the nucleus is invariant when z' is reversed; moreover, at least for large j, the states with the maximum projection $m = \pm j$ are shifted up while the states with minimum projection $m = \pm 1/2$ are shifted down. This is understandable in semiclassical terms: the wave function should be concentrated

[6]It can be found in any textbook on angular momentum and spherical tensors, but also in the appendices of nuclear structure textbooks.

in the plane perpendicular to the angular momentum and therefore in the case of maximum (minimum) projection over z' it is mainly in the plane $x'y'$ (along the z' axis) which is the region where the potential shrinks (becomes shallower).

There is another case that can be solved exactly, that is, the case of extremely large deformation in which one can assume a harmonic oscillator with cylindrical symmetry around the z' axis. Although the realistic cases are in between the two limits of the small and large deformations, the labels associated with the cylindrical symmetry (large deformation) are often used in the literature.

The exact quantum numbers that are valid for any value of ϵ are the projection of the total angular momentum on the z' axis (the quantity Ω of the above discussion) and the parity π. The quantum numbers that are valid in cylindrical symmetry but only asymptotically valid (for large ϵ) in the case at hand can be shown to be: the principal quantum number of the harmonic oscillator N, the quantity associated with the number of nodes in the z' direction n_z (the number of nodes is $n_z - 1$), and the projection over z' of the orbital angular momentum Λ. In cylindrical symmetry the relation

$$N = n_z + 2n_r + \Lambda \tag{5.32}$$

holds, where n_r is the quantity associated with the number of nodes in the radial direction (the number of nodes is $n_r - 1$).

The notation

$$\Omega^{\pi}\left[N, n_z, \Lambda\right]$$

is used with the aim of distinguishing the exact quantum numbers from the approximate ones (in square brackets). In reality, one solves the Hartree-Fock or BCS equations without assuming any symmetry. The nucleons find the arrangement that allows them to occupy states that are as lowest as possible in energy, that is, in order to minimise the total energy. In many instances, deformed solutions arise. These usually correspond to the cases in which both protons and neutrons have open shells.

Chapter 6

Electromagnetic moments and transitions

In the previous Chapter, we have already made use of the concepts of quadrupole electromagnetic operator and associated reduced transition probability. Although the reader may have already encountered these concepts in an introductory nuclear physics course, we deem it useful to present, in this Chapter, a concise review of the basic notions associated with electromagnetic static moments and transitions. In particular, the goal is to provide the students with the proper definition of: electric and magnetic multipole transitions, the associated operators in the long-wavelength limit and, eventually, their relevant matrix elements.

Expectation values of these operators on the nuclear ground state correspond to the electromagnetic nuclear moments. Electric quadrupole moments lie at the basis of the discussion in the previous Chapter; however, electric octupole and magnetic dipole moments play also an important role in low-energy nuclear physics.

Transition matrix elements of the electromagnetic operators are also of paramount importance. We have already mentioned them, and in general they always appear when discussing vibrational and rotational states. In this Chapter, we will introduce the typical values of the transition matrix elements associated with single-particle transitions, that is, the so-called single-particle units. We will give some ground, then, to the idea that there exist collective vibrational and rotational states: in this Chapter, collective states will emerge as the excited states whose transition matrix elements are much larger than the single-particle ones.

By means of this discussion, some other concepts (e.g., the lifetime of the excited states) will be also highlighted. On the other hand, we will not cover all possible aspects related to electromagnetic moments and transitions. In particular, we will restrict ourselves to the realm of nuclear structure and refrain from giving any connection with the physics of the nucleons (or hadrons). Nucleons will be taken, as in the rest of this textbook, as point-like nonrelativistic particles. Protons will be characterised by their electric charge, and protons and neutrons also by their internal spin. The internal structure of these particles will not be considered.

6.1 Multipole expansion of the electromagnetic interaction

The electromagnetic scalar and vector potentials[1] $(V, \mathbf{A})$ are often expanded in plane waves. This is not the proper formulation to describe the interaction with nuclei, that we have often described in the last Chapters using a spherical basis. It is possible, nonetheless, to introduce an expansion of the vector potential in components that have good angular momentum and parity.

We will use $\lambda\mu$ as labels for the quantum numbers associated with the angular momentum and its z-projection. This means that the components $\mathbf{A}_{\lambda\mu}$ obey

$$\begin{aligned} J^2\mathbf{A}_{\lambda\mu} &= \lambda\left(\lambda+1\right)\mathbf{A}_{\lambda\mu}, \\ J_z\mathbf{A}_{\lambda\mu} &= \mu\mathbf{A}_{\lambda\mu}. \end{aligned} \tag{6.1}$$

We also need to distinguish the components with different parity. This amounts to distinguishing a term $\mathbf{A}_{\lambda\mu}(EL)$ with parity $(-1)^{\lambda}$, and a term $\mathbf{A}_{\lambda\mu}(MA)$ with parity $(-1)^{\lambda+1}$. The two labels refer obviously to electric (EL) and magnetic (MA).

If we write down these two terms, in the case of a monochromatic com-

[1] Their definition is subject to the choice of a specific gauge. We shall use the Coulomb gauge, in which $\nabla\cdot\mathbf{A}=\mathbf{0}$, in what follows. Our discussion will be restricted to the vector potential.

ponent of the vector potential charaterised by the frequency ω, we obtain

$$\begin{aligned} \mathbf{A}_{\lambda\mu,EL} &= \frac{-i}{k\sqrt{\lambda(\lambda+1)}} \left(\nabla \times \mathbf{L}\right) \left(j_\lambda(kr) Y_{\lambda\mu}(\theta,\phi)\right), \\ \mathbf{A}_{\lambda\mu,MA} &= \frac{1}{\sqrt{\lambda(\lambda+1)}} \mathbf{L} j_\lambda(kr) Y_{\lambda\mu}(\theta,\phi), \end{aligned} \tag{6.2}$$

where $k = \frac{\omega}{c}$, j_λ is a Bessel function, and $\mathbf{L} = -i\left(\mathbf{r} \times \nabla\right)$ is the angular momentum operator. The derivation of these formulas is not related to any nuclear physics concept. It is omitted in all recent textbooks but it can be found, for instance, in Ref. [43]. This source can be used to check other details that will be omitted in the treatment of this Chapter, together with the more recent textbook [44].

The interaction between matter and radiation, in this gauge, can be written as

$$H_{\text{int}} = -\frac{1}{c} \int d^3r \; \mathbf{j}(\mathbf{r}) \cdot \mathbf{A}(\mathbf{r}), \tag{6.3}$$

where $\mathbf{j}$ is the current density. By inserting the previous expressions (6.2) into (6.3), one can directly analyse the interaction of the system under study with the radiation of a given type and multipole.

In the nuclear case, the current $\mathbf{j}$ can be written as the sum of a convection part (associated with the motion of the charged protons) and of a magnetic part. This latter is written, in turn, as a function of a magnetization current μ. This means

$$\mathbf{j} = \mathbf{j}_{\text{C}} + \mathbf{j}_{\text{M}} = \mathbf{j}_{\text{C}} + \nabla \times \mu. \tag{6.4}$$

In the following Section, we analyse the electric multipoles of (6.3).

6.2 Electric multipole operators and moments

In the electric case,

$$H_{\lambda\mu,EL} = -\frac{1}{\omega\sqrt{\lambda(\lambda+1)}} \int d^3r \; \mathbf{j} \cdot \left[\nabla \times (\mathbf{r} \times \nabla)\right] j_\lambda Y_{\lambda\mu}, \tag{6.5}$$

where the dependence on radial and angular coordinates has been omitted for simplicity. Using a vector identity that reads

$$i\nabla \times \mathbf{L} = \mathbf{r}\nabla^2 - \nabla\left(1 + r\frac{\partial}{\partial r}\right),$$

as well as the fact that $j_\lambda Y_{\lambda\mu}$ are solutions of the Helmholtz equation[2], one arrives with algebraic steps at

$$H_{\lambda\mu,EL} = -\frac{1}{\omega\sqrt{\lambda(\lambda+1)}}\int d^3r\ \mathbf{j}\cdot\left[-k^2\mathbf{r}j_\lambda Y_{\lambda\mu} - \nabla\left(\frac{\partial}{\partial r}\left(rj_\lambda\right)Y_{\lambda\mu}\right)\right]. \quad (6.6)$$

In the second term, we can integrate by parts and use the continuity equation that reads

$$\nabla\cdot\mathbf{j} = \nabla\cdot\mathbf{j}_{\rm C} = -\frac{\partial\rho}{\partial t} = i\omega\rho, \quad (6.7)$$

where the last equality is related to the fact that we are considering the monochromatic case with frequency ω [cf. before Eq. (6.2)]. By writing the second term in the new form before the other term, Eq. (6.6) becomes

$$\begin{aligned} H_{\lambda\mu,EL} = &- \frac{i}{\sqrt{\lambda(\lambda+1)}}\int d^3r\ \rho\left(\frac{\partial}{\partial r}\left(rj_\lambda\right)Y_{\lambda\mu}\right) \\ &+ \frac{k^2}{\omega\sqrt{\lambda(\lambda+1)}}\int d^3r\ \mathbf{j}\cdot\mathbf{r}j_\lambda Y_{\lambda\mu}. \end{aligned} \quad (6.8)$$

At this point, we perform the aforementioned long wavelength approximation. Densities and currents are non-negligible in the range between zero and R given by Eq. (2.1). Consequenty, the largest value of kr is

$$kR \approx \frac{E}{\hbar c}1.25{\rm A}^{1/3}[{\rm fm}] \approx 6\ 10^{-3}\ {\rm A}^{1/3}\ E\ [{\rm MeV}], \quad (6.9)$$

where E is the energy of the electromagnetic radiation. In the range of our interest, $E \approx 1-10$ MeV, we can safely assume that $kr \ll 1$ and use the following approximation for the Bessel functions,

$$j_\lambda(kr) \xrightarrow[kr\to 0]{} \frac{(kr)^\lambda}{(2\lambda+1)!!}. \quad (6.10)$$

Inserting this into Eq. (6.8), we obtain

$$\begin{aligned} H_{\lambda\mu,EL} = &- i\sqrt{\frac{\lambda+1}{\lambda}}\frac{k^\lambda}{(2\lambda+1)!!}\int d^3r\ \rho r^\lambda Y_{\lambda\mu} \\ &+ \frac{1}{c\sqrt{\lambda(\lambda+1)}}\frac{k^{\lambda+1}}{(2\lambda+1)!!}\int d^3r\ \mathbf{j}\cdot\mathbf{r}j_\lambda Y_{\lambda\mu}. \end{aligned} \quad (6.11)$$

[2]This means that $\left(\nabla^2+k^2\right)j_\lambda(kr)Y_{\lambda\mu} = 0$.

Because of Eq. (6.7), it turns out that the second term in the latter equation is a factor $\approx kr$ smaller than the first one and is usually neglected.

It is customary to introduce an extra normalization factor in Eq. (6.5) and define

$$\begin{aligned} H_{\lambda\mu,EL} &= -\frac{1}{\omega\sqrt{\lambda(\lambda+1)}}\frac{i(2\lambda+1)!!}{k^\lambda}\sqrt{\frac{\lambda}{\lambda+1}}\int d^3r\ \mathbf{j}\cdot[\nabla\times(\mathbf{r}\times\nabla)]\, j_\lambda Y_{\lambda\mu} \\ &= \frac{-i(2\lambda+1)!!}{ck^{\lambda+1}(\lambda+1)}\int d^3r\ \mathbf{j}\cdot[\nabla\times(\mathbf{r}\times\nabla)]\, j_\lambda Y_{\lambda\mu}. \end{aligned} \tag{6.12}$$

This normalization allows obtaining a simpler form for (6.11), that is

$$\boxed{H_{\lambda\mu,EL} = \int d^3r\ \rho r^\lambda Y_{\lambda\mu} = \sum_i e_i r_i^\lambda Y_{\lambda\mu}(\theta_i,\phi_i).} \tag{6.13}$$

In the last step, we have inserted the definition of the charge density,

$$\rho(\mathbf{r}) = \sum_i e_i \delta(\mathbf{r}-\mathbf{r}_i), \tag{6.14}$$

where the sum runs over all nucleons but the electric charge is $e_i = 1$ for protons and $e_i = 0$ for neutrons. The equalities in (6.13) point to the fact that we can interpret the single-particle operator in the r.h.s. as the *electric multipole operator*, $O_{\lambda\mu,EL}$. Its matrix elements have dimension e fm$^\lambda$. Its expectation value over a nuclear state, like e.g. the ground-state,

$$\mathcal{M}_{\lambda\mu,EL} = \langle 0|\sum_i e_i r_i^\lambda Y_{\lambda\mu}(\theta_i,\phi_i)|0\rangle = \langle 0|O_{\lambda\mu,EL}|0\rangle, \tag{6.15}$$

is an *electric multipole moment*. As we have seen, different normalizations are possible for such moment. The discussion in this Section gives a solid ground to the discussion of quadrupole properties that has been made throughout the previous Chapter.

6.3 Electric multipole transitions and single-particle units

The concepts discussed in the previous Section can be extended to the case in which the electric multipole operator induces a transition from an initial

state i to a final state f, namely

$$\mathcal{A}_{\lambda\mu,EL} = \langle f|O_{\lambda\mu,EL}|i\rangle. \tag{6.16}$$

The symbol $\mathcal{A}$ stands for amplitude. The quantity which can be measured is the transition probability, that is the square of $\mathcal{A}$. As we already hinted when we wrote Eq. (5.17), in most of the cases we do not measure the polarization of the initial and final states. In all these cases, we actually measure a transition probability which is averaged over initial (degenerate) states and summed over final (degenerate) states. In the case in which these states have quantum numbers J and M, the transition probability that is defined in this way is called *reduced transition probability*. It is written as

$$\begin{aligned} B(E\lambda, i \to f) &= \frac{1}{2J_i+1} \sum_{M_i,M_f,\mu} |\langle J_f, M_f|O_{\lambda\mu,EL}|J_i, M_i\rangle|^2 \\ &= \frac{1}{2J_i+1} \sum_{M_i,M_f,\mu} \frac{\langle J_i M_i \lambda\mu|J_f M_f\rangle^2}{2J_f+1} \langle J_f||O_{\lambda\mu,EL}||J_i\rangle^2 \\ &= \frac{1}{2J_i+1} \langle J_f||O_{\lambda\mu,EL}||J_i\rangle^2, \end{aligned} \tag{6.17}$$

where in the second line we use the Wigner-Eckhart theorem for spherical tensors $T_{\lambda\mu}$,

$$\langle J_f, M_f|T_{\lambda\mu}|J_i, M_i\rangle = \frac{\langle J_i M_i \lambda\mu|J_f M_f\rangle}{\sqrt{2J_f+1}} \langle J_f||T_\lambda||J_i\rangle,$$

that introduces the reduced matrix elements (those with the double bar). In the next line we have used the orthonormality property of the Clebsch-Gordan coefficients.

Reduced transition probablilities characterise the electromagnetic excitation and decay of all the states that we have discussed so far. It is natural, then, to ask the question which is the natural scale for these probabilities. In the Tables, they are provided in units of $\mathrm{e}^2\mathrm{fm}^{2\lambda}$. However, these units do not give an idea if only one nucleon, or many of them, are involved in the process.

This is the motivation for introducing the so-called *single-particle units*. A single-particle unit, or s.p.u., characterises a transition in which only one nucleon is involved as the wording suggests. Let us suppose that a nucleon

undergoes a transition of type $E\lambda$ from an orbital j_i to an orbital j_f. If we assume[3] that $j_i = \lambda + \frac{1}{2}$ and $j_f = \frac{1}{2}$, and we evaluate with the use of a standard textbook the reduced matrix element in Eq. (6.17), we find

$$\begin{aligned} B(E\lambda, j_i = l + \frac{1}{2} \rightarrow j_f = \frac{1}{2}) &= \frac{2\lambda+1}{4\pi} \langle \lambda + \frac{1}{2}\frac{1}{2}\lambda 0 | \frac{1}{2}\frac{1}{2}\rangle^2 \left(\int dr\ R_f\ e\ r^\lambda R_i \right)^2 \\ &= \frac{1}{4\pi} \left(\int dr\ R_f\ e\ r^\lambda R_i \right)^2 . \end{aligned} \tag{6.18}$$

In going from the first to the second line we have taken into account that $\langle \lambda + \frac{1}{2}\frac{1}{2}\lambda 0 | \frac{1}{2}\frac{1}{2}\rangle^2 = \frac{1}{2\lambda+1}$. For the estimate of the radial integral, we perform a further simplification. We take wave functions $R_{i,f}(r) \equiv \frac{u_{f,i}(r)}{r}$ [cf. Eq. (2.7)] that are constant in the interval between 0 and the nuclear radius given by Eq. (2.1) and called a in this context[4]. Due to normalization,

$$\int_0^a dr\ r^2\ R_{i,f}^2 = 1 \quad \Rightarrow \quad R_{i,f} = \sqrt{\frac{3}{a^3}}, \tag{6.19}$$

and then

$$\int_0^a dr\ R_f r^{\lambda+2} R_i = \frac{3}{a^3}\frac{a^{\lambda+3}}{\lambda+3}. \tag{6.20}$$

With this assumption, and by replacing a with the value of Eq. (2.1), we arrive at the standard definition of s.p.u.:

$$B_{\text{s.p.u}}(E\lambda) = \frac{1}{4\pi}\left(\frac{3}{\lambda+3}\right)^2 1.2^{2\lambda} A^{\frac{2\lambda}{3}}\ [\text{e}^2\text{fm}^{2\lambda}]. \tag{6.21}$$

We have now a way to understand, in the electromagnetic case, the meaning of collectivity. A collective state is a state whose transition probability is large with respect to the s.p.u.

6.4 The magnetic sector

We do not repeat, for the magnetic multipoles, the detailed steps that we have outlined in the electric case. These steps are indeed similar in the

[3]This assumption is made in such a way that the factors associated with the specific orbitals can be simplified. We remind that these s.p.u. are merely intended to provide an order or magnitude of the reduced transition probability.

[4]Note that one should not mix up the wave function R_i or R_f with the nuclear radius.

general spirit. Thus, we describe them briefly, and we refer again to Refs. [43, 44] in case one is interested in repeating the whole calculation[5].

One has to start from the expressions already given in Eqs. (6.2) and (6.3), that give

$$H_{\lambda\mu,MA} = -\frac{1}{c\sqrt{\lambda(\lambda+1)}} \int d^3r \; \mathbf{j} \cdot \mathbf{L} j_\lambda Y_{\lambda\mu}. \tag{6.22}$$

In close analogy with the electric case, a factor is usually added so that the final expression in the long wavelength limit is eventually simpler to handle. This means, in practice, that one defines

$$H_{\lambda\mu,MA} = -\frac{(2\lambda+1)!!}{ck^\lambda(\lambda+1)} \int d^3r \; \mathbf{j} \cdot (\mathbf{r} \times \nabla) \, j_\lambda Y_{\lambda\mu}. \tag{6.23}$$

This equation is the analogous of Eq. (6.12). We state without formal proof that, in the long wavelength limit and taking care of the overall properties of nucleons (charge and spin), the latter formula becomes

$$\boxed{H_{\lambda\mu,MA} = \sum_i \left[g_s(i)\mathbf{s}_i + g_\ell(i)\frac{2\ell_i}{2\lambda+1} \right] \cdot \nabla_i \left(r_i^\lambda Y_{\lambda\mu}(\theta_i, \phi_i) \right).} \tag{6.24}$$

In this equation, which is the analogous of (6.13), ℓ and $\mathbf{s}$ are the single-particle orbital and spin angular momentum (cf. Chapter 2), whereas

$$g_\ell(i) = \begin{cases} 1\mu_N & \text{for protons} \\ 0 & \text{for neutrons,} \end{cases} \tag{6.25}$$

and

$$g_s(i) = \begin{cases} +5.586\mu_N & \text{for protons} \\ -3.826\mu_N & \text{for neutrons} \end{cases} \tag{6.26}$$

(μ_N is the nuclear magneton).

As in the electric case, we can interpret the single-particle operator in the r.h.s. of (6.24) as the *magnetic multipole operator* $O_{\lambda\mu,MA}$. Its expectation value over a nuclear state, like e.g. the ground-state, is a *magnetic multipole*

[5]The student can also ask for notes that can be made available by the author of this text.

moment. Magnetic reduced transition probabilities can also be defined, together with the corresponding s.p.u. We do not dwell on the magnetic case but we refer to standard textbooks for details. We only stress, as it is useful for the next Section, that the matrix elements of the operator (6.24) have units of μ_N fm$^{\lambda-1}$.

6.5 Lifetimes

From the reduced transition probability, we can also calculate the lifetime of the excited states. This is done using the Fermi Golden rule. We avoid here the tedious calculation of the density of final photon states [44] and simply provide the result.

The transition rate for a given multipole transition is given by

$$T(E\lambda \text{ or } M\lambda) = \frac{8\pi(\lambda+1)}{\lambda[(2\lambda+1)!!]^2}\frac{1}{\hbar}\left(\frac{E}{\hbar c}\right)^{2\lambda+1} B(E\lambda \text{ or } M\lambda). \qquad (6.27)$$

E is, as above, the transition energy that is the energy of the photon. The reduced transition probabilities B are given in e^{2}fm$^{2\lambda}$ and μ_N^2fm$^{2\lambda-2}$, in the electric and magnetic case respectively. One should remember that we are using units in which e^2 corresponds to MeV fm, while μ_N^2 to MeV fm^3. Then, it is straightforward to check that T turns out to be in s^{-1} as it should.

Transition rates given by Eq. (6.27) allow the comparison of different multipoles. The ratio between two multipole transitions having $\lambda+1$ and λ is given by a factor $(kR)^2$. k^2 comes from $\left(\frac{E}{\hbar c}\right)^2$. R^2 comes from the radial operator inside the matrix element that gives B. Since, as we have seen in Sec. 6.2, $kR \ll 1$, the transition rate associated with a higher multipole becomes negligible when a lower one is allowed by the transition rules:

$$\begin{aligned} T(E\lambda) &\gg T(E(\lambda+1)), \\ T(M\lambda) &\gg T(M(\lambda+1)). \end{aligned} \qquad (6.28)$$

Chapter 7

Direct nuclear reactions

7.1 Introduction and classification of reactions

The study of nuclear reactions is a very broad domain, and the border between nuclear and hadronic reactions is somehow blurred. In the present Chapter, we will have in mind only reactions in which both the initial and final systems are either nucleons or nuclei, disregarding in this way the production of other types of particles. We will also leave aside electro-weak reactions, where electrons, muons or neutrinos interact with nuclei. In this respect, a typical nuclear reaction can be written as

$$\mathrm{A} \; + \; \mathrm{a} \; \rightarrow \; \mathrm{B} \; + \; \mathrm{b}, \tag{7.1}$$

although the presence of more than two particles in the final state cannot be excluded. In the initial state, reactions involving three or more particles have increasingly small cross sections. We shall keep the notation (7.1) for the sake of simplicity.

There are important conservation laws that dictate which reactions are possible, and which are the available final states for the particles that are involved: total energy, linear momentum, angular momentum, total electric charge, baryon number are conserved quantities, as well as parity since we negect the contribution of the weak interaction. The reaction Q-value is defined as the difference between the masses of the particles in the initial and final channels, turned into rest energies via the factor c^2. This means

$$Q \equiv \left(M_A + M_a - M_B - M_b\right) c^2 = \sum_f T_f - \sum_i T_i, \tag{7.2}$$

where the notation of Eq. (7.1) has been followed. The second equality follows from the energy conservation. In the r.h.s., i and f label the particles in the initial and final states, respectively, with their kinetic energies T_i and T_f. From the definition of the Q-value it is clear that if $Q > 0$ (exothermic reaction), the reaction can occur for any initial kinetic energy. This is not the case if $Q < 0$ (endothermic reaction): in this case, a threshold exists.

While the Q-value is of course a scalar quantity that does not depend on the chosen reference frame, the partition of kinetic energies among particles does. How the threshold kinetic energy for endothermic reactions depends on the specific frame will not discussed here. In fact, we will not detail any of the formulas associated to the kinematics of nuclear reactions. These are a simple application of elementary mechanics and can be found in many textbooks[1]. We simply provide here a few important comments on the laboratory and center-of-mass systems. As in previous Chapters, we stick to non-relativistic kinematics.

The laboratory (LAB) system is clearly defined. Usually, in it there is a target particle at rest[2] and this will be the particle A in the notation of Eq. (7.1). This is not the case in the center-of-mass (COM) frame. A simple calculation, carried out in the Appendix 7.A.1, leads to

$$\sum_i T_i^{(\mathrm{COM})} = \frac{A}{A+a} T^{(\mathrm{LAB})}, \tag{7.3}$$

where the l.h.s. is the total kinetic energy available in the COM system whereas in the r.h.s. we have the kinetic energy in the LAB system of the incident particle a, multiplied by a factor that includes the mass numbers of projectile and targets. In a reaction induced by a light particle, like a nucleon, on a heavy nucleus A, the two energies can be mixed up because the factor $\frac{A}{A+a}$ is close to 1. In fact, the COM essentially coincides with the heavy particle and remains idle, while this is not the case in a symmetric reaction where the energy in the COM is one half of the LAB energy.

In what follows, we will study the properties of some reactions as a function of the energy, and it is clear that such dynamics must be studied in the COM system. The COM energy wil be referred to simply as *incident energy*. The associated velocity, or momentum, will be simply written as $\mathbf{v}$, or $\mathbf{p}$. We also shall use the name momentum, in this Chapter, for the wave

[1] See e.g. Sec. 10.3 of Ref. [45].

[2] We leave aside the case of experiments performed with two colliding beams.

vector $\mathbf{k}$ which is the momentum in units of $\hbar$. We shall keep implicit that in the COM system $T = \frac{1}{2}\mu v^2$ where μ is the reduced mass (cf. the Appendix 7.A.1).

The main observables associated with a reaction are the differential and the total cross section[3]. In keeping with the huge variety of possible reactions, the cross sections vary from negligibly small to large values[4] of the order of $\approx$ barn. We remind that

$$1 \text{ b} = 10^{-24} \text{ cm}^2 = 100 \text{ fm}^2.$$

We can classify the reactions according to their type or to the incident energy.

Elastic reactions are those in which neither the configuration of the systems that are involved nor the relative energy change between the initial and final state, and we can write the reaction as A+a $\rightarrow$ A+a. Inelastic reactions are those in which the particles in the initial and final states do not change, but some amount of energy is transferred from the relative kinetic energy to intrinsic excitations; in other words, one of the two particles (or both) can be excited. If we assume that A has been excited, we write $\text{A} + \text{a} \rightarrow \text{A}^* + \text{a}$. Transfer reactions are those in which B and b are different nuclei with respect to A and a, namely some nucleons have been transferred between projectile and target. We may have in mind one-neutron transfer, one proton-transfer, or multi-nucleon trasfer.

At high energies, like 100 MeV/nucleon, nuclear reactions can be assumed to take place through one single step. The projectile is usually not much deviated from its trajectory, in a semiclassical picture, so that the angular distributions are forward-peaked and have specific shapes that are well reproduced by theory if we calculate them through first-order perturbation theory, as we shall discuss below. The fact that only a single interaction takes place can be roughly justified through an estimate of the interaction time, that is,

$$\begin{aligned} \Delta t &\approx \frac{R}{v} = \hbar \, \frac{R}{\hbar c} \sqrt{\frac{\mu c^2}{2T}} \approx 7 \cdot 10^{-22} \text{ MeV} \cdot \text{s} \, \frac{5 \text{ fm}}{200 \text{ MeV} \cdot \text{fm}} \sqrt{\frac{10^3}{2T}} \\ &\approx 10^{-23} \text{ s} \sqrt{\frac{10^3}{2T}}, \end{aligned} \tag{7.4}$$

[3]The definitions are assumed to be known.

[4]On the nuclear scale.

where T is assumed in MeV. For T of the order of hundreds of MeV, this interaction time is of the order of the typical time between two nuclear collisions that has been estimated in Eq. (2.33). These reactions are called, therefore, *direct* reactions.

At the other extreme, reactions around 1 MeV/nucleon are characterised by interaction times that are one order of magnitude longer, or by a number of collisions that are one order of magnitude larger. Not surprisingly, as it will be discussed in some detail below, in these reactions the large number of collisions produce an equlibrated, or thermalized, projectile-target compound system that is called *compound nucleus* (CN). The CN lasts long enough so to loose memory of the way in which it has been formed, and decays to a final state independently of the initial state. Only the energy of the compound nucleus is a relevant parameter. Cross sections are isotropic.

These two kinds of reactions will be discussed, while we leave aside the intermediate case of partial equilibration (that is, the so called *multi-step* or *pre-equilibrium* reactions), in keeping with the higher complexity. After this phenomenological introduction, we discuss some formal theory of the scattering process and a general formula for the associated cross section, that will be prone to several approximations.

7.2 Formal theory

We consider the two nuclei A and a, and we define in the following way the degrees of freedom and the associated Hamiltonian. $\mathbf{R}$ is the relative coordinate (i.e. the distance between the centre-of-mass of A and a), so that the relative kinetic energy can be written as $T = -\frac{\hbar^2}{2\mu}\nabla^2_{\mathbf{R}}$, where μ is the reduced mass and $\nabla_{\mathbf{R}}$ is the gradient with respect to the coordinate $\mathbf{R}$. The coordinates of the nucleons belonging to A (a) are denoted by $\mathbf{r}_A$ ($\mathbf{r}_a$); accordingly, the intrinsic Hamiltonians will be written $H_A(\{\mathbf{r}_A\})$ and $H_a(\{\mathbf{r}_a\})$, and the dependence on the set of intrinsic coordinates will be dropped for simplicity. Of course, H_A contains the kinetic energies of the nucleons of A, in the system which is fixed in its centre of mass, as well as the interaction among all these nucleons. The same holds true in the case of H_a. Eventually, the remaining part of the Hamiltonian will be the interaction V_{Aa} between every nucleon belonging to A and every nucleon belonging to a. The term aA of this potential depends on $\mathbf{R} + \mathbf{r}_a - \mathbf{r}_A$.

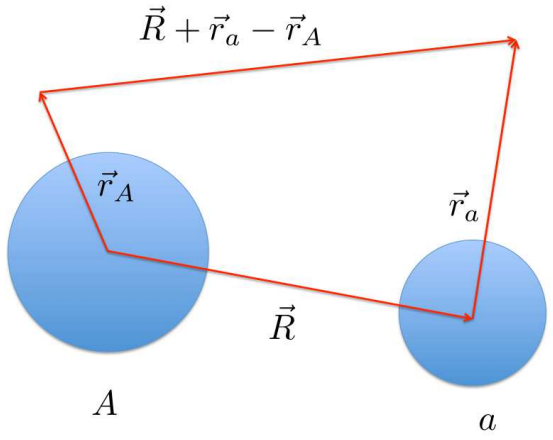

Figure 7.1: Appropriate coordinates for the collision between nuclei A and a, as described in the main text.

All this discussion should be more clear by looking at Fig. 7.1[5]. The Hamiltonian that we have just described is

$$H = H_A + H_a + T + V_{Aa} = H_0 + V, \tag{7.5}$$

where, in the second step, we make it clear that we assume that H_A and H_a are known, together with their eigenvalues and eigenvectors. In other words, the problem in which $V \equiv V_{Aa}$ vanishes and the total Hamiltonian is H_0 has a known solution. We call Φ the eigenfunctions of H_0. These wave functions are products of the intrinsic wave functions ϕ_A and ϕ_a of H_A and H_a, respectively, and of the eigenfunction of T which is a plane wave. Thus, they read

$$\Phi^{\pm}_{\mathbf{k}}(\mathbf{R}) = e^{\pm i\mathbf{k}\cdot\mathbf{R}}\phi_A\phi_a, \tag{7.6}$$

where the $+$ and $-$ sign refers, respectively, to outgoing and ingoing boundary conditions (from now on, we will not carry on the $\pm$ notation as we will

[5]One should note that all this is intended to explain elastic and inelastic reactions. The situation will be to some extent different in the case of transfer reactions, because of the change in configurations between the initial and final channel.

essentially have in mind the case of outgoing boundary conditions only). The equation

$$(E - H_0)\,\Phi_{\mathbf{k}} = 0 \tag{7.7}$$

holds, with

$$E = \frac{\hbar^2 k^2}{2\mu} + E_A + E_a. \tag{7.8}$$

The complete Schrödinger equation is

$$(E - H_0)\,\Psi_{\mathbf{k}} = V\Psi_{\mathbf{k}}, \tag{7.9}$$

namely we label as Ψ the exact wave function. $\Psi_{\mathbf{k}}$ is the product of ϕ_A, ϕ_a and the exact wave function for the relative motion. Φ and Ψ depend both on the quantum number associated with the momentum, $\mathbf{k}$, and on two quantum numbers associated with the specific eigenstates of A and a (say, n_A and n_a). However, in what follows we keep these latter two quantum numbers implict, and write only the momentum explicitly. We shall also keep the intrinsic wave functions implicit until it is needed for the derivation.

In the next subsection, we derive an exact equation for Ψ.

7.2.1 The Lippmann-Schwinger equation

The exact wave function $\Psi_{\mathbf{k}}$ can be expanded in terms of the set $\Phi_{\mathbf{k}'}$ in the following way:

$$\Psi_{\mathbf{k}}(\mathbf{R}) = \int d^3k'\; a(\mathbf{k}')\Phi_{\mathbf{k}'}(\mathbf{R}), \tag{7.10}$$

where a labels the (at this stage unknown) coefficients. We notice that the set Φ corresponds to a continuum spectrum, and obey the completeness and closure relations in the following, generalised sense:

$$\begin{aligned} \int d^3R\; \Phi^*_{\mathbf{k}}(\mathbf{R})\Phi_{\mathbf{k}'}(\mathbf{R}) &= (2\pi)^3\delta(\mathbf{k}-\mathbf{k}'), \\ \int d^3k\; \Phi^*_{\mathbf{k}}(\mathbf{R})\Phi_{\mathbf{k}}(\mathbf{R}') &= (2\pi)^3\delta(\mathbf{R}-\mathbf{R}'). \end{aligned} \tag{7.11}$$

We can replace the expansion (7.10) into the l.h.s. of the Schrödinger equation (7.9), and use the fact that Φ is eigenfunction of H_0, to get

$$\int d^3k'\;\; (E - E')\, a(\mathbf{k}')\Phi_{\mathbf{k}'} = V\Psi_{\mathbf{k}}. \tag{7.12}$$

We now multiply both sides from left by $\Phi^*_{\mathbf{k}''}(\mathbf{R})$ and integrate over $\mathbf{R}$, to obtain, using the first of the equations (7.11),

$$(2\pi)^3 a(\mathbf{k}'')(E - E'') = \int d^3R\ \Phi^*_{\mathbf{k}''}(\mathbf{R}')V(\mathbf{R})\Psi_{\mathbf{k}}(\mathbf{R}). \tag{7.13}$$

We change the notation from $''$ to $'$, and we use the latter equation to derive an expression for the coefficient a. We insert back such expression in the expansion (7.10), so that

$$\begin{aligned}\Psi_{\mathbf{k}}(\mathbf{R}) &= \int d^3k'\ a(\mathbf{k}')\Phi_{\mathbf{k}'}(\mathbf{R}) = \int d^3k' \int d^3R'\ \frac{1}{(2\pi)^3}\frac{\Phi_{\mathbf{k}'}(\mathbf{R})\Phi^*_{\mathbf{k}'}(\mathbf{R}')}{E - E'}V(\mathbf{R}')\Psi_{\mathbf{k}}(\mathbf{R}') \\ &= \int d^3R'\ G_0(\mathbf{R}, \mathbf{R}'; E)V(\mathbf{R}')\Psi_{\mathbf{k}}(\mathbf{R}'). \end{aligned} \tag{7.14}$$

In the last step, we have introduced the Green's function G_0 defined as

$$G_0(\mathbf{R}, \mathbf{R}'; E) = \frac{1}{(2\pi)^3}\int d^3k'\ \frac{\Phi_{\mathbf{k}'}(\mathbf{R})\Phi^*_{\mathbf{k}'}(\mathbf{R}')}{E - E'}. \tag{7.15}$$

Since all the quantities at the r.h.s. of Eq. (7.15) are known, the Green's function can be explicitly calculated. The result reads[6]

$$G_0(\mathbf{R}, \mathbf{R}'; E) = -\frac{\mu}{2\pi\hbar^2}\frac{e^{ik|\mathbf{R}-\mathbf{R}'|}}{|\mathbf{R} - \mathbf{R}'|}. \tag{7.16}$$

Eq. (7.14) shows one particular solution of the Schrödinger equation (7.9). The general solution of the inhomogeneous equation (7.9) can be written as the general solution of the associated homogeneous equation, that is Φ, plus the particular solution (7.14):

$$\Psi_{\mathbf{k}} = \Phi_{\mathbf{k}} + \int d^3R'\ G_0(\mathbf{R}, \mathbf{R}'; E)V(\mathbf{R}')\Psi_{\mathbf{k}}(\mathbf{R}'). \tag{7.17}$$

More schematically, we can write Eq. (7.17) as

$$\Psi = \Phi + \int\ G_0\ V\ \Psi. \tag{7.18}$$

[6]It is a result that can be derived by using the residue theorem. The derivation is available under request.

This is called Lippmann-Schwinger equation: it is an integral equation which is equivalent to the Schrödinger equation we have started from, but its advantage is that it is written in a form that allows solutions by iteration, or anyway increasingly accurate solutions as a series in V, In fact, one can also write it as

$$\Psi = \Phi + \int G_0\ V\ \Phi + \int\int G_0\ V\ G_0\ V\ \Phi + \dots \tag{7.19}$$

This will be used in what follows, as we shall actually stop at the lowest (i.e. Born) approximation where V appears only once.

At the end of our derivation, we can explicity re-introduce the internal coordinates of the two nuclei, $\mathbf{r}_1 \dots \mathbf{r}_a$ and $\mathbf{r}_1 \dots \mathbf{r}_A$ (cf. Fig. 7.1). We can also re-introduce the exact wave functions of the two nuclei ϕ_A and ϕ_a, either in their initial or final states. We do it while showing the relationship between the somehow formal Lippmann-Schwinger equation and the actual experimental observable, that is, the cross section.

7.2.2 The scattering amplitude and the cross section

In the asymptotic region, $R \gg R'$, we can make the following approximations:

$$\begin{aligned} |\mathbf{R} - \mathbf{R}'|^{-1} &\approx \frac{1}{R}\ , \\ k|\mathbf{R} - \mathbf{R}'| &= k\left(R^2 + R'^2 - 2\mathbf{R}\cdot\mathbf{R}'\right)^{1/2} \approx kR\left(1 - \frac{\mathbf{R}\mathbf{R}'}{R^2}\right) = kR - \mathbf{k}'\cdot\mathbf{R}', \end{aligned} \tag{7.20}$$

where in the last step we have defined $\mathbf{k}'$ as the projection of $\mathbf{k}$ along the direction of $\mathbf{R}$, namely $\mathbf{k}'R \equiv k\mathbf{R}$. Such direction defines the scattering angle θ, having assumed the initial momentum $\mathbf{k}$ along the z-axis.

In this way, we can write the form of the Lippmann-Schwinger equation (7.17) for $R \to \infty$:

$$\begin{aligned} \Psi_{\mathbf{k}}(\vec{R}) \ \to\ & e^{ikz}\phi_A\phi_a - \frac{\mu}{2\pi\hbar^2}\frac{e^{ikR}}{R}\int d^3R'\ e^{-i\mathbf{k}'\cdot\mathbf{R}'}\int d^3r_1 \dots d^3r_a\ d^3r_1 \dots d^3r_A \\ & \phi_f^{(a)*}(\mathbf{r}_1 \dots \mathbf{r}_a)\phi_f^{(A)*}(\mathbf{r}_1 \dots \mathbf{r}_A)V(\mathbf{R}', \{\mathbf{r}\})\phi_i^{(A)}(\mathbf{r}_1 \dots \mathbf{r}_A)\phi_i^{(a)}(\mathbf{r}_1 \dots \mathbf{r}_a)\ \Psi_{\mathbf{k}}(\mathbf{R}'). \end{aligned} \tag{7.21}$$

This equation allows one to identify an exact expression for the scattering amplitude, that is,

$$f(\theta) = -\frac{\mu}{2\pi\hbar^2}\int d^3R'\; e^{-i\mathbf{k}'\cdot\mathbf{R}'}\int d^3r_1\ldots d^3r_a\; d^3r_1\ldots d^3r_A \\ \phi_f^{(a)*}(\mathbf{r}_1\ldots\mathbf{r}_a)\phi_f^{(A)*}(\mathbf{r}_1\ldots\mathbf{r}_A)V(\mathbf{R}',\{\mathbf{r}\})\phi_i^{(A)}(\mathbf{r}_1\ldots\mathbf{r}_A)\phi_i^{(a)}(\mathbf{r}_1\ldots\mathbf{r}_a)\;\Psi_{\mathbf{k}}(\mathbf{R}'). \tag{7.22}$$

Often, in the literature, one leaves the explicit integration on the reative coordinate $\mathbf{R}'$, and uses bra and ket notation, $\langle$ and $\rangle$, for the integration on the internal coordinates. We shall do the same and also use the short-hand notations $\langle f|$ and $|i\rangle$, respectively for $\phi_f^{(a)*}\phi_f^{(A)*}$ and $|i\rangle$ for $\phi_i^{(A)}\phi_i^{(a)}$. Then, we write

$$\boxed{f(\theta) = -\frac{\mu}{2\pi\hbar^2}\int d^3R'\; e^{-i\mathbf{k}'\cdot\mathbf{R}'}\;\langle f|V|i\rangle\;\Psi_{\mathbf{k}}(\mathbf{R}').} \tag{7.23}$$

Eq. (7.23) has the remarkable feature of being an exact equation for the scattering amplitude. It is for spinless particles, though. The quantity $\langle f|V|i\rangle$, which is a function of the relative distance $\mathbf{R}'$ and represents the interaction between the nucleons of the two nuclei when such relative distance is fixed, is often called *form factor*.

In the case of eleastic scattering, the cross section can be readily derived as

$$\frac{d\sigma}{d\Omega} = |f(\theta)|^2. \tag{7.24}$$

This equation has to be modified in the case of inelastic scattering as follows,

$$\frac{d\sigma}{d\Omega} = \frac{k'}{k}|f(\theta)|^2. \tag{7.25}$$

7.3 Elastic scattering

7.3.1 Kinematics

In the case of elastic scattering, the transferred momentum $\mathbf{q}$ is defined by

$$\mathbf{q} \equiv \mathbf{k} - \mathbf{k}', \tag{7.26}$$

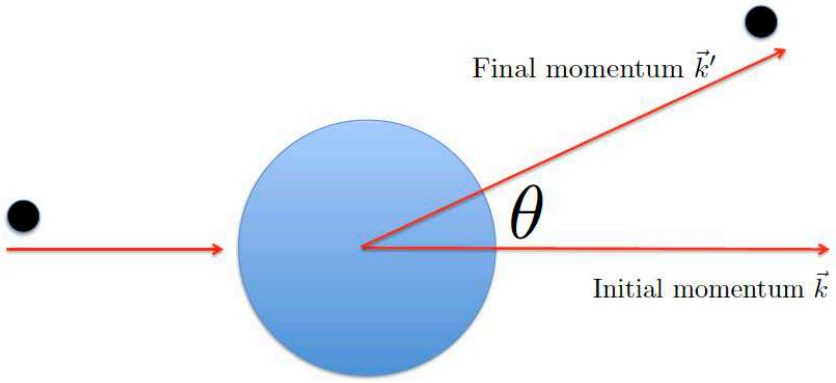

Figure 7.2: Initial and final momenta $\mathbf{k}$ and $\mathbf{k}'$. $\mathbf{q}$ is defined as $\mathbf{k} - \mathbf{k}'$ (see the text). θ is the scattering angle.

where $\mathbf{k}$ and $\mathbf{k}'$ are equal in modulus. We can also write

$$\begin{aligned} q^2 &= k^2 + k'^2 - 2\mathbf{k}\cdot\mathbf{k}' cos\theta = 2k^2\,(1 - cos\theta) \\ &= 4k^2 sin^2\frac{\theta}{2}, \\ q &= 2k sin\frac{\theta}{2}. \end{aligned} \tag{7.27}$$

From this equation, one can see the explicit form in which the angle θ appears in the scattering amplitude (cf. also Fig. 7.2).

7.3.2 Cross section within the Born approximation

We stick to the Born approximation, in which the interaction V acts only once. The plane-wave Born approximation (PWBA) is the simplest possible approximation for elastic scattering: in it, starting from the exact expression for the scattering amplitude (7.23), the unknown wave function $\Psi_{\mathbf{k}}$ is replaced with the corrsponding plane wave, that is,

$$\begin{aligned} f_{\rm PWBA}(\theta) &= -\frac{\mu}{2\pi\hbar^2}\int d^3R'\; e^{-i\mathbf{k}'\cdot\mathbf{R}'}\langle 0|V|0\rangle e^{i\mathbf{k}\cdot\mathbf{R}'} \\ &= -\frac{\mu}{2\pi\hbar^2}\int d^3R'\; e^{i\mathbf{q}\cdot\mathbf{R}'}\langle 0|V|0\rangle. \end{aligned} \tag{7.28}$$

In the independent particle approximation,

$$\langle 0|V|0\rangle = \sum_{Aa}\langle 0|V(\mathbf{R}+\mathbf{r}_a-\mathbf{r}_A)|0\rangle = \int d^3r_A d^3r_a\ \rho_A(\mathbf{r}_A)V\rho_a(\mathbf{r}_a). \quad (7.29)$$

This is often called *folding model* for obvious reasons, or *double folding model* for the elastic form factor. We can also mention the special case in which the projectile a is a point particle (a neutron or a proton). Then, we have the corresponding *single folding model* in which

$$\langle 0|V|0\rangle = \sum_{A}\langle 0|V(\mathbf{r}-\mathbf{r}_A)|0\rangle = \int d^3r_A\ \rho_A(\mathbf{r}_A)V \equiv U(\mathbf{R}). \quad (7.30)$$

As the latter equivalence hints, this is nothing but a kind of mean field potential (at point $\mathbf{R}$). The scattering amplitude,

$$f_{\rm PWBA}(\theta) = -\frac{\mu}{2\pi\hbar^2}\int d^3R'\ e^{i\mathbf{q}\cdot\mathbf{R}'}U(\mathbf{R}'), \quad (7.31)$$

becomes simply the Fourier transform of the potential U.

If we consider a neutron impinging on a nucleus, the potential could be represented with a Woods-Saxon shape or, with a more crude approximation, with a potential well. If the well has a radius a and a depth V_0, the scattering amplitude becomes quite simple to evaluate. We introduce here the development of the plane wave into spherical components that will be useful many times later on, namely

$$e^{i\mathbf{q}\cdot\mathbf{R}} = 4\pi\sum_{\lambda\mu} i^\lambda j_\lambda(qR)Y^*_{\lambda\mu}(\hat{q})Y_{\lambda\mu}(\hat{R}), \quad (7.32)$$

where j_λ is the spherical Bessel function and the notation $\hat{q}$ ($\hat{R}$) corresponds to the polar angles of $\mathbf{q}$ ($\mathbf{R}$). Then,

$$\begin{aligned} f_{\rm PWBA}(\theta) &= -\frac{\mu V_0}{2\pi\hbar^2}\int_0^a dR\ R^2\ d\hat{R}\ e^{i\mathbf{q}\cdot\mathbf{R}} = -\frac{2\mu V_0}{\hbar^2}\int_0^a dR\ R^2\ j_0(qR) \\ &= -\frac{2\mu V_0}{\hbar^2 q^3}\int_0^{qa} dx\ x^2\ j_0(x) = -\frac{2\mu V_0 a^2}{\hbar^2 q}j_1(qa), \end{aligned} \quad (7.33)$$

where we have used the expansion (7.32) in the first step, and the integral $\int dx\ x^2\ j_0(x) = x^2\ j_1(x)$ in the last step. We can use Eq. (7.27) and, if we restrict to small angles, approximate

$$q = 2ksin\frac{\theta}{2} \approx k\theta.$$

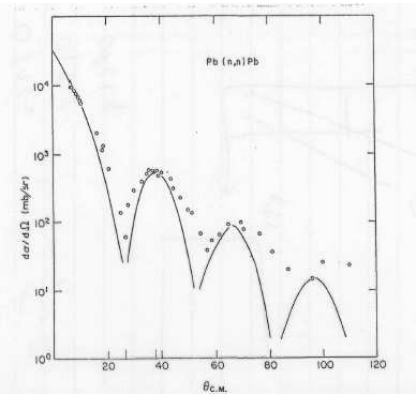

Figure 7.3: Elastic cross section for neutrons on Pb. The incident energy is about 14.5 MeV. The points correspond to measured values, whereas the line is a theoretical calculation. See the text for a discussion.

In this way, the elastic cross section turns out to be

$$\frac{d\sigma}{d\Omega} = \frac{4\mu^2 V_0^2 a^4}{\hbar^4 k^2 \theta^2} |j_1(ka\theta))|^2. \tag{7.34}$$

We check this approximate cross section against experimental data. A set of measured points for the elastic cross section of neutrons impinging on ^{208}Pb at 14.5 MeV is displayed in Fig. 7.3. The value of k associated with neutrons impinging at 14.5 MeV is ≈ 0.84 fm^{-1}. The separation between two zeros of the Bessel function turns out to be $\delta\theta \approx \pi/ka$. Therefore, to reproduce the separation between two minima in Fig. 7.3, which is $\approx 27^\circ = 0.47$ rad, we must assume

$$a = \frac{\pi}{0.47k} = 7.96 \text{ fm}.$$

This value is very close to the radius of ^{208}Pb calculated by means of Eq. (2.1).

Eq. (7.34) is actually analogous to what is known from basic diffraction theory. It corresponds to treating the nucleus as a black object, and it belongs to the class of formulas that go under the name of "black sphere approximation". In this respect, it can be understood why Eq. (7.34) cannot account for the strong reduction in the height of the peaks as the scattering angle increases. In simple terms, from the discussion so far we cannot understand the logaritmic scale on the vertical axis of Fig. 7.3. Eq. (7.34) makes sense when *absorbtion* is negligible. But this is not the case when dealing with nuclear elastic scattering.

The physical picture that corresponds to absorbtion and that is missing so far, is that only part of the incident neutrons undergo elastic scattering,

that is, they do not remain all in the *elastic channel*. Part of the incident flux is lost because neutrons perform inelatic or transfer reactions and should be found in other *reaction channels*. Usually this is dealt with by means of the introduction of an *optical potential*. Optical potentials replace the mean-field U and have the form

$$U_{\rm opt} = V(\mathbf{R}) + iW(\mathbf{R}). \tag{7.35}$$

The imaginary part of the potential corresponds to an absorbtion of the particles and is related to the concept of mean free path. We explain this concept in the case of unform matter, to make it more transparent.

7.3.3 Absorbtion and the optical potential

In uniform nuclear matter (cf. 2.3.1), the wave functions can be assumed to be plane waves. The Schrödinger equation for a neutron in uniform matter can be written as

$$\left(-\frac{\hbar^2}{2\mu}\nabla^2 + V + iW\right) e^{ikz} = Ee^{ikz}, \tag{7.36}$$

if we insert a uniform potential of the type (7.35) and if we take the momentum along the z-direction for the sake of simplicity. Then, we can write

$$\begin{aligned} \frac{\hbar^2 k^2}{2\mu} + V + iW &= E, \\ k^2 &= \frac{2\mu}{\hbar^2}\left(E - V - iW\right). \end{aligned} \tag{7.37}$$

The quantity k becomes a complex number, and we can more easily write it in the hypohesis (to be verified *a posteriori*) that in absolute value W is significantly smaller than $E - V$:

$$k = \sqrt{\frac{2\mu(E-V)}{\hbar^2}}\left(1 - i\frac{W}{E-V}\right)^{1/2} \approx \sqrt{\frac{2\mu(E-V)}{\hbar^2}}\left(1 - \frac{i}{2}\frac{W}{E-V}\right). \tag{7.38}$$

The momentum assumes an imaginary part, that is, the wave function becomes

$$e^{i(k_{\rm R}+ik_{\rm I})z} = e^{ik_{\rm R}z}e^{-k_{\rm I}z}. \tag{7.39}$$

The square modulus of this wave function is not 1, but it takes a factor $e^{-2k_{\rm I}z}$ that implicitly defines a *mean free path* l through the identification

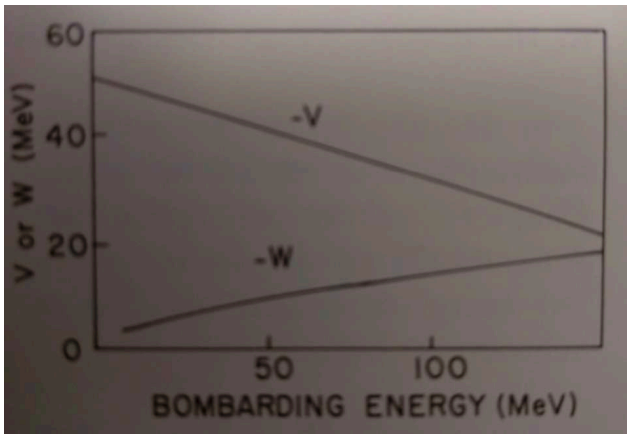

Figure 7.4: Schematic trend of the strength of the real and imaginary parts of the optical potential (7.35). Figure taken from Ref. [46].

$e^{-2k_{\rm I}z} \equiv e^{-z/l}$. Of course we expect W to be negative so that $k_{\rm I}$ is positive. Thus, we conclude that

$$l = \frac{1}{2k_{\rm I}} = \sqrt{\frac{\hbar^2}{2\mu}} \frac{\sqrt{E-V}}{|W|}. \tag{7.40}$$

In Fig. 7.4, values for the strength V and W of the real and imaginary part of the optical potential (7.35) are displayed. By using Eq. (7.40) and the values of Fig. 7.4, we can see that the mean free part of a low-energy neutron can be very large, of the order of the radius of a heavy nucleus or larger, as we have argued at the start of Chapter 2.

In finite nuclei, $V(\mathbf{R})$ and $W(\mathbf{R})$ may have a Woods-Saxon shape, although sometimes an imaginary part given by the derivative of a Woods-Saxon is preferred (the corresponding function is peaked on the surface and almost zero elsewhere, that is, it simulates a surface absorbtion). Generally speaking, a given shape, depending on few parameters, is assumed. Such parameters are fitted on experimental data like those shown in Fig. 7.3. At present, global optical model (OM) parameters exist although it still customary to fit them on a specific set of data, namely in a narrow range of isotopes and/or incident energies.

The calculations of elastic cross sections through optical potentials can be performed only numerically. It is instructive to discuss, in the next subsection, a very simple approach for this aim.

7.3.4 Eikonal approximation

This approximation is, strictly speaking, valid at high energy. However, its advantage is that it provides very simple expressions for the elastic cross section, which are amenable to a quite straightforward numerical treatment. The name of this approximation comes from optics, where it corresponds to the limit in which physical optics coincides with geometrical optics since the scale on which the refraction index n varies is large compared to the wavelength λ. In nuclear physics, this wavelength is the De Broglie one associated with the relative motion: if λ is small enough, or k is large enough, the approximation is valid. While for neutrons or protons it has been shown that one needs to go to quite large energies of the order or 500 MeV or 1 GeV, the same approximation can be safely used at much lower energies in the case of heavy ions: in fact, k also scales with $\sqrt{A}$.

In the eikonal approximation one assumes trajectories that are straight lines. The wave function of the initial state (also assumed to have momentum along the z-axis) has the form e^{ikz} times a minimal distortion given by a scalar function φ. Cylindrical coordinates will be used, that is, z and the two-dimensional vector $\mathbf{b}$ on the orthogonal plane (it is written in this form because it concides with the impact parameter). The rotation angle around z will not play any role. The function $\Psi_{\mathbf{k}}$ is therefore written as[7]

$$\Psi_{\mathbf{k}}(\mathbf{R}) = e^{ikz}\varphi(z, b). \tag{7.41}$$

We replace this wave function in the Schrödinger equation for the relative motion,

$$-\frac{\hbar^2}{2\mu}\nabla^2\Psi_{\mathbf{k}} + V\Psi_{\mathbf{k}} = E\Psi_{\mathbf{k}}, \tag{7.42}$$

and we make the assumption that the term containing the Laplacian of φ can be neglected, namely that

$$|\nabla^2\varphi| \ll k\,|\nabla\varphi|.$$

This equation represents, in mathematical terms, the fact that the distortion is minimal, and is eventually valid for large enough values of k. It is easy to verify that the Schrödinger equation (7.42) simplifies to

$$\frac{\partial\varphi}{\partial z} = -\frac{i}{\hbar v}V\varphi, \tag{7.43}$$

[7] As above, we keep intrinsic coordinates and intrinsic wave functions implicit until needed.

with $v = \hbar k/\mu$. The solution reads

$$\varphi(b,z) = \exp\left[-\frac{i}{\hbar v}\int_{-\infty}^{z} dz'\ V(b,z')\right] = e^{i\chi(b,z)}. \tag{7.44}$$

This is a very simple equation, in which the second equality is just a definition of the quantity $\chi(b,z)$. Re-inserting at this point intrinsic coordinates and wave functions the proper definition of $\chi(b,z)$ becomes

$$\chi(b,z) = -\frac{1}{\hbar v}\int_{-\infty}^{z} dz'\ \langle f|V(b,z')|i\rangle. \tag{7.45}$$

We now show how to deduce the elastic cross section. In this case, the quantity that enters the above equation for $\chi(b,z)$ is $\langle 0|V|0\rangle$, and this can be written as U as we did in our previous discussion.

$$\begin{aligned} f_{\rm eiko}(\theta) &= -\frac{\mu}{2\pi\hbar^2}\int d^3R'\ e^{-i\mathbf{k}'\cdot\mathbf{R}'}\ U\ e^{ikz}e^{i\chi(b,z)} \\ &= -\frac{\mu}{2\pi\hbar^2}\int d^2b\ e^{i(\mathbf{k}-\mathbf{k}')\cdot\mathbf{b}}\ \int dz\ e^{i(k_z-k'_z)z}\ U\ e^{i\chi(b,z)}. \end{aligned} \tag{7.46}$$

We shall use the approximation that the momentum variation is small enough so that it is perpendicular to z. Then, $\mathbf{k}-\mathbf{k}'$ has only component parallel to $\mathbf{b}$ and the last integral of (7.46) simplifies to

$$\begin{aligned} &\int_{-\infty}^{+\infty} dz\ U\ e^{-\frac{i}{\hbar v}\int_{-\infty}^{z} dz'\ U} = i\hbar v\left(e^{-\frac{i}{\hbar v}\int_{-\infty}^{+\infty} dz'\ U} - 1\right) \\ &= i\hbar v\left(e^{i\chi(b)} - 1\right), \end{aligned} \tag{7.47}$$

where the last step is a definition of $\chi(b) \equiv \chi(b, z = +\infty)$. With this simplification, and the usual definition of the momentum transfer already given,

$$f_{\rm eiko}(\theta) = -\frac{ik}{2\pi}\int d^2b\ e^{i\mathbf{q}\cdot\mathbf{b}}\left(e^{i\chi(b)} - 1\right). \tag{7.48}$$

Finally, if ϕ is the angle around z, we express the integral in d^2b as $db\ b\ d\phi$ and we use the definition of the Bessel function J_0 in terms of

$$\int_0^{2\pi} d\phi\ e^{iqbcos\phi} = 2\pi J_0(qb).$$

We arrive at the final equation

$$f_{\rm eiko}(\theta) = -ik \int db\ b\ J_0(qb) \left(e^{i\chi(b)} - 1\right). \tag{7.49}$$

The two equations (7.44) and (7.49) provide the full solution of the elastic cross section in the eikonal approximation, by means of just two simple one-dimensional integrals. Of course the elastic cross section is just $|f(\theta)|^2$.

7.4 Inelastic scattering

7.4.1 General considerations and kinematics

Inelastic scattering experiments are, as a rule, carried out with the aim of obtaining information on the excitation spectra of nuclei (vibrational states, rotational bands, or other kinds of excitations). The main problem is the reaction selectivity. If we produce a beam with given energy, and the particles interact with target nuclei, in the simplest possible experimental set-up only the energy lost by the projectile is measured, together with the scattering angle. First, it would be relevant to make sure that only one of the two nuclei, say the target[8] is excited. To this aim, one can use as a projectile either protons, or α-particles that do not have excited states below 20 MeV, or other nuclei that allow distinguishing in some way the case of projectile excitation[9].

Another issue is that, even if one is sure to deal only with target excitation, the identification of the quantum numbers of the excited states is not straighforward. At times, this can be done only with the guidance of theoretical calculations, or of systematics. In the case of spherical nuclei, J and the parity π are good quantum numbers as we have stressed already. To a good approximation, we can also consider L and S as valid quantum numbers. If the nucleus is even-even, $J = L = S = 0$ in the ground-state, and we can identify J, L and S both with the quantum numbers of the final state and with those exchanged in the projectile-target interaction [that can

[8] We have in mind the usual configuration in which stable nuclei are studied. Of course, in the case of exotic nuclei that are produced in-beam, the situation is reversed and the roles of projectile and target in this and in the following sentences should be exchanged.

[9] In the case of ^{17}O, just to make one example, the low energy threshold for neutron emission allows studying the target excitations above that threshold without ambiguity.

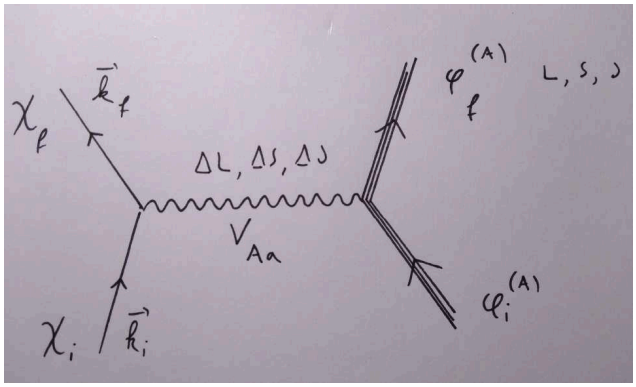

Figure 7.5: Representation in terms of a Feynman diagram of the projectile-target interaction in the case of inelastic scattering. We are assuming that the initial state of the target, whose associated wave function is $\phi_i^{(A)}$, has $L = S = J = 0$ and that the final state, $\phi_f^{(A)}$, has L, S, J. These coincide with the quantum numbers labelled by $\Delta L, \Delta S, \Delta J$, as discussed in the text.

be labelled as ΔJ, ΔL and ΔS, respectively (cf. Fig. 7.5)]. We may add isospin to this discussion although we shall not do it for the sake of simplicity. The main specific aspect that is at variance with the case of the other quantum numbers, is that most of the nuclei have $T \neq 0$ in the ground state. Thus, we cannot identify ΔT wih the isospin of the final state.

The selectivity in ΔS can be achieved in few cases. For instance, α-particles are widely used in inelastic scattering experiments because they lead exclusively to $S = 0$ states[10]. As for ΔL, in order to estimate it we can use semi-classical considerations. The angular momentum of the relative motion will be written (in units of $\hbar$) as kb, where b is the impact parameter. If we equate the angular momentum acquired by the nucleus, ΔL, with the angular momentum lost in the relative motion, then

$$\Delta L = \Delta k \cdot b = qR. \tag{7.50}$$

In the last step we have assumed a so-called "grazing" collision, that is, we have replaced the impact parameter with the target radius. We make another simplifying approximation: we assume that inelastic scattering is performed at sufficiently high energy so that the absolute value of $\mathbf{k_f}$, although smaller than $\mathbf{k_i}$, can be confused with it. Thus, using a common symbol k for the

[10] $\Delta T = 0$ is also guaranteed.

absolute value of those vectors,

$$\Delta L^2 = (k_i^2 + k_f^2 - 2\mathbf{k_i} \cdot \mathbf{k_f}\ cos\theta)R^2 \approx 4k^2 sin^2\frac{\theta}{2}\ R^2. \tag{7.51}$$

For small angles, where $sin\theta$ can be replaced by θ,

$$\Delta L \approx kR\theta. \tag{7.52}$$

One can identify ΔL from the angle θ at which the angular distribution has a maximum for a given excitation energy (the excitation energy coincides with the energy lost by the projectile).

As an example, we could consider α particles having energy $E = 172$ MeV. The value of k can be calculated from $\sqrt{2\mu E}/\hbar$ and turns out to be approximately 5.8 fm^{-1}. From Eq. (7.52) we learn that, for e.g. Sn nuclei that have a radius of about 6 fm, the cross section should be peaked at 3.3 degrees for $\Delta L = 2$. In this way, it has been possible to identify the main peak appearing in Fig. 7.6 as the Giant Quadrupole Resonance as it shows up at 4 degrees.

7.4.2 The Distorted Wave Born Approximation (DWBA)

Let us start again from the general expression for the scattering amplitude (7.23) that we have provided above:

$$f(\theta) = -\frac{\mu}{2\pi\hbar^2}\int d^3R'\ e^{-i\mathbf{k'}\cdot\mathbf{R'}}\ \langle f|V|i\rangle\ \Psi_{\mathbf{k}}(\mathbf{R'}).$$

Now i and f are typically the ground-state and some excited state of one of the colliding particles, respectively (as discussed in the previous subsection). The quantity $\langle f|V|i\rangle$ is called *inelastic form factor* or *transition amplitude* T_{fi}. As in the elastic case, it depends only on the coordinate $\mathbf{R'}$ as the integration on the internal coordinates has been performed.

We can use approximations that are the same as we have already discussed in the case of elastic scattering. For instance, PWBA or the eikonal approximation can be used. In the case of PWBA, the scattering amplitude will be proportional to the Fourier transform of the inelastic form factor.

However, the most widely used approximation is the Distorted Wave Born Approximation (DWBA). It relies on the numerical solution of the elastic scattering with an Hamiltonian

$$H = H_0 + V_{\rm opt}, \tag{7.53}$$

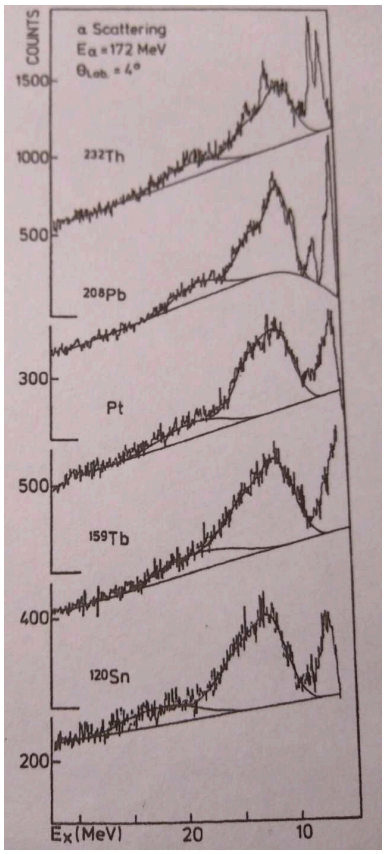

Figure 7.6: Energy spectra of inelastically scattered α-particles having a bombarding energy of 172 MeV and a scattering angle of 4 degrees. Taken from [39].

where H_0 has been given in Eq. (7.5) (it includes the kinetic energy of the relative motion and the two intrinsic Hamiltonian) while $V_{\rm opt}$ is an effective interaction that is chosen so that the elastic scattering solution is known and reproduces experiment at best. In other words, this operator is chosen so that $\langle 0|V_{\rm opt}|0\rangle$ corresponds to $U_{\rm opt}$ of Eq. (7.35). The complete Hamiltonian will be

$$H = H_0 + V_{\rm opt} + (V - V_{\rm opt})\,, \tag{7.54}$$

and the treatement of Sec. 7.2 can be repeated as it is, but with H_0 replaced by $H_0 + V_{\rm opt}$ in the role of the unperturbed Hamiltonian and V replaced by $V - V_{\rm opt}$ in the role of the perturbation.

The eigenfunctions of $H_0 + V_{\rm opt}$, that replace the plane waves (eigenfunctions of H_0), are usually denoted by χ and called *distorted waves*. The quantity $V - V_{\rm opt}$ is written as V for simplicity. If we then write the corresponding equation of (7.23) with the unknown wave funtion Ψ replaced by

χ, and $V - V_{\rm opt}$ rewritten simply as V, we obtain

$$f_{\rm DWBA}(\theta) = -\frac{\mu}{2\pi\hbar^2}\int d^3R'\ \chi^*_{\mathbf{k}'}(\mathbf{R}')\ \langle f|V|i\rangle\ \chi_{\mathbf{k}}(\mathbf{R}'). \qquad (7.55)$$

This is the DWBA expression for the transition amplitude.

Within all possible approximations, we remind that the cross section is given by

$$\frac{d\sigma}{d\Omega} = \frac{k_f}{k_i}|f(\theta)|^2. \qquad (7.56)$$

We complete this Section with two specific examples. In the next subsection we treat the special case of Coulomb excitation, in which the external perturbation is exactly known. In the following and last subsection, we show how, within the PWBA, the nuclear excitation can be treated in a simple way, so that the excitation cross section is proportional to the strength associated with simple operators. This latter argument has a pedagogical value. It shows that there is a relationship between the cross section and the transition matrix elements associated with the operators F that have been introduced in Sec. 4.3.

7.4.3 Coulomb excitation

We assume that we are able to single out scattering events in which the impact parameter is large and, thus, only the long-range Coulomb force is active. We also assume that the projectile remains in its ground-state, and its action within the form factor is the same as that of a point charge Z_a. Under this hypothesis, we can write the form factor in terms of the degrees of freedom of the target only, that is,

$$\begin{aligned} T_{fi} &\equiv \langle f|V_{\rm Coul}|i\rangle \\ &= \int d^3r_1 \ldots d^3r_A\ \phi_f^{(A)*}(\vec{r}_1 \ldots \vec{r}_A)\ V_{\rm Coul}\ \phi_i^{(A)}(\vec{r}_1 \ldots \vec{r}_A). \end{aligned} \qquad (7.57)$$

We work again within the independent particle approximation. The description of nuclear excited states in terms of a superposition of single-particle excitations has already been carried out in Sec. 4.3. In this spirit, the operator $V_{\rm Coul}$ plays exactly the role of F, that has been introduced in Eq. (4.4). If we call $|LM\rangle$ the excited state (using the quantum numbers that

are appropriate in the case of a spherical nucleus), and we use (4.29) and the related equations, then

$$\begin{aligned} T_{fi} &= \langle LM|V_{\rm Coul}|0\rangle = \sum_{\rm ph} X_{\rm ph}\langle ph^{-1}|V_{\rm Coul}|0\rangle \\ &= \sum_{\rm ph}\langle 0|\delta\rho|ph^{-1}\rangle\langle ph^{-1}|V_{\rm Coul}|0\rangle = \int d^3r\ V_{\rm Coul}(\vec{R}-\vec{r})\delta\rho_{LM}(\vec{r}), \end{aligned} \tag{7.58}$$

where the completeness relation has been used in the last step. The quantity $\delta\rho$ is usually called *transition density*. It must have the form

$$\delta\rho(\vec{r}) = \delta\rho_{LM}(\vec{r}) = \delta\rho_{LM}(r)\ Y^*_{LM}(\hat{r}), \tag{7.59}$$

because the density variation associated with the creation (annihilation) of a state with angular momentum LM must involve the function Y^*_{LM} (Y_{LM}).

It is useful, at this point, to expand the Coulomb interaction into multipoles,

$$\begin{aligned} V_{\rm Coul}(\vec{R}-\vec{r}) &= \frac{e^2Z_AZ_a}{|\vec{R}-\vec{r}|} \\ &= e^2Z_AZ_a\ \sum_{\lambda\mu}\frac{4\pi}{2\lambda+1}\frac{r^\lambda_<}{r^{\lambda+1}_>}Y^*_{\lambda\mu}(\hat{R})Y_{\lambda\mu}(\hat{r}), \end{aligned} \tag{7.60}$$

where $r_<$ ($r_>$) are the smaller (larger) between r and R. In the case under study, clearly $r_> = R$ and $r_< = r$, so that the previous equation (7.58) becomes

$$\begin{aligned} T_{fi} &= e^2Z_AZ_a\ \sum_{\lambda\mu}\frac{4\pi}{2\lambda+1}\int d\hat{r}\ Y_{\lambda\mu}(\hat{r})Y^*_{LM}(\hat{r})\ \frac{1}{R^{\lambda+1}}Y^*_{\lambda\mu}(\hat{R})\ \int dr\ r^{\lambda+2}\ \delta\rho_{LM}(r) \\ &= \frac{4\pi e^2Z_AZ_a}{2L+1}\frac{1}{R^{L+1}}Y^*_{LM}(\hat{R})\ \int dr\ r^{L+2}\delta\rho_{LM}(r). \end{aligned} \tag{7.61}$$

If this form factor is inserted into a reliable expression for the scattering amplitude, it is clear that the only unknown is the transition density. In other words, due to the fact that the Coulomb interaction is known, the measurement of the cross section for Coulomb excitation allows a direct determination of the transition density of the excited state.

An example is that of the excitation of small-amplitude surface modes. A small variation of the density can be taken as proportional to its derivative, that is, one can assume

$$\delta\rho_{LM} \equiv \beta_L \, \frac{d\rho_0}{dr}, \tag{7.62}$$

where ρ_0 is the g.s. density and β_L is the only free parameter, that can be determined by means of a fit to experimental data.

7.4.4 Plane Wave Born Approximation (PWBA) with a zero-range force

The use of the PWBA and of a projectile-target interaction which is proportional to a Dirac delta is not realistic but has a pedagogical value, as we will show at the end. The interaction V can be expanded in multipoles, in analogy with Eq. (7.60), as

$$V(\vec{R}-\vec{r}) = V_0\delta(\vec{R}-\vec{r}) = \sum_{\lambda\mu} \frac{\delta(r-R)}{r^2} Y_{\lambda\mu}(\vec{r}) Y^*_{\lambda\mu}(\vec{R}). \tag{7.63}$$

The form factor can be obtained in the same way that has led to Eq. (7.61) and becomes

$$T_{fi} = V_0 \; \delta\rho_{LM}(R) \; Y^*_{LM}(\hat{R}). \tag{7.64}$$

We now calculate the scattering amplitude within PWBA, that is,

$$f(\theta) = -\frac{\mu}{2\pi\hbar^2} \int d^3R' \; e^{i\vec{q}\cdot\vec{R}'} T_{fi}(\vec{R}'). \tag{7.65}$$

We employ, accordingly, the development (7.32) and obtain

$$f(\theta) = -\frac{2\mu}{\hbar^2} i^L Y^*_{LM}(\hat{q}) \; V_0 \; \int dR' \; R'^2 j_L(qR) \delta\rho_{LM}(R). \tag{7.66}$$

Often, the momentum transfer is such that over the distance scale in which the transition density is not negligible (typically, the scale associated with the nuclear surface) the condition $qR \ll 1$ holds. The spherical Bessel functions for small arguments behave as $j_L(qR) \approx (qR)^L$, and the scattering amplitude can be written

$$f(\theta) = -\frac{2\mu}{\hbar^2} i^L q^L V_0 \; Y^*_{LM}(\hat{q}) \; \int dR' \; R'^{L+2} \; \delta\rho_{LM}(R), \tag{7.67}$$

so that the corresponding cross section becomes

$$\begin{aligned}\frac{d\sigma}{d\Omega} &= \frac{k_f}{k_i}\frac{4\mu^2 q^{2L} V_0^2}{(2L+1)\hbar^4}\sum_M Y^*_{LM}(\hat{q})Y_{LM}(\hat{q}) \mid \int dR' \; R'^{L+2} \; \delta\rho_{LM}(R)|^2 \\ &= \frac{k_f}{k_i}\frac{\mu^2 q^{2L} V_0^2}{\pi\hbar^4} \mid \int dR' \; R'^{L+2} \; \delta\rho_{LM}(R)|^2. \end{aligned} \tag{7.68}$$

We have supposed that the cross section is averaged over all possible final M-substates since we are unable to distinguish them with unpolarised beams and targets. It turns out that the cross section is proportional, via known factors, to the square of the radial matrix element associated with the action of an operator like R'^L. This operator has the same form as the electric multipole operator that we have introduced in (6.13).

This decomposition in two factors, a kinematical one and the square of the action of a radial multipole operator, is strictly speaking only valid within this not fully realistic plane-wave approximation; however, it possesses a conceptual validity as a guideline even for more realistic cases.

7.A Appendices

7.A.1 Tranformation between the LAB and COM system for the incident energy

We consider a reaction of the type (7.1) and we assume that A is at rest in the LAB system, while a impinges on it with a kinetic energy $T^{(\mathrm{LAB})} \equiv \frac{1}{2}M_a v_a^2$. The origin of the COM system is defined by the coordinate,

$$\vec{r}_{\mathrm{COM}} = \frac{M_A\vec{r}_A + M_a\vec{r}_a}{M_A + M_a}, \tag{7.69}$$

and its velocity by

$$\vec{v}_{\mathrm{COM}} = \frac{M_a\vec{v}_a}{M_A + M_a}. \tag{7.70}$$

The Galilean transformations provide the velocities of A and a in the COM systems, that are

$$\begin{aligned}\vec{v}_a^{(\mathrm{COM})} &= \vec{v}_a - \vec{v}_{\mathrm{COM}} = \frac{M_A\vec{v}_a}{M_a + M_a}, \\ \vec{v}_A^{(\mathrm{COM})} &= -\vec{v}_{\mathrm{COM}} = -\frac{M_a\vec{v}_a}{M_A + M_a}. \end{aligned} \tag{7.71}$$

From this latter equation, the sum of the kinetic energies in the COM frame results as

$$\begin{aligned}\sum_i T_i^{(\mathrm{COM})} &= \frac{1}{2}M_a\frac{M_A^2 v_a^2}{(M_A+M_a)^2}+\frac{1}{2}M_A\frac{M_a^2 v_a^2}{(M_A+M_a)^2} \\ &= \frac{1}{2}\frac{M_A M_a}{M_A+M_a}v_a^2 = \frac{M_A}{M_A+M_a}T^{(\mathrm{LAB})} \approx \frac{A}{A+a}T^{(\mathrm{LAB})},\end{aligned} \tag{7.72}$$

where in the last step we have approximated the masses with the mass numbers. The quantity $\frac{M_A M_a}{M_A+M_a}$ is the reduced mass μ.

Chapter 8

Compound nucleus reactions

At low energy, particles that participate to the reaction have quite a long time to interact with one another. As a consequence, one can imagine that a complete thermalization takes place, that is, the energy brought into the projectile plus target compound system by the relative motion is shared by all nucleons, like in the case of the equipartition that defines the concept of temperature. This picture, in which the system that has been formed has also, by definition, lost memory of the initial reaction, is the so called *compound nucleus* hypothesis. There are experimental evidences for such a picture, so that the concept of nuclear temperature can be defined.

Before coming to it in some detail, we describe specifically neutron reactions and charged particles reactions in the next two subsections. There is a crucial difference between the two cases since these reactions take place at incident energies below the Coulomb barrier. What is common to the different cases is that compound nucleus reactions are isotropic (memory is also lost regarding the incident projctile direction). Thus, we shall discuss total cross sections instead of angular distributions.

8.1 Neutron reactions

We shall discuss these reactions by means of one example, and extrapolating from it their general features. The example of neutrons on ^{16}O is displayed in Fig. 8.1. The main feature of the cross section is the presence of narrow peaks, called *resonances*. We expect them to correspond to excited states in ^{17}O. The relation between the incident neutron energy T_n and the excitation

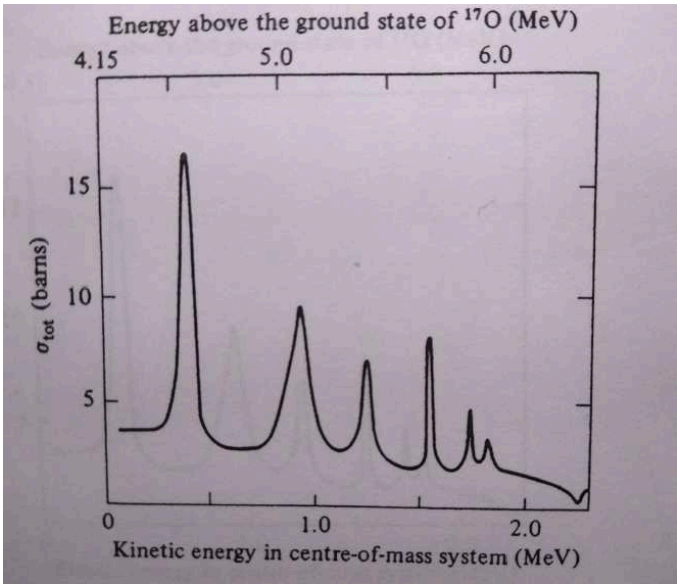

Figure 8.1: Total cross section for neutrons interacting with ^{16}O as a function of the center-of-mass energy. Figure taken from [47].

energy E_x in this nucleus reads

$$T_n - \mathrm{BE}(^{16}\mathrm{O}) = E_\mathrm{x} - \mathrm{BE}(^{17}\mathrm{O})$$
$$E_\mathrm{x} = T_n + \mathrm{BE}(^{17}\mathrm{O}) - \mathrm{BE}(^{16}\mathrm{O}) \approx T_n + 4.15 \text{ MeV}.$$

The excitation energy can be read from the upper scale in Fig. 8.1. It is straighforward, for instance, to identify the first peak in the figure with the state at 4.56 MeV in ^{17}O having spin and parity $3/2^-$. This peak has a width Γ of about 0.04 MeV. The associated half-life is therefore $\tau = \hbar/\Gamma \approx 10^{-20}$ s. If we compare this time with the interaction time defined above in Eq. (7.4), we see that this latter is of the order of 10^{-22} s. In other words, the system lives much longer than the time scale on which it is formed. Therefore, we use time-dependent perturbation theory to describe its formation and subsequent decay.

In this Section we call 1, 0, and f, respectively, the initial channel of the reaction (neutron plus ^{16}O in the example under study), the state that is formed (excited state of ^{17}O), and the final state of the decay. There are, in general, different final states available. The compound nucleus can decay through neutron emission, proton emission (although this hindered by the

Coulomb barrer) and γ-decay (this is less likely because it is an electromagnetic decay). f labels a specific final state but we often do not detect the specific final state. Nevertheless, we shall calculate the *inclusive* or *exclusive* cross section, respectively: the former corresponds to all possible final state decays and the latter is associated with a specific decay channel. For the sake of simplicity, we shall do it first by neglecting the intrinisic degrees of freedom of the particles, i.e. their spins. Spin factors will be added at the end of the derivation.

The general equation of time-dependent perturbation theory, from quantum mechanics textbooks, reads

$$i\hbar\dot{a}_n = \sum_{m\neq n} V_{mn} e^{-i(E_m-E_n)t/\hbar} a_m, \tag{8.1}$$

where m, n are eigenstates of the unperturbed Hamiltonian H_0 (in this case, the one corresponding to the non-interacting neutron and ^{16}O) with corresponding energies E, a labels the probability amplitudes to find the interacting system in the given state, and V is the interaction. In the case under study, we could imagine a simple Woods-Saxon potential for the neutron-nucleus potential but the following derivation is more general. If we restrict to the states 1 and 0, the previous equation becomes

$$i\hbar\dot{a}_0 = V_{01} e^{-i(E_1-E_0)t/\hbar} a_1. \tag{8.2}$$

In this case $a_0^2 + a_1^2 = 1$ and, while $a_0(t=0) = 0$ and $a_1(t=0) = 1$, we also assume that a_0 will remain quite small and we can approximate a_1 as being 1 for all times. These assumptions, that go together with the more general one of stopping time-dependent perturbation theory at the lowest (i.e., first) order, shoud be checked *a posteriori*.

We do not want at this stage to consider the possible final states as explicit states. We would just like to consider the possibility that, once in the state 0, the system can decay to the set of states f with a total width Γ that we can measure experimentally. It is a simple exercise to show that this decay can be simply taken into account by changing the latter equation (8.2) into

$$i\hbar\dot{a}_0 = V_{01} e^{-i(E_1-E_0)t/\hbar} a_1 - i\frac{\Gamma}{2} a_0. \tag{8.3}$$

In fact, if we integrate the equation

$$i\hbar\dot{a}_0 = -i\frac{\Gamma}{2} a_0 \tag{8.4}$$

we easily find $a_0 = e^{-\frac{\Gamma}{2\hbar}t}$ that corresponds to $a_0^2 = e^{-t/\tau}$ with $\tau = \hbar/\Gamma$. We then go back and integrate Eq. (8.3). The solution is

$$a_0(t) = V_{01}\frac{e^{-\frac{i}{\hbar}(E_1-E_0)t} - e^{-\frac{\Gamma}{2\hbar}t}}{E_1 - E_0 + i\frac{\Gamma}{2}}. \tag{8.5}$$

The last term in the numerator can be neglected for large values of t. Then,

$$|a_0(t)|^2 = \frac{|V_{01}|^2}{(E_1 - E_0)^2 + \frac{\Gamma^2}{4}}. \tag{8.6}$$

This expression shows already the existence of a resonant-shape excitation probability. We are, nonetheless, interested in the cross section rather than in the probability of exciting each single state; also, we would like to get rid of the matrix element V_{01} of the potential V, in order to express the result in terms of measurable quantities only. To do so, we consider the full process that includes the decay, $1 \to 0 \to f$. The number of events per unit time (i.e., the transition rate R) is equal to the probability amplitude to excite the state 0, divided by the half-life for the process $0 \to f$:

$$R_{1\to 0\to f} = |a_0(t)|^2\frac{1}{\tau_{0\to f}} = \frac{|V_{01}|^2}{(E_1 - E_0)^2 + \frac{\Gamma^2}{4}}\frac{\Gamma_f}{\hbar}. \tag{8.7}$$

The trick is now to select the decay back to the initial state 1, that obeys the Fermi Golden Rule

$$\Gamma(E_1) = 2\pi|V_{10}|^2 n(E_1). \tag{8.8}$$

We have preferred to label the state with its energy E_1 rather than simply with 1. One reason is that we need the density of states $n(E_1)$. This can be calculated by assuming that the states of the impinging particle are quantized in a box having volume Ω. An elementary calculations proves that

$$n(E_1) = \frac{\Omega}{(2\pi)^3}4\pi k^2\frac{1}{\hbar v}, \tag{8.9}$$

where k is such that $\frac{\hbar k^2}{2\mu} = E_1$ and v is the associated velocity. Finally, the cross section is the transition rate R divided by the incident flux. The flux, with one particle in a box having volume Ω as we have assumed so far, is v/Ω. Therefore, we write

$$\sigma(1 \to 0 \to f) = \frac{\Omega}{v}R_{1\to 0\to f}, \tag{8.10}$$

and we insert here the expression of the transition rate (8.7), with the matrix element $|V_{01}|^2$ written by means of Eq. (8.8) and, then, the density of states $n(E_1)$ taken from Eq. (8.9). The result is

$$\sigma(1 \to 0 \to f) = \frac{\pi}{k^2} \frac{\Gamma(E_1)\Gamma_f}{(E_1 - E_0)^2 + \frac{\Gamma^2}{4}}. \tag{8.11}$$

As it has been anticipated, spin factors are missing, so that the previous equation is, strictly speaking, only valid for collisions between two nuclei having spin zero. It is easy to insert the spin factors, as the cross section is expected to depend on a sum over final states and average over initial states. Therefore, if the initial particles are in the spin states j_1 and j_2, respectively, and the compound nucleus has spin j, we can write

$$\boxed{\sigma(1 \to 0 \to f) = \frac{\pi}{k^2} \frac{(2j+1)}{(2j_1+1)(2j_2+1)} \frac{\Gamma(E_1)\Gamma_f}{(E_1 - E_0)^2 + \frac{\Gamma^2}{4}}.} \tag{8.12}$$

The formula is called *Breit-Wigner*. As we have mentioned, in many instances the exclusive cross section is not measured. The inclusive cross section, or total one, is simply the sum of the cross secions to the various final states. The only factor in (8.12) that depends on f is Γ_f. Since $\sum_f \Gamma_f = \Gamma$, we immediately deduce

$$\boxed{\sigma(1 \to 0) = \frac{\pi}{k^2} \frac{(2j+1)}{(2j_1+1)(2j_2+1)} \frac{\Gamma(E_1)\Gamma}{(E_1 - E_0)^2 + \frac{\Gamma^2}{4}}.} \tag{8.13}$$

This formula for the inclusive cross section explains indeed Fig. 8.1 above. In this figure one can see several resonances, each of one can be interpreted with the formula (8.13) and the height of the peaks decreases as the factor $\sim \frac{1}{k^2}$ predicts. Although Fig. 8.1 refers to a specific case, neutron resonances exist in all nuclei. The key point is that as the mass number increases the density of such resonances increases. When they overlap, the treatment in terms of independent resonances is no longer valid.

8.2 Charged particles reactions

In order to appreciate the difference with the case of the previous Section, let us now assume to form the nucleus ^{17}O in a different reaction like α+^{13}C.

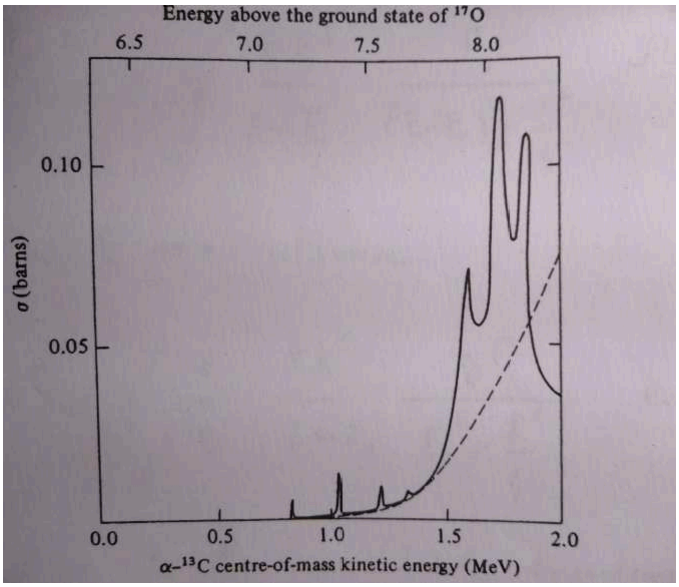

Figure 8.2: Total cross section for α-particles interacting with ^{13}C as a function of the center-of-mass energy. Figure taken from [47]. See the text for a discussion, in particular for an explanation of the exponential dashed curve.

We expect to populate the same states, i.e. to find the same resonances of the compound system. The resonances should be at the same excitation energy in the compound nucleus: this clearly implies a different center-of-mass energy, that is readily obtained by applying to this case the equation analogous to Eq. (8.1) above.

However, the resulting cross section displayed in Fig. 8.2 displays those peaks on top of an exponential background (the dashed curve) that makes them negligibly small as the energy decreases. We recognize the signature of the Coulomb barrier penetration. In fact, the Coulomb barrier height is generally given by

$$V_B = \frac{e^2 Z_A Z_a}{R_A + R_a}, \tag{8.14}$$

and at low energy the charged particle must tunnel this barrier. The probability P for tunneling is invariant under time-reversal, that is, it is the same

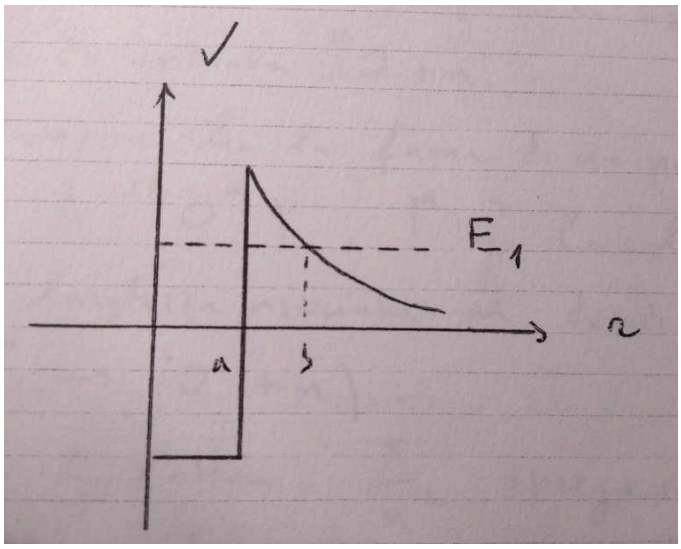

Figure 8.3: Schematic plot for the barrier penetration. See the text for a discussion.

that has been calculated for the α-decay:

$$\begin{aligned} P &= e^{-2G} \\ G &= \sqrt{\frac{2\mu}{\hbar^2}} \int_a^b dr \ [V(r) - E_1]^{1/2} . \end{aligned} \tag{8.15}$$

The barrier is assumed here to be spherically symmetric and its radial shape is depicted in Fig. 8.3. a and b are the inner edge of the barrier and the outer edge associated with the incident energy E_1, respectively, and μ is the reduced mass. In the case of α-decay, if τ_0 is the typical time interval between successive encounters with the barrier, the transition rate is

$$R = \frac{1}{\tau_0} P = \frac{1}{\tau_0} e^{-2G}, \tag{8.16}$$

and the half-life is then

$$\tau = \tau_0 e^{2G}. \tag{8.17}$$

If we identify this with $\hbar/\Gamma(E_1)$ in Eq. (8.13), we obtain from it

$$\boxed{\sigma(1 \to 0) = \frac{\pi\hbar}{k^2} \frac{(2j+1)}{(2j_1+1)(2j_2+1)} \frac{\Gamma}{(E_1 - E_0)^2 + \frac{\Gamma^2}{4}} \frac{e^{-2G(E_1)}}{\tau_0},} \tag{8.18}$$

where the exponential form has been put in evidence. As $G(E_1)$ is manifestly a decreasing function of E_1, the cross section exponentially increases as shown in Fig. 8.2. In the next Chapter, we shall study the case of $E_1 \to 0$, evaluate and use the factor $G(E)$ in that case.

8.3 Experimental findings and the nuclear temperature

The compound nucleus hypothesis was proposed by Niels Bohr back in 1936. It has been verified much later in many cases. As we stated at the start of the Chapter, according to this hypothesis the reaction process is slow enough so that the participating nuclei form a compound system in which energy and angular momentum are statistically shared among all nucleons. In this situation, no memory is kept about the initial state: the decay is independent from the initial state. One example is provided by the two reactions

$$\begin{aligned} \mathrm{p} + {}^{63}\mathrm{Cu} &\to {}^{64}\mathrm{Zn}^* \\ \alpha + {}^{60}\mathrm{Ni} &\to {}^{64}\mathrm{Zn}^*. \end{aligned}$$

It has been proved [48] that the final decays of the compound nucleus ^{64}Zn*, like ^{63}Zn+n, ^{62}Zn+2n, ^{62}Cu+n+p ... have the same cross section in the two reactions provided the compound nucleus is formed at the same excitation energy.

In this respect, the Breit-Wigner formula (8.12) can be factorized as

$$\begin{aligned} \sigma(1 \to 0 \to f) &= \sigma(1 \to 0)\ B_f, \\ B_f &= \frac{\Gamma_f}{\Gamma}, \end{aligned} \tag{8.19}$$

where $\Gamma(E_1)$ has been simply written as Γ and B_f is the *branching ratio*. As we said before, we expect that neutron and proton decays are possible only above threshold, but as soon as they are possible $\Gamma_n \gg \Gamma_p \gg \Gamma_\gamma$. In many cases one can approximate Γ with Γ_n, or B_n with 1.

Let us now assume that one can measure the energy spectrum of the emitted neutrons. The assumption of nuclear thermalization is supported by those cases in which the neutrons obey the energy dependence which can be expected in case of a thermalized source, i.e. they obey a Maxwell-Boltzmann distribution like

$$n(E)dE \sim \sqrt{E}\ e^{-E/T} dE, \tag{8.20}$$

where $n(E)$ is the number of neutrons with energy between E and $E + dE$, the normalization is omitted for the sake of simplicity, and the temperature T is written in units of MeV. Whenever the experimental energy spectra are fitted by a curve of the type (8.20), one can extract a value for T from the fit. Since the compound nucleus excitation energy E is known, the purpose is now to find a relation between E and T.

In a standard thermodynamic picture one would expect

$$\begin{aligned} \frac{1}{T} &= \frac{dS}{dE}, \\ S &= ln\ \omega(E), \end{aligned} \tag{8.21}$$

where S is the entropy and $\omega(E)$ is the density of states at the energy E. In principle, it is possible to calculate with modern nuclear structure methods the density of states. A schematic calculation that can be done analytically, albeit with some effort, is based on the Fermi gas model. The key parameter in this case is the single-particle level density at the Fermi surface g_0. This is the inverse of the gap between the last occupied and first unoccupied state. We write, in the case of $N = Z = A/2$,

$$\frac{\delta\varepsilon}{\varepsilon} = 2\frac{\delta k}{k} = \frac{2}{3}\frac{\delta A}{A}, \tag{8.22}$$

where ε is a s.p. energy, $\varepsilon = \frac{\hbar^2 k^2}{2m}$, and the last equality follows if we take k around k_F and we use Eq. (2.30) since of course ρ is proportional to A. The latter equation, in the case $\delta A = 1$ and $\varepsilon = \varepsilon_F$ provides

$$\delta E = \frac{2}{3}\frac{\varepsilon_F}{A} \quad \Rightarrow \quad g_0 = \frac{3}{2}\frac{A}{\varepsilon_F}. \tag{8.23}$$

A parameter which is proportional to the single-particle level density around the Fermi energy, and which is defined for the sake of practicity, is

$$a = \frac{\pi^2}{6}\frac{3}{2}\frac{A}{\varepsilon_F}. \tag{8.24}$$

At this point, one should count in how many ways particles can be distributed on the single-particle energy levels of the Fermi gas in such a way that the difference between the total energy of the nucleus and that of the g.s. is

equal to E. Although tedious, this counting can be accomplished (cf. the Appendix 2B in [49]) and the result is

$$\omega(A, E) = \frac{6^{1/4} g_0}{12(g_0 E)^{5/4}} e^{2\sqrt{aE}}. \tag{8.25}$$

If we use this result, by keeping only the dominant exponential dependence on E, to obtain the temperature from Eq. (8.21) we arrive simply at the equation

$$E = aT^2. \tag{8.26}$$

While the theoretical value in the case of the Fermi gas calculation is $a = A/16$ MeV^{-1}, experiments give values of the order of $a = A/8$ MeV^{-1}.

Chapter 9

Selected topics in Nuclear Astrophysics

This Chapter is not intended to give a complete view of the broad domain of Nuclear Astrophysics, to which numerous available textbooks are devoted. Rather, we shall just illustrate a few pedagogical cases in which nuclear physics is highly instrumental to tackle and solve astrophysical problems.

9.1 Nuclear reactions inside stars

9.1.1 The origin of the energy emitted by the sun

There are simple arguments that show that the sun cannot produce energy but through nuclear reactions. The solar luminosity, $L_\odot$, is known to be about $3.83\ 10^{26}$ W. Let us assume that this energy is the outcome of usual chemical reactions. As an example, we take the reaction

$$\mathrm{C}\ +\ \mathrm{O}_2\ \rightarrow\ \mathrm{CO}_2,$$

for which it is known that 1 kg of C provides $3.35\ 10^7$ J. The mass of the sun is known to be $1.99\ 10^{30}$ kg, so that if our closest star were made by one third of C and two thirds of O, the total energy available would be

$$E = \frac{1}{3}\ 1.99\ 10^{30}\ 3.35\ 10^7\ \mathrm{J} = 2.22\ 10^{37}\ \mathrm{J}. \tag{9.1}$$

This energy would be all exhausted within a time t simply given by

$$t = \frac{E}{L_\odot} = 1.8\ 10^3 \text{ y}. \tag{9.2}$$

Obviously this time is too short, and this fact was perceived as a great puzzle already back in the 19th century. We know now that the sun has an age of the order of 10^9 years and the missing factor 10^6 can be understood, after the discovery of the atomic nucleus, as the scale factor between chemical (i.e. atomic) energies of the order of eV and nuclear energies of the order of MeV.

9.1.2 Hydrostatic equilibrium and average properties of the sun

The sun, as other stars, can be thought to be a sphere in hydrostatic equilibrium. We consider the thin region between r and $r + dr$, where a mass $4\pi r^2 dr\rho(r)$ is found if $\rho(r)$ is the density. The gravitational attraction between this mass and the total mass $M(r)$ between zero and r can be written as if $M(r)$ were concentrated in the origin, and reads

$$dF_G = -G\frac{4\pi r^2\rho(r)M(r)dr}{r^2} = -4\pi G\rho(r)M(r)dr, \tag{9.3}$$

where G is the Newton's constant. If we divide the force (9.3) by $4\pi r^2$, we obtain the gravitational pressure that is directed inward (as the minus sign in the latter equation implies) and must be balanced by the difference between internal pressures on the outer and inner edges of the region, $p(r+dr)-p(r)$. This means

$$\frac{p(r+dr)-p(r)}{dr} = \frac{dp(r)}{dr} = -\frac{dF_G}{4\pi r^2 dr} = -G\frac{M(r)\rho(r)}{r^2}. \tag{9.4}$$

This equation, together with the definition of $M(r)$, that is,

$$M(r) = \int_0^r dr'\ 4\pi r'^2\rho(r'), \tag{9.5}$$

could be solved if p as a function of the density were known.

Here, we limit ourselves to the extraction of a few average numbers from our empirical knowledge of the solar properties[1]. We take Eq. (9.4),

$$\frac{dp}{dr} = -G\frac{M(r)\rho(r)}{r^2},$$

[1]The standard solar model (SSM) is described in textbooks and provides a full description of the inner dynamics of the sun.

we multiply both sides by $4\pi r^3$, and integrate from zero to the radius R which is defined as the point where the pressure vanishes. This amounts to writing

$$\int_0^R 4\pi r^3 \frac{dp}{dr} dr = -G \int_0^R \frac{M(r)\rho(r)}{r} 4\pi r^2 dr. \tag{9.6}$$

The r.h.s. is simply the gravitational energy, that is

$$E_{\rm G} = -G \int_0^R \frac{M(r)\rho(r)}{r} 4\pi r^2 dr = -k\frac{GM_\odot^2}{R}, \tag{9.7}$$

where k is 3/5 for a uniform density distribution. We shall approximate $k \approx 1$. The l.h.s can be integrated by parts to give

$$4\pi r^3 p(r)\Big|_0^R - 3\int_0^R p(r) 4\pi r^2 dr = -3\bar{p}V. \tag{9.8}$$

The first term in the l.h.s. is manifestly zero while the second one defines an average pressure $\bar{p}$. Therefore,

$$\bar{p} = -\frac{E_{\rm G}}{3V} \approx \frac{GM_\odot^2}{4\pi R_\odot^4}. \tag{9.9}$$

From the latter equation, and knowing the radius of the sun which is 6.96 10^8 m, one extracts an average pressure of $\approx 10^{14}$ Pa. We can also extract an average temperature by means of the perfect gas equation. If $\bar{m}$ is an average mass of the constituents[2], then

$$\begin{aligned} \bar{p} &= \frac{Nk_BT}{V} = \frac{N\bar{m}}{V}\frac{1}{\bar{m}}k_BT = \frac{\bar{\rho}}{\bar{m}}k_BT, \\ k_BT &= \frac{\bar{p}\bar{m}\frac{4}{3}\pi R_\odot^3}{M_\odot} \approx 0.4 \text{ keV}, \end{aligned} \tag{9.10}$$

where k_B is the Boltzann's constant and $\bar{\rho}$ is the average density. The value of k_BT, although it corresponds to a rather high temperature on the terrestrial scale ($\approx$ millions of K), is quite small on the nuclear scale. In this regime, nuclear reactions are very much below the barrier and are extremely hindered. This explains the long life of the sun (and of the life on Earth, by the way).

[2]The composition of the sun includes about 71% of H, 27% of He as well as small amounts of heavier elements. If only H were present, the average mass of one proton and one electron is ≈ 0.5 amu. Including He we can write $\bar{m} \approx 0.61$ amu.

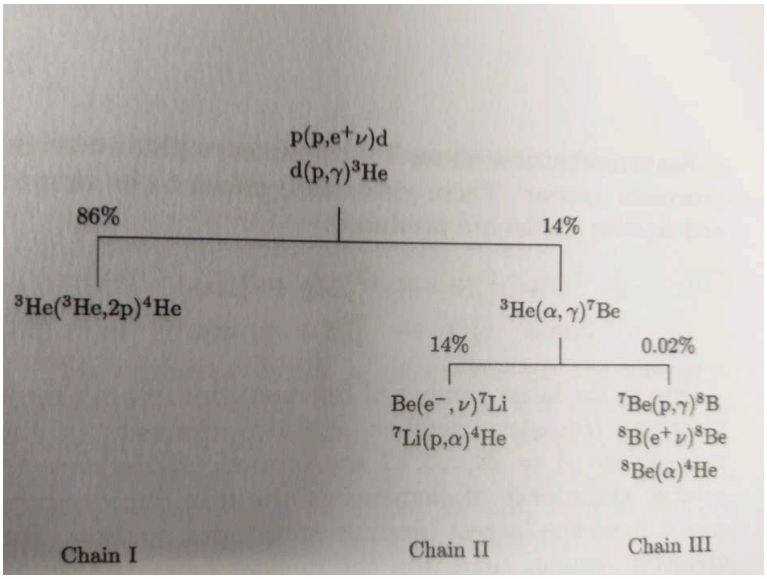

Figure 9.1: Main cycles that contribute to H burning, that is, possible transmutations of H into He, in the sun. Figure taken from [50].

9.1.3 Nuclear reactions in the sun

Bethe and Cricthfield [51] were the first to propose a cycle of reactions that is able to turn H into He. Nowadays, this is known as pp1-cycle. Bethe is also responsible for pointing out the existence of the so-called CNO-cycle, and these discoveries were awarded with the Nobel prize. The pp-cycle reactions are depicted in Fig. 9.1, whereas the CNO cycle is described in specialized textbooks.

9.1.4 The case of other stars

The main observable that determines the properties of a star is its mass. As is evident from our discussion about the sun in 9.1.2, had we taken a star with larger mass we would have found larger values of T and p. In fact, the sun belongs to the low-mass stars (masses equal to 0.4-2 $M_\odot$). It is relatively young, and at the present stage it still converts H into He as we have just decribed in 9.1.3. Stars of this type are prone to exhaust H, contract themselves, increase the values of T, and start burning He. Eventually, they may end up in a white dwarf made up with mainly C and O.

Massive stars behaves quite differently. If we take, as an extreme case, a star that starts from a mass around 25 $M_\odot$, after burning H and He it can further contract due to gravitational forces, increase internal temperature and pressure, and start ignition of heavier elements; thus, such stars go through C-, Ne-, O-, and Si-burning. We do not discuss the details of the nuclear reactions that take place, nor we attempt to estimate the time scales and the amount of energy released.

The only point we want to make here is that in other stars than the sun, obviously different reactions can take place and the temperature can be higher. In the next Section we shall discuss how to estimate the reaction rates of these reactions in a general fashion, once astrophysical considerations have provided a reliable number for the temperature.

After Si is exhausted in a star, most of it is composed of nuclei like ^{56}Fe. Then, no further energy can be released via fusion reactions and the equilbrium between gravitational energy, that tends to contract the system, and energy generated by nuclear processes that opposes the contraction, breaks down. The so-called core collapses, and the electron degeneracy pressure is able to counteract this contraction only when the mass is smaller than the so-called Chandrasekhar limit ($\approx 1.4\ M_\odot$). The core collapse is accelerated by electron capture by iron nuclei (the so-called neutronization), and actually by other complex phenomena that reduce the available energy density and pressure. When the core reaches such a high density that neutrons feel the short-range hard-core repulsion (that we have described in Chapter 1), the core bounces back and a shock wave produces the so-called supernova explosion. How this happens in detail, is not yet well understood.

9.2 The Gamow peak

Let us take a generic reaction $k \to j$. The cross section will depend strongly on energy because it is associated with barrier penetration, as we have seen in Chapter 8. The center-of-mass energy is, in turn, related to the relative velocity between k and j, $v \equiv |\vec{v}_k - \vec{v}_j|$, by $E = \frac{1}{2}\mu v^2$. At a given energy E, the cross section is the number of reactions per unit time [i.e. the transition rate $r(E)$] and per target nucleus, divided by the incident flux. We call d^3n_k and d^3n_j the number of particles of the species k and j with velocities in a three-dimensional infinitesimal volume of the phase space around $\vec{v}_k$ and $\vec{v}_j$,

respectively. Then, we can write

$$\sigma(E) = \frac{r(E)/d^3n_j}{d^3n_k\ v}, \tag{9.11}$$

while the total reaction rate $r_{k\to j}$ integrated over all possible velocities of the particles k and j reads

$$r_{k\to j} = \int r(E) = \int \sigma(E)v\ d^3n_j d^3n_k. \tag{9.12}$$

This reaction rate can be calculated by assuming a Maxwell-Boltzmann distribution for the particle velocities, namely

$$d^3n_j = n_j \left(\frac{m_j}{2\pi k_B T}\right)^{3/2} \exp\left(-\frac{m_j v_j^2}{2k_B T}\right) d^3v_j, \tag{9.13}$$

where n_j is the total number of particles j, m_j is their mass, and T is the temperature of the environment in which the reaction takes place. Exactly the same equation holds for d^3n_k. It is convenient to change variables to the center-of-mass and relative coordinates,

$$\begin{cases} \vec{R} = \dfrac{m_j\vec{r}_j + m_k\vec{r}_k}{m_j + m_k}, \\ \vec{r} = \vec{r}_j - \vec{r}_k \end{cases} \tag{9.14}$$

[this latter equation is a generalisation of Eq. (1.5)]. Then, velocities must be transformed accordingly and the following well-known result can be found:

$$\frac{1}{2}m_j v_j^2 + \frac{1}{2}m_k v_k^2 = \frac{1}{2}MV^2 + \frac{1}{2}\mu v^2 = E_{\rm COM} + E, \tag{9.15}$$

where M is the total mass and $\vec{V}$ is the velocity associated with $\vec{R}$. With this choice,

$$r_{k\to j} = n_j n_k \frac{m_j^{3/2} m_k^{3/2}}{(2\pi k_B T)^3} \int \sigma(E)v\ e^{-\frac{1}{k_B T}\left(\frac{1}{2}MV^2 + \frac{1}{2}\mu v^2\right)} d^3V d^3v. \tag{9.16}$$

The integral over the center-of-mass veocity $\vec{V}$ can be done straightforwardly since the cross section does not depend on it, and one is left with a standard Gaussian integration. The result is

$$r_{k\to j} = n_j n_k \frac{\mu^{3/2}}{(2\pi k_B T)^{3/2}} \int \sigma(E)v\ e^{-\frac{\mu v^2}{2k_B T}} 4\pi v^2 dv. \tag{9.17}$$

We change the integration variable to $E = \frac{1}{2}\mu v^2$ and obtain our final result

$$\boxed{r_{k\to j} = n_j n_k \left(\frac{8}{\pi\mu}\right)^{1/2} (k_B T)^{-3/2} \int dE\ \sigma(E)\ E\ e^{-E/k_B T}.} \qquad (9.18)$$

This latter equation would imply that one has to know the cross section at incident energies between 0 and ∞ in order to extract the reaction rate. However, this is not the case: we shall demonstrate that only a limited range of incident energies must be actually explored. The cross section $\sigma(E)$, because of the Coulomb barrier, is an exponentially growing function of E whereas the exponential (Boltzmann) factor is decreasing with E. There will be a limited region around the maximum of the integrand that allows obtaining the result of a complete integration, to a very good approximation.

The maximum of the integrand, i.e. the product between the two exponential factors $\sigma(E)$ and $e^{-E/k_B T}$, is called the *Gamow peak*. The linear function E is negligible in the present context. We calculate the position of the Gamow peak by starting from Eq. (8.18). As anticipated at that stage, we first evaluate the Gamow factor $G(E)$ at extremely low energy.

We re-write the cross section that we have already written in Eq. (8.18) as

$$\sigma(E) = \frac{1}{E} S(E) e^{-2G(E)}, \qquad (9.19)$$

where the dominant exponential factor has been kept, the quantity $1/E$ corrsponds to the factor $1/k^2$ in Eq. (8.18), and the other factors, either constants or factors that have a mild dependence on E, have been gathered under the symbol $S(E)$. $S(E)$ is called *astrophysical factor*. We remind that the Gamow factor, already defined in Eq. (8.15), reads

$$G(E) = \sqrt{\frac{2\mu}{\hbar^2}} \int_a^b dr\ \left[V(r) - E\right]^{1/2},$$

and the points a and b are defined in Fig. 8.3. Let us identify a with the nuclear radius, and b with the classical turning point r_C, that is defined through

$$E = V(r_C) = \frac{Z_i Z_j e^2}{r_C} \quad \Rightarrow \quad r_C = \frac{Z_i Z_j e^2}{E}. \qquad (9.20)$$

In such a case, the integral appearing in the Gamow factor can be evaluated

analytically with the replacement $r = r_C cos^2\theta$. The result is

$$G(E) = \frac{r_C}{\hbar}\ \sqrt{2\mu E}\left[cos^{-1}\sqrt{\frac{R}{r_C}} - \sqrt{\frac{R}{r_C}\left(1-\frac{R}{r_C}\right)}\right]. \qquad (9.21)$$

For energies in the range between fractions of keV [like in Eq. (9.10)] and 10 keV the assumption $r_C \gg R$ is extremely appropriate. Then, we can definitely write

$$G(E) = \frac{r_C}{\hbar}\frac{\pi}{2}\sqrt{2\mu E}. \qquad (9.22)$$

We derive r_C from Eq. (9.20) and we consider that $e^2 = \alpha\hbar c$ where α is the fine structure constant. Then

$$e^{-2G(E)} = \exp\left[-\frac{\pi\alpha Z_i Z_j\sqrt{2\mu c^2}}{\sqrt{E}}\right] \equiv e^{-b/\sqrt{E}}, \qquad (9.23)$$

and, thus, the integrand of Eq. (9.18) behaves as

$$f(E) = \exp\left[-\frac{E}{k_B T} - \frac{b}{\sqrt{E}}\right] \qquad (9.24)$$

if we just neglect $S(E)$. We define E_0 as the maximum of the function $f(E)$. A simple maximization of this function yields

$$E_0 = \left(\frac{bK_B T}{2}\right)^{2/3} = 1.22\ \left(Z_i^2 Z_j^2 A_{\rm red} T_6^2\right)^{1/3}\ \text{keV}, \qquad (9.25)$$

where in the last step we have defined $A_{\rm red} = A_i A_j/(A_i + A_j)$ (with obvious notation) as well as the quantity T_6 which is the temperature in units of 10^6 K. The opportune constants have been grouped. E_0 is the energy of the Gamow peak.

9.3 The nucleosynthesis problem

After having laid out the main features of reactions in stars, and especially the fact that these reactions take place at low energies around the Gamow peak, many further questions arise. How did these reactions produce, and how do they keep producing, the elements that we find in the Universe? This

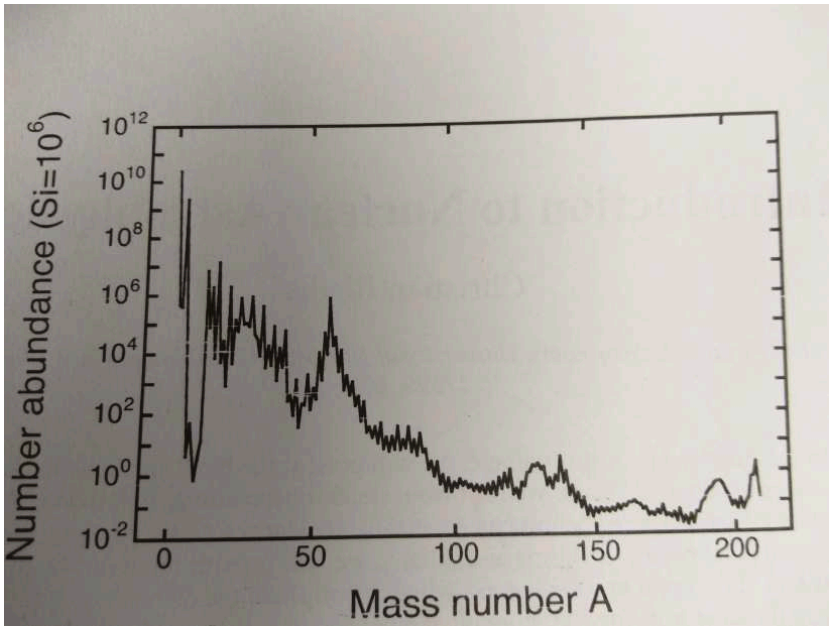

Figure 9.2: Abundance of the elements in the solar system, normalized to the number of Si atoms which is taken as 10^6.

is perhaps the main question, and it has been listed among the most crucial unanswered problems in physics.

Fig. 9.2 shows the relative abundances of elements in the solar system. H and He are the most abundant and their formation happened during the Big Bang. There is a big drop in abundances in correspondence with Li, Be and B, and a sharp increase at C and O (which explains, among the rest, the existence of life on the Earth). After that, the curve on the average decreases but there is a huge peak around Fe, Co and Ni which is referred to as the iron peak, plus other peaks that can be connected with nuclei having magic or double-magic character. The reactions among charged particles, and the associated reaction rates defined by Eq. (9.18), can explain the abundances up to the iron peak. To explain the production of heavier elements, that are characterised by a neutron excess, neutron capture processes need to be invoked.

Neutron capture, or (n,γ) processes, point towards increasingly neutron-rich nuclei. If nuclei become neutron-rich, they undergo β-decay. To understand, or simulate in detail, what happens in a neutron-rich environment, one needs to know the nuclear masses, the decay lifetimes, and the low-lying

states. β-decay has a well-defined lifetime, while the neutron capture rate obeys a formula like (9.12) and depends strongly on the neutron density. Hence, the needs to look for environments in which such density may be large.

In usual conditions, the neutron density is not very large and the neutron capture is slowed down by β-decay. A nucleosynthesis process that takes place in such conditions is called the s-process (s stands for slow). Only much larger neutron densities can give rise to the so-called rapid, or r-process. In such a case, the neutron capture rate is so high that the process can proceed to more neutron-rich systems without being hindered by β-decays.

Reaction network equations, in which the number of particles i as a function of time is written in terms of the reaction rates that create or destroy them, can be devised. One of the difficulties is identifying the appropriate astrophysical environment. The exact site of the r-process is for instance not yet known with certitude. While for a certain time the common belief was that supernova explosion was the most likely r-process site, this has idea has been questioned lately.

The recent observation of neutron star merging has been a kind of breakthrough in this quest. In the merging, together with the detection of gravitational waves and of neutrinos, an electomagnetic signal called "kilonova" has been detected [52]. This points to the huge relevance of such event for the synthesis of the heavy elements.

9.4 Neutron stars

The existence of systems composed only by neutrons, and bound by the gravitational force, was predicted by Landau long time ago, at the beginning of the 1930s[3]. The discovery of neutron stars came only much later, in 1967.

[3]At least, this is often said. For those who are interested in reading a review of what may have happened in the early 1930s, specifically in an hyopthetical discussion between Landau, Bohr and Rosenfeld about neutron stars, can consult the arxiv paper at `https://arxiv.org/abs/1210.0682`.

9.4.1 A crude argument

The existence of a netron star can be, at our level, understood by means of a simple exercise based on the semi-empirical mass formula,

$$\mathrm{BE}(A,Z) = a_{\mathrm{V}}A - a_{\mathrm{S}}A^{2/3} - a_{\mathrm{A}}\frac{(N-Z)^2}{A} + \text{pairing term.}$$

A system with only neutrons has no Coulomb, and is expected to be very large if the binding energy of the latter formula, which is negative, must be counterbalanced by the gravitational energy (9.7), that we can take with $k = 3/5$ assumung that the density is uniform. Being the system very large, we can neglect the surface energy and obviously the pairing contribution. We arrive at the following balance between nuclear and gravitational energies, namely

$$a_{\mathrm{V}}A - a_{\mathrm{A}}A + \frac{3}{5}\frac{Gm^2}{r_0}A^{5/3} = 0, \tag{9.26}$$

where m is the nucleon mass and the radius is taken as usual from Eq. (2.1).

If we replace reasonable values for the parameters of the mass formula, like $a_{\mathrm{V}} = 15.85$ MeV and $a_{\mathrm{A}} = 23.21$ MeV, we obtain

$$A \approx 5\ 10^{55}. \tag{9.27}$$

The corresponding mass and radius are

$$M = mA \approx 10^{29}\ \mathrm{kg} \approx 0.05\ M_\odot \qquad R = r_0 A^{1/3} \approx 5\ \mathrm{km}. \tag{9.28}$$

These estimates are qualitatively important in order to show that a neutron star can exist, but they turn out to be very crude. The actual mass of a neutron star is between 1 and 2 solar masses, and the radius is around 10 km. $1.4M_\odot$ is a kind of canonical mass that characterises many observed stars. Most of the particles are neutrons but there is a small fraction of protons and electrons, whose number can be fixed once the number of neutrons is given, thanks to the two conditions of charge neutrality and equilibrium with respect to the weak processes, namely direct and inverse β-decays.

The error in the estimates comes mainly from the unrealistic assumptions that the density is constant and that, whatever the microscopic structure of the star, the standard formulas for binding energy and radius hold still true as if the star were a giant nucleus. We know, to some extent, that while in the inner part the density can reach several times the nuclear saturation

density, it goes down to fractions of the saturation density before the surface of the star is reached. In other words, the neutron stars have a non-trivial structure.

In the next subsection, we will explore how we can arrive at better estimates for the mass and radius of a neutron star, using a microscopic description.

9.4.2 The Tolman-Oppenheimer-Volkov (TOV) equation

The calculation of the mass and radius of a neutron star can be performed by assuming hydrostatic equilibrium. The classical (i.e. Newtonian) version of this assumption has been elucidated in 9.1.2 and has led to Eq. (9.4). We could, for pedagogical purposes, solve the Newtonian hydrostatic equilibrium equation for a neutron star but the results would be not realistic.

Actually neutron stars are so compact (that is, the local mass density is so large) that corrections from general relativity cannot be neglected. We cannot discuss here how one can deduce from general relativity, with assumptions that include the spherical symmetry, the corrections to Eq. (9.4). We merely write down the result, which is the celebrated Tolman-Oppenheimer-Volkov (TOV) equation:

$$\frac{dp(r)}{dr} = -G\frac{M(r)\rho(r)}{r^2}\left(1+\frac{p}{\rho c^2}\right)\left(1+\frac{4\pi p r^3}{M(r)c^2}\right)\left(1-\frac{2GM(r)}{c^2 r}\right)^{-1}. \tag{9.29}$$

ρ is here the energy density $\mathcal{E}$ divided by c^2. In the case of the Newtonian version of this equation we can replace it with the mass density. We remind that the pressure p can be related to the energy density $\mathcal{E}$ (or to the total energy E or the energy per particle E/A):

$$p = -\frac{\partial E}{\partial \Omega} = \rho^2 \frac{d}{d\rho}\frac{E}{A} = \rho\frac{d\mathcal{E}}{d\rho} - \mathcal{E}. \tag{9.30}$$

Here, as in the rest of this text, Ω is the volume and the assumption of constant particle number A is made. Because of Eq. (9.5),

$$M(r) = \int_0^r dr'\ 4\pi r'^2 \rho(r'),$$

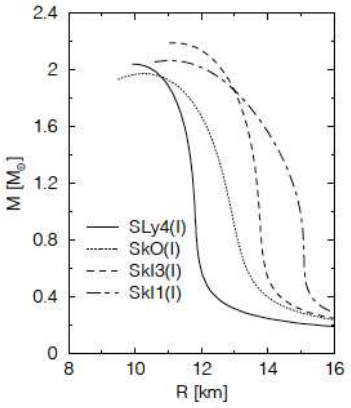

Figure 9.3: Gravitational masses (in units of the solar mass) and radii (in km) of neutron stars deduced from the TOV equation by using the EoS deduced from some Skyrme forces. The different labels refer to different Skyrme sets. The figure is taken from Ref. [54], that the reader can consult for details.

the problem of determining the three functions $p(r)$, $\rho(r)$ and $M(r)$ can be solved if $\mathcal{E}$ or E/A are given. Of course, the solution is not unique but there is a class of solutions, each for a given value of the boundary condition. In fact, one integrates the coupled differential equations (9.29), (9.30) and (9.5) by starting from an ansatz for the central pressure $p_c \equiv p(r = 0)$. A very pedagogical introduction to this topic can be found in Ref. [53].

The issue is, then, to have a model and an expression of the *equation of state* (EoS) for the matter that exists in neutron stars, in the form of Eq. (9.30)[4]. In many cases, the assumption has been made that neutron stars are merely made of pure neutron matter. While this assumption is not realistic, as we discuss in the next subsection, it leads to a reasonable first approximation to solve the TOV equation. In Sec. 2.3.1 we have discussed a simple approach to the EoS of symmetric nuclear matter. This can be extended to asymmetric matter or pure neutron matter. In other words, there exist indeed many attempts to calculate masses and radii of neutron stars by using Skyrme forces. Many other models, basically all those have been discussed in the first Chapters of this text, have been employed to calculate those masses and radii.

In Fig. 9.3 we show, for the sake of mere illustration, a few calculations based on Skyrme forces. The reader may note the vertical slope that the curves tend to display. There is a qualitative argument to explain this feature. Let us start again from the hydrostatic equation, in the Newtonian version

[4]The temperature is assumed to vanish in this context, so that the equation of state is a relationship between pressure and density.

(for the sake of simplicity). We can approximate

$$\frac{dp}{dr} = -G\frac{M\rho}{r^2} \quad \Rightarrow \quad \frac{p}{R} \sim -G\frac{M}{R^2}\frac{M}{R^3}. \tag{9.31}$$

The nuclear pressure is produced by the short-range repulsion among neutrons; if we take it as a two-body interaction, by neglecting the three-body contribution, we obtain that $\mathcal{E}$ goes like ρ^2 and E/A goes like ρ. This argument can be checked by going through, once again, Sec. 2.3.1: in particular, the second term at the r.h.s. of Eq. (2.41) testifies to our statement. Then, Eq. (9.30) provides a pressure that goes like ρ^2, and Eq. (9.31) predicts that

$$\frac{1}{R}\frac{M^2}{R^6} \sim -G\frac{M^2}{R^5}. \tag{9.32}$$

In this approximate equation, the mass simplifies and a sort of rough independence of the value of the radius from the mass shows up. This provides a qualitative explanation of the vertical slope that we have spotted.

From the discussion of the TOV equation, the most important take-home message is that the measurement of the mass and radius of neutron stars provides a strong constraint on the EoS and, in turn, on the nuclear models for the neutron stars components and their mutual interactions. A few years ago, it has been shown that neutron stars exist whose mass is equal to, or slightly larger than, two solar masses. This observation has ruled out many models than predict only smaller values of the mass.

The constraints on the radii have been for quite a long time rather loose. Moreover, masses and radii had been, until very recently, observed for different systems only. While this text was being written, NICER has observed for the first time the mass and radius of the *same* compact object.

This latest constraint, as well as those coming from the gravitational wave (GW) observations during the merging of neutron stars (that we do not discuss here) are setting new constraints for nuclear physics. All this testifies to a current "Renaissance" period for the physics of astrophysical compact objects.

9.4.3 Brief discussion of the neutron star structure

There are many reasons to imagine that neutron stars cannot be simple "gigantic nuclei". The densities that characterise them, namely the density profiles $\rho(r)$ from the integration of the TOV equation, span several orders

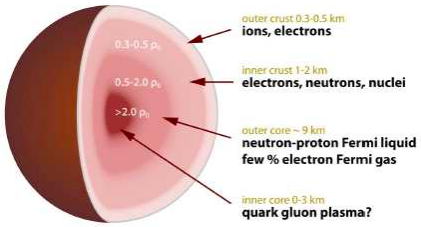

Figure 9.4: Schematic picture of the different layers of a neutron star. A more thorough discussion can be found in [55].

of magnitude. The inner density is unknown but it must be of the order of, or higher than, the nuclear saturation density. The outer layers of neutron stars display values of the density that are two or three orders of magnitude smaller. There are excellent reviews on our current understanding of the neutron star structure [55]. Generally speaking, starting from the surface and moving inward, we believe that the following layers are found:

- outer crust: fully ionized atoms are disposed in a lattice, and are surrounded by an electron gas;
- inner crust: neutron-rich nuclei in a lattice co-exist with the electron gas and with free neutrons;
- outer core: nuclei dissolve and nuclear matter shows up;
- inner core: the composition is unknown, although it may have a very exotic character: hyperons or even deconfined quarks may exist therein.

A simple picture of these layers is displayed in Fig. 9.4. In the following, we shall not discuss the physics of these layers as this would imply a quite considerable effort. We limit ourselves to simple, qualitative arguments that are meant to elucidate *why* we expect such succession of layers. In this respect, our discussion follows the simple sketch prvided by Ref. [56]: this short lecture note is a concise source that allows understanding the basic physics that govern dense matter, thanks to a format similar to FAQs (Frequently Asked Questions).

At the outer surface of the star, at vanishing density, the configuration will be the most favourable energetic configuration that we imagine also on Earth, namely ^{56}Fe atoms. With increasing density, atoms are ionized and the electrons acquire higher and higher energies and reach the relativistic regime. At high densities and high energies, the Coulomb interaction be-

comes unimportant[5]. This brings us to the picture for the outer crust: nuclei (that is, fully ionized atoms) in a lattice, surrounded by an electron gas. By going inward, as density and pressure increase, electron capture by nuclei becomes more important and the nuclei are neutron-rich.

As we learnt, nuclei cannot accommodate too many neutrons. Here, nuclear physics comes in as the position of the neutron drip-line determines tre transition from the outer to the inner crust. This latter, in fact, starts when nuclei "drip neutrons out" and is composed by very neutron-rich nuclei in a lattice, surrounded by neutrons in addition to electrons. The properties of this neutron gas or liquid are not easy to extrapolate from terrestrial studies. The role of neutron superfluidity has still to be fully understood, for instance.

It is intuitive that, by further increasing density and pressure, we must go towards a phase in which nuclei and free neutrons coalesce. This defines the so-called outer core. It is far from obvious to determine which shapes emerge from this coalescence. Whereas matter has sooner or later to become uniform at some density, what happens before that value is attained is subject of debate. The question is, here, whether elongated systems in which the surface is non-zero (rods or "spaghetti", flat surfaces or "lasagna") have a lower energy, at a given density, than uniform matter. We do not dwell on this question as the energy balance is governed by a very subtle interplay between surface energy and Coulomb energy.

Completely uncertain is the composition of neutron stars at even higher densities. Above the nuclear saturation density, the energy density may be large enough so that new particles are produced: other leptons like μ's, or hyperons like the Σ, Λ or Ξ particles. Unfortunately, at present we have poor knowledge, if any, about the interactions between hyperons and nuclei, or between hyperons themselves. It is impossible, so far, to draw conclusions about the presence of these species and their contribution to the bulk properties of neutron stars. The same can be said regarding the possible emergence of quark matter. The properties of the inner core are subject of many speculations.

[5]We leave it as an exercise, with the following hints: take the electron gas at given density ρ, derive the average distance between electrons as well as the typical (Fermi) momentum, and deduce that the ratio between interaction energy and kinetic energy goes to zero when the velocity goes to c.

Chapter 10

Fusion and fission reactions

10.1 Heavy-ion fusion reactions

We do not treat here hydrogen fusion. Instead, we are interested in the case of heavy ions. Fusion is often the only method, starting from two colliding nuclei, to synthetize super-heavy elements. Fusion is also an important reaction in stellar environments (cf. the discussion in Chapter 9). Last but not least, as we will see below, heavy-ion fusion is one of the best physics cases to elucidate the subtle features of quantum tunneling.

Let us assume we want to study the fusion between two ions (A_1, Z_1) and (A_2, Z_2). Fusion is classically possible if the potential between the ions can be overcome, but is also possible below any potential barrier because nuclei are quantal objects. The problem can be treated by separating different partial waves characterised by their angular momentum l. In other terms, if we reason using only the radial coordinate r, the effective potential between the ions reads

$$V_l(r) = V_{Nuclear}(r) + V_{Coulomb}(r) + \frac{\hbar^2 l(l+1)}{2\mu r^2}. \tag{10.1}$$

The nuclear potential $V_{Nuclear}$ can be taken, e.g., with a Woods-Saxon shape, the Coulomb potential $V_{Coulomb}$ can be approximated as that of two uniformely charged spheres, and the last term is the well-known centrifugal potential. μ is the reduced mass.

By choosing the example of ^{16}O and ^{154}Sm we find the behaviour that is displayed in Fig. 10.1 (in the figure caption we mention the parameters that have been used), as far as the nuclear and Coulomb term are concerned. We

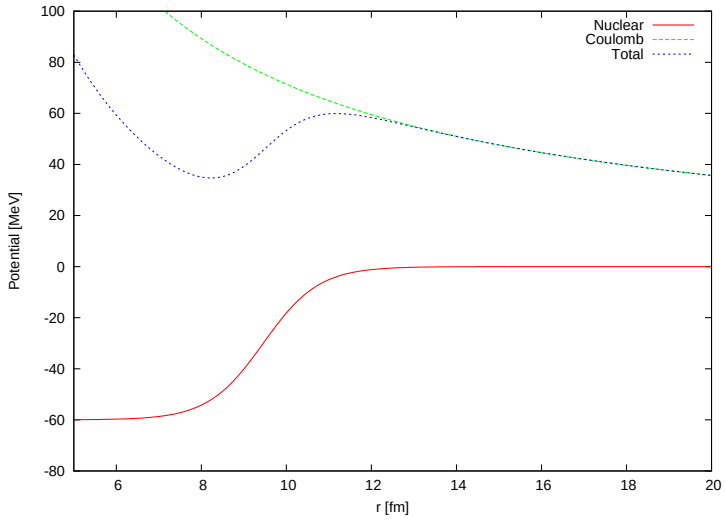

Figure 10.1: Potential among the two nuclei ^{16}O and ^{154}Sm. The nuclear potential has the Woods-Saxon shape (2.3) with radius R given by $1.2\left(A_1^{1/3}+A_2^{1/3}\right)$ [fm] and depth equal to 60 MeV, while the Coulomb potential is that of two point charges Z_1 and Z_2. Figure taken from K. Hagino.

now consider the role of the angular momentum of the relative motion. We start from a simple classical approximation in which the relationship between the impact parameter b and the angular momentum l is simply

$$l = kb, \tag{10.2}$$

where $k = \sqrt{\frac{2\mu E}{\hbar^2}}$.

We define a *grazing* angular momentm l_g in the following way: the system is characterised by this angular momentum if the corresponding incident energy E is equal to the potential at its maximum. If R is the radial value corresponding to this maximum, then l_g is the solution of the implicit equation

$$E = V_{l_g}(R) = V_{Nuclear}(R) + V_{Coulomb}(R) + \frac{\hbar^2 l_g(l_g+1)}{2\mu R^2}. \tag{10.3}$$

In order to have a simple estimate of this solution, we employ Eq. (10.2) and define accordingly $b_g = l_g/k$. We can then write

$$E = V + \frac{\hbar^2 \left(kb_g\right)^2}{2\mu R^2}, \tag{10.4}$$

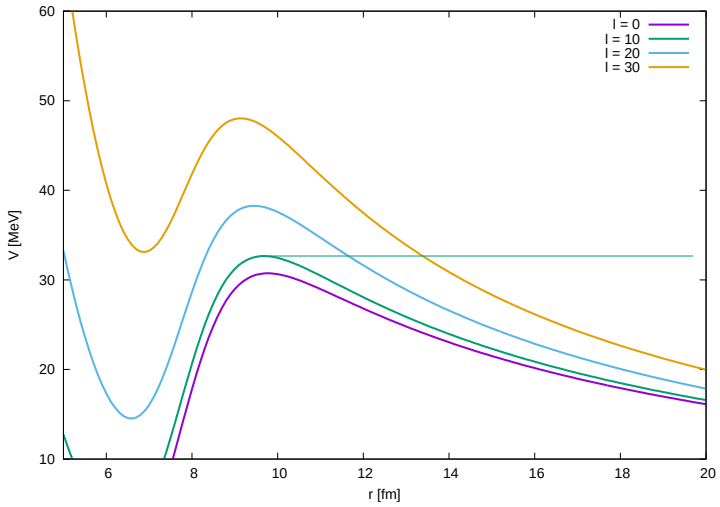

Figure 10.2: Potential among the two nuclei ^{16}O and ^{58}Ni. In this case, the total effective potential is displayed, including the centrifugal term, for different values of l. If the energy is the one indicated by the horizontal line, the meaning of the approximation that fusion takes place when $l > l_g$ which is equal to 10 in this case, becomes evident. Figure taken from K. Hagino.

where V is a shorthand notation for the sum of the nuclear and Coulomb potentials. We can see such simple estimate in Fig. 10.2. As we discuss in the next subsection, the correspondingly simple estimate for the fusion cross section consists in assuming that as soon as the impact parameter is equal to, or smaller than, the grazing one b_g, then fusion takes place.

10.1.1 Classical approximation

In the purely classical approximation, fusion takes place in all those events in which the impact parameter b is smaller than the grazing one b_g. In terms of cross section, this means

$$\sigma^{\text{cl.}} = \int_0^{b_g} 2\pi b \, db = \pi b_g^2. \tag{10.5}$$

We take b_g from Eq. (10.4) and we also use the fact that $E = \frac{\hbar k^2}{2\mu}$. With simple manipulations we arrive at

$$\sigma^{\text{cl.}} = \pi R^2 \left(1 - \frac{V}{E}\right), \tag{10.6}$$

where V is the barrier height, that is the maximum value of the potential V, and R is its radial position. Data taken at different energies above the barrier obey such law and interpolation allows extracting the values of V and R. As soon as we go below the barrier we must take into account the penetration factor.

10.1.2 Sub-barrier fusion and Wong's formula

The correspondence between l and b that has been approximately described by Eq. (10.2) should be replaced by

$$kb = l + \frac{1}{2}.$$

This is Eq. (10.28) and is proven in the Appendix. Note that the difference with the previous estimate, $kb = l$, is not relevant for large values of kb.

Then, the classical value (10.5) can be written in terms of the angular momentum l and complemented by a transmission coefficient for each partial wave $P_l(E)$, that gives precisely the probability that such partial wave penetrates the potential barrier,

$$\sigma = \int 2\pi b \; db = \frac{\pi}{k^2} \sum_l (2l+1) \quad \rightarrow \quad \frac{\pi}{k^2} \sum_l (2l+1) \, P_l(E). \tag{10.7}$$

Since we may use this formula around the barrier, the best approximation for the transmission coefficient is

$$P_l(E) = \left[1 + e^{2G(E)}\right]^{-1}, \tag{10.8}$$

with

$$G(E) = \sqrt{\frac{2\mu}{\hbar^2}} \int_a^b dr \left[V + \frac{\hbar^2 \left(l + \frac{1}{2}\right)^2}{2\mu r^2} - E \right]^{1/2} \tag{10.9}$$

[a and b are the inner and outer edge of the barrier, as in Fig. 8.3 and Eq. (8.15)]. Note that the previous Eq. (10.8) reduces to $P(E) = e^{-2G(E)}$, exactly in the form of Eq. (8.15), if we are well below the barrier and the Gamow factor $G(E)$ is large. Note also that in Eq. (10.9) we have written the angular momentum squared consistently with (10.28).

There is a way to evaluate anlytically the Gamow factor if one approximates the shape of the barrier by using a reversed parabola, that is, with the replacement

$$V(r) + \frac{\hbar^2 \left(l+\frac{1}{2}\right)^2}{2\mu r^2} \quad \rightarrow \quad V_B - \frac{1}{2}\mu\omega^2 \left(r-R\right)^2 , \tag{10.10}$$

where V_B is the maximum of the barrier, R is its radial position as it was above, and ω is a parameter to be fitted to reproduce the barrier shape at best (at least close to the maximum). Note that we aim at reproducing the shape of the barrier for $l = 0$. One can find, by direct inspection, that the height of the barrier changes with l but the change of the curvature can be safely neglected. Then, the Gamow factor becomes

$$\begin{aligned} G(E) &= \sqrt{\frac{2\mu}{\hbar^2}} \int_a^b dr \left[V_B - E - \frac{1}{2}\mu\omega^2 \left(r-R\right)^2\right]^{1/2} \\ &= \frac{\pi}{\hbar\omega}\left(V_B - E\right). \end{aligned} \tag{10.11}$$

Eventually,

$$P_0 = \left[1 + e^{\frac{2\pi}{\hbar\omega}(V_{B0}-E)}\right]^{-1}, \tag{10.12}$$

$$P_l = \left[1 + e^{\frac{2\pi}{\hbar\omega}(V_{B}-E)}\right]^{-1} = \left[1 + e^{\frac{2\pi}{\hbar\omega}\left(V_{B0}+\frac{\hbar^2\left(l+\frac{1}{2}\right)^2}{2\mu R^2}-E\right)}\right]^{-1}, \tag{10.13}$$

where V_{B0} is the barrier height in the case of $l = 0$, and we have worked within the aforementioned approximation, that is, we have assumed that for different values of l only the barrier height V_B changes and not its shape. The total cross section is

$$\sigma = \frac{\pi}{k^2}\sum_l \left(2l+1\right)\frac{1}{1+\exp\left\{\frac{2\pi}{\hbar\omega}\left[V_{B0}+\frac{\hbar^2\left(l+\frac{1}{2}\right)^2}{2\mu R^2}-E\right]\right\}}, \tag{10.14}$$

and the sum can be replaced by an integral to find an analytical solution. The result is the famous Wong's formula [57], that is,

$$\sigma = \frac{\hbar\omega R^2}{2E}\ln\left[1 + e^{\frac{2\pi}{\hbar\omega}(E-V_{B0})}\right]. \tag{10.15}$$

It is easy to show that this formula reduces to the classical one, Eq. (10.6), in the case $E \gg V$, that is, far above the barrier.

10.1.3 Failure of potential models below the barrier: fusion enhancement

Wong's formula works well, except when one goes well below the Coulomb barrier and the parabolic approximation (10.10) fails. One can estimate more precisely the transmission coefficient P_l, by solving numerically the Schrödinger equation with a realistic potential, and calculate the cross section from Eq. (10.7). This procedure goes under the name of "potential model".

These potential models work relatively well for light systems, but fail to reproduce the experimental findings for a number of heavy systems at energies below the barrier (for the same systems, they do work for energies above the barrier). In particular, potential models underestimate the fusion cross sections so that this phenomenon has been given the name of "subbarrier enhancement" of the fusion cross section, around the turn of the 1970s and during the 1980s. The origin of this enhancement could not be traced back to the choice of the specific potential.

The detailed treatment of this enhancement goes beyond our scope here. The interested reader can look at [58] and references therein. In the case of deformed nuclei, for instance, one must evaluate the barrier penetration by taking into account the rotational motion: different relative orientations of the two nuclei lead to barriers with different shapes. Also other kinds of nuclear excitations, like the low-lying vibrations that we have discussed in Chapter 4, affect the fusion processes.

10.2 Nuclear fission

10.2.1 General aspects

After the discovery of the neutron, in 1932, there was immediately much interest in the possible reactions that this new projectile could induce, without the hindrance associated with the Coulomb repulsion. One of the directions was the exploration whether neutron capture could lead to the production of elements with atomic number Z larger than 92 (so-called "transuranic" elements). There were difficulties, at that time, to identify the final products of neutron-induced reactions. O. Hahn and F. Strassmann showed in 1939 that elements with mass equal roughly to one half of U were produced, when neutrons impinged on that target. L. Meitner and O. Frisch gave the correct

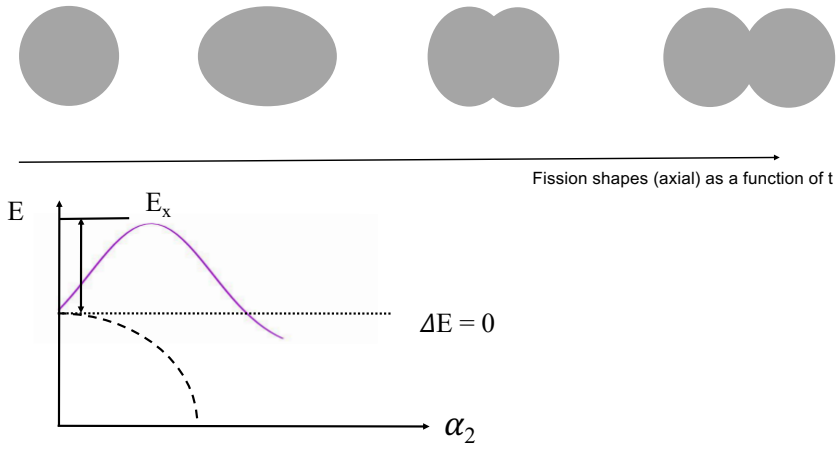

Figure 10.3: In a simple way, we sketch in the upper part of the figure the elongated shapes through which the nucleus is supposed to evolve before undergoing fission. In the lower part, we show the energy as a function of the deformation parameter α_2. The dashed line corresponds to the case of spontaneous fission ($\Delta E < 0$). The full line displays the case in which initially $\Delta E > 0$ and there is a barrier, that the system can pass by means of tunneling (spontaneous fission), or that can be overcome if an initial energy $E_{\rm x}$ is provided (induced fission). The dashed line indicates the critical line $\Delta E = 0$. See the text for a discussion.

interpretation of the phenomenon which is now called *fission*.

A typical fission process is

$$^{235}\mathrm{U} + \mathrm{n} \;\rightarrow\; ^{140}\mathrm{Ba} + ^{93}\mathrm{Kr} + 3\mathrm{n},$$

and this reaction releases about 200 MeV. There are many possible outcomes of a fission reaction. Another one is, for instance,

$$^{235}\mathrm{U} + \mathrm{n} \;\rightarrow\; ^{140}\mathrm{Xe} + ^{94}\mathrm{Sr} + 2\mathrm{n}.$$

A thorough discussion of the statistical distribution of the possible fission channels can be found in the specialized literature. Here, we just stress a few basic facts. First, the fact of being highly exoenergetic is common to all fission channels. Observing 2-3 neutrons with energies of the order of $\approx$ MeV is another typical feature. Last but not least, the fragments are neutron-rich and they typically undergo β-decay.

The first question is how fission occurs, why it is not spontaneous for U and needs to be induced, and why it is spontaneous for some heavier elements

like Cf. The standard modelization introduced by Bohr and Wheeler [59] is based on the idea that the the nucleus goes through increasingly elongated shapes, like those that are schematically drawn in the upper part of Fig. 10.3. Once the two centers that appears in the shapes that are displayed are separated by a thin "neck", Coulomb repulsion pushes the two sub-systems apart.

The deformed shapes can be better defined by going back to the general formula (5.1). If we specialise it to the case of axial symmetry, one has

$$R(\theta) = R_0 \left[1 + \alpha'_2 P_2(cos\theta) + \alpha'_3 P_3(cos\theta) + \ldots\right]. \tag{10.16}$$

The parameters α' are related to α in Eq. (5.1) by simple relationships since

$$Y_{l0}(\theta) = \sqrt{\frac{2l+1}{4\pi}} P_l(cos\theta).$$

We will use α instead of α' in what follows, for the sake of simplicity.

For pedagogical reasons, we further restrict to the case of quadrupole deformation, namely we assume that (at least in the first steps) the shape is simply described by the parameter α_2. We aim at understanding the behaviour of the energy when α_2 is small, namely for small deviations from the spherical symmetry. The relevant plot is visibile in the lower part of Fig. 10.3: if the energy decreases ($\Delta E < 0$) fission can happen spontaneously, but this is not the case of the energy increases and the spherical shape is a local minimum ($\Delta E > 0$).

If we take the energy from the semi-emprical mass formula, as a function of deformation the volume energy does not change if the volume is conserved, and also the asymmetry energy remains constant. We can calculate both the change in the surface energy and in the Coulomb energy. The surface energy increases as the surface increases. In fact, the surface energy can be written as σS, where S is the surface and σ is the surface tension. The sphere has the smallest possibile surface for the given volume. The change associated with the ellisoidal shape can be analytically calculated at lowest order in α_2. A detailed calculation can be found in Ref. [60]. The result is

$$E_{\rm surf} = E_{\rm surf,0} \left(1 + \frac{2}{5}\alpha_2^2\right), \tag{10.17}$$

where $E_{\rm surf,0}$ is the surface energy of the sphere having radius R, that is, $E_{\rm surf,0} = a_S A^{-2/3}$.

Even more tedious is the calculation of the Coulomb energy. It is straightforward, though: one assumes a uniform charge distribution and just integrates the contributions from the Coulomb interaction between pairs of charges in two points. The result reads, again at lowest order in α_2,

$$E_{\rm Coul} = E_{\rm Coul,0}\left(1 - \frac{1}{5}\alpha_2^2\right), \tag{10.18}$$

where now $E_{\rm Coul,0} = a_C Z^2 A^{-1/3}$.

The net result is that the variation of the energy for small values of α_2 is given by

$$\frac{\Delta E}{\alpha_2^2} = \frac{2}{5}a_{\rm S}A^{2/3} - \frac{1}{5}a_{\rm C}Z^2A^{-1/3}. \tag{10.19}$$

This quantity in the r.h.s. can be evaluated by using the typical parameters of the mass formula. $\Delta E = 0$ if

$$\frac{Z^2}{A} = \frac{2a_{\rm S}}{a_{\rm C}} \approx 50. \tag{10.20}$$

For smaller (larger) values than ≈ 50, the change ΔE is positive (negative). This fact explains why only very heavy elements can undergo spontaneous fission. The parameter Z^2/A is often called *fissility parameter*.

In Fig. 10.4 we show the known life-times for spontaneous fission and the role played by the fissility parameter. While the dashed line shows a possibile, plausible fit of some of the data[1], we should stress that the microscopic study of fission is an active field of research and the fine structure of the data can be seen as resulting from shell effects and other subtle phenomena that we do not treat here.

We move now our attention to induced fission. In the lower plot of Fig. 10.3, one can also see that, if an external source can give the nucleus an initial excitation energy $E_{\rm x}$, the barrier can be overcome even in case of nuclei that would have a very long half-life (sometimes infinite, in practice) associated to spontaneous fission. The energy can be supplied by neutrons, photons but also charged particles. In the case of the capture of very low-energy neutrons, the energy of the compond system and the barrier heights are known in the case of U, Th and Pu isotopes. We shall consider U in the next subsection, because of its practical interest.

[1]It is an empirical law which was proposed *before* many of the displayed data have become available.

We end this part by stressing that many interesting aspects of fission are not treated here: the case of double barriers and fission isomers, the role of triaxiality, the distribution of masses and kinetic energy among the fission fragments, the case of ternary fission (to name only a few).

10.2.2 The case of U and the role of pairing

Some fission barriers have been known for quite some time. For instance, in ^{236}U, the barrier height is 5.3 MeV while in ^{239}U the barrier height is 5.5 MeV. The two are not markedly different, as one expects. However, when a very low-energy neutron is captured by ^{235}U the energy of the compound system ^{236}U becomes 6.55 MeV. On the other hand, the energy of ^{238}U plus a thermal neutron (i.e., of the compound system ^{239}U) is 4.81 MeV. This is why the former is a fissile material while the second is not. We see here the role played by pairing: energies are higher in an even system than in an odd one.

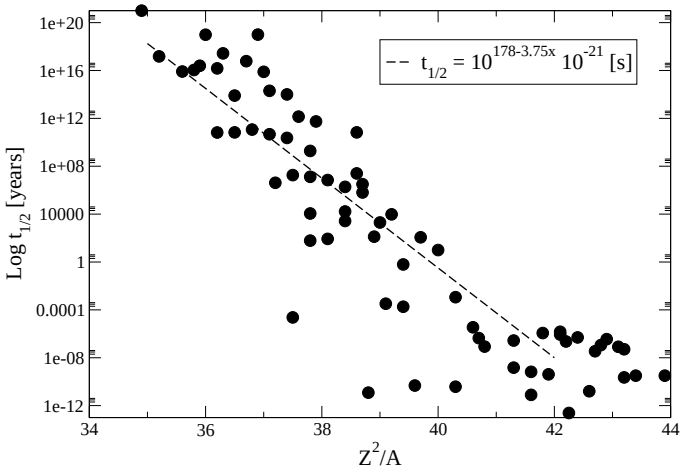

Figure 10.4: The known lifetimes for spontaneous fission (taken from `https://fr.wikipedia.org/wiki/Fission_spontanée`) are displayed as a function of the fissility parameter $x = Z^2/A$. The dashed line shows the linear trend (in log scale) predicted by one of the many available empirical formulas.

10.2.3 The fission chain reaction

As we have anticipated in Sec. 10.2.1, a low-energy neuron impinging on ^{235}U produces fission with a release of $\approx$ 200 MeV of energy. This is of course relevant for energy production. The ratio of energy released vs. mass of fuel, $E/m_{\rm fuel}c^2$ is of the order of 10^{-3}. We can compare this number with a typical one associated with the release from chemical reactions. In Chapter 9 (Sec. 9.1.1), we have considered carbon and pointed out that 1 kg of it produces $E = 3.35\ 10^7$ J: in this case the ratio is 10^{-9}.

We should point out, however, that not 100% of the released energy from U fission is immediately available under the form of heat or radiation. In a typical fission like the one mentioned at the start of the Section, 167 MeV go into kinetic energy of the fragments, 5 MeV go into kinetic energy of the neutrons, and 6 MeV are found in γ-rays. This is the energy which is readily available. About 15 MeV are released after β-decays, either in terms of electron energies or delayed γ-rays: as a consequence, this energy may appear with a large time delay, even years. Finally, 12 MeV are carried away by neutrinos and this energy is not deposited anywhere.

Energy release from a single fission is not the only point to be kept in mind. If one wants to produce energy, the fission process must have a sufficiently large rate, and be self-sustained. Every fission event produces 2-3 neutrons. We will denote this number by ν in what follows, and assume $\nu = 2.5$. These neutrons can ignite a chain process under given circumstances as we explain here below.

As for the cross section, we show in Fig. 10.5 the total cross section of neutrons on ^{235}U. For thermal neutrons, below 0.1 eV, this cross sections reaches almost 10^3 b, which is a huge value, but it drops to about 7 b in the MeV range. As we said, one is interested here in the fission cross section, which is about 84% of the total one at very low energy, while in the MeV range fission takes place about 1 time over 6. However, having a 100% ^{235}U enriched sample is, in practice, impossible. The natural abundances are 99.28% for ^{238}U and 0.72% for ^{235}U. A so-called "enriched" sample may reach 3% of ^{235}U. As for ^{238}U, this is not fissile, as the fission cross section is negligible when the neutron energy is below the $\approx$ MeV scale. The total neutron cross section is approximately constant in a broad energy range, and is about 10 b. There are jumps above this value in the resonance region but resonances are narrow and we will not consider their presence here.

We briefly discuss how these numbers impact the estimate of the outcome

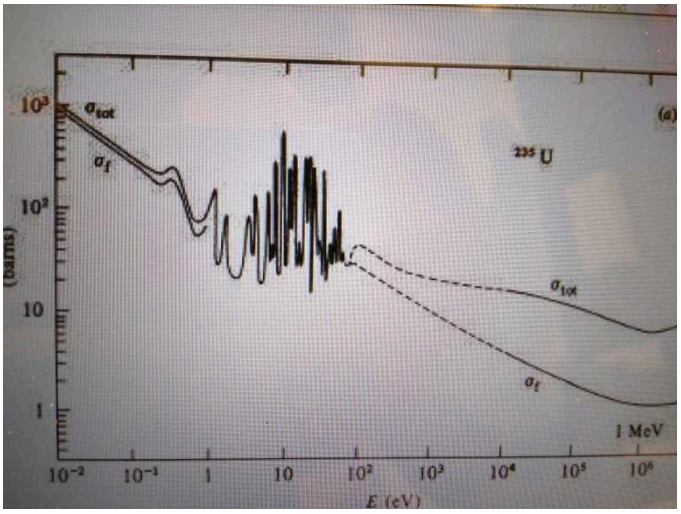

Figure 10.5: Cross section of neutrons on ^{235}U as a function of the neutron energy. $\sigma_{\rm tot}$ is the total cross section, while $\sigma_{\rm f}$ is the cross section for fission. Taken from [47].

of a chain reaction. The typical density of a U sample is 4.8 10^{28} nuclei/m^3. The total neutron cross section will depend on the neutron energy and the enrinchment in ^{235}U. For a quick estimate, we consider a value around 10 b, which correponds to the value for neutrons with energies around 1 MeV, more or less for both isotopes (^{235}U and ^{238}U). The reaction rate for one neutron on U is $\rho v \sigma$, where v is the neutron velocity. Thus, the time between two reactions is

$$\tau = \frac{1}{\rho v \sigma}, \tag{10.21}$$

and the mean free path is simply

$$l = \frac{1}{\rho \sigma} = \frac{1}{4.8\ 10^{28}\ 7\ 10^{-28}}\ \text{m} \approx 3\ \text{cm}. \tag{10.22}$$

As we said, we expect $\nu = 2.5$ neutrons for each reaction carrying away 5 MeV all together. With an energy of 2 MeV, the velocity of the neutron is 2 10^7 m/s and the time τ is about 1.5 10^{-9} s.

Let us denote as $n(t)$ the neutron number at time t. This quantity will obey the following equation,

$$n(t+dt) = n(t) + (\nu q - 1)\,\frac{dt}{\tau} n(t), \tag{10.23}$$

where the second term describes the increase due to new fission processes. Each interaction eliminates one neutron and, if fission occurs with a probability q, it produces $\nu = 2.5$ new neutrons. The time step dt must be compared to the time τ that we have previously defined. The solution of Eq. (10.23) is

$$n(t) = n(0)e^{(\nu q-1)\frac{t}{\tau}}. \tag{10.24}$$

This solution shows that the reaction can sustain itself if q is larger than $1/\nu = 0.4$.

q is not only determined by the cross section value, but also by all the physical conditions that affect the neutron transport. Controlling a nuclear reactor means basically to control q. An uncontrolled increase of q may lead to catastrophic events due, for instance, to a lack of the control of the temperature.

10.3 Appendix: relation between b and l

We start by reminding the formula for the scattering amplitude,

$$f(\theta) = \frac{1}{k}\sum_l (2l+1)e^{i\delta_l} sin\delta_l P_l(cos(\theta)), \tag{10.25}$$

where the partial wave expansion has been introduced, δ_l is the phase shift associated to each partial wave, and P_l is a Legendre polynomial. The Legendre polynomials obey the well-known orthonormality condition,

$$\int_{-1}^{+1} d\mu\ P_l(\mu)P_{l'}(\mu) = \frac{2}{2l+1}\delta_{ll'},$$

and by exploiting it one readily obtains

$$\sigma = \int d\Omega\ |f(\theta)|^2 = \frac{4\pi}{k^2}\sum_l (2l+1)sin^2\delta_l. \tag{10.26}$$

The largest possible value is found for $\delta_l = 1$. We equate this value to the classical expression in terms of the impact parameter b:

$$\sigma = \frac{4\pi}{k^2}\sum_l (2l+1) = 2\pi\int db\ b. \tag{10.27}$$

This latter equation provides the required relationship

$$kb = l + \frac{1}{2}, \tag{10.28}$$

that is used in this Chapter.

Bibliography

[1] J. Carlson, S. Gandolfi, F. Pederiva, S. C. Pieper, R. Schiavilla, K. E. Schmidt, and R. B. Wiringa, "Quantum monte carlo methods for nuclear physics," *Rev. Mod. Phys.*, vol. 87, pp. 1067–1118, Sep 2015.

[2] J. Lynn, I. Tews, S. Gandolfi, and A. Lovato, "Quantum monte carlo methods in nuclear physics: Recent advances," *Annual Review of Nuclear and Particle Science*, vol. 69, no. 1, p. null, 2019.

[3] H. Hergert, S. Bogner, T. Morris, A. Schwenk, and K. Tsukiyama, "The in-medium similarity renormalization group: A novel ab initio method for nuclei," *Physics Reports*, vol. 621, pp. 165 – 222, 2016. Memorial Volume in Honor of Gerald E. Brown.

[4] G. Hagen, T. Papenbrock, M. Hjorth-Jensen, and D. J. Dean, "Coupled-cluster computations of atomic nuclei," *Reports on Progress in Physics*, vol. 77, p. 096302, sep 2014.

[5] C. Barbieri, F. Raimondi, and C. McIlroy, "Recent applications of self-consistent green's function theory to nuclei," *Journal of Physics: Conference Series*, vol. 966, p. 012015, feb 2018.

[6] S. Shen, H. Liang, W. H. Long, J. Meng, and P. Ring, "Towards an ab initio covariant density functional theory for nuclear structure," *Progress in Particle and Nuclear Physics*, vol. 109, p. 103713, 2019.

[7] B. R. Barrett, "The no core shell model in an effective field theory framework," *Journal of Physics: Conference Series*, vol. 403, p. 012013, dec 2012.

[8] M. Hjorth-Jensen, M. P. Lombardo, and U. van Kolck, eds., *An advanced course in computational nuclear physics: Bridging the scales from quarks to neutron stars*, vol. 936 of *Lecture notes in physics*. Springer, 2017.

[9] L. Coraggio, S. Pastore, and C. Barbieri, "Editorial: The future of nuclear structure: Challenges and opportunities in the microscopic description of nuclei," *Frontiers in Physics*, vol. 8, p. 597, 2021.

[10] G. Colò, "Heavy nuclei: Introduction to density functional theory and variations on the theme," *The European Physical Journal Plus*, vol. 133, p. 553, Dec 2018.

[11] W. Huang, G. Audi, M. Wang, F. Kondev, S. Naimi, and X. Xu, "The ame2016 atomic mass evaluation (i). evaluation of input data; and adjustment procedures," *Chinese Physics C*, vol. 41, no. 3, p. 030002, 2017.

[12] M. Wang, G. Audi, F. Kondev, W. Huang, S. Naimi, and X. Xu, "The ame2016 atomic mass evaluation (ii). tables, graphs and references," *Chinese Physics C*, vol. 41, no. 3, p. 030003, 2017.

[13] I. Sick, "Form factors and radii of light nuclei," *Journal of Physical and Chemical Reference Data*, vol. 44, no. 3, p. 031213, 2015.

[14] R. F. Casten, *Nuclear Structure from a Simple Perspective*. New York, NY: Oxford Univ. Press, 1990.

[15] R. B. Wiringa, V. G. J. Stoks, and R. Schiavilla, "Accurate nucleon-nucleon potential with charge-independence breaking," *Phys. Rev. C*, vol. 51, pp. 38–51, Jan 1995.

[16] E. Matsinos, "A brief history of the pion-nucleon coupling constant," 2019.

[17] D. B. Kaplan, M. J. Savage, and M. B. Wise, "Nucleon-nucleon scattering from effective field theory," *Nuclear Physics B*, vol. 478, no. 3, pp. 629 – 659, 1996.

[18] K. Hebeler, "Three-nucleon forces: Implementation and applications to atomic nuclei and dense matter," *Physics Reports*, vol. 890, pp. 1–116, 2021.

[19] A. Deur, S. J. Brodsky, and G. F. de Taramond, "The QCD running coupling," *Progress in Particle and Nuclear Physics*, vol. 90, pp. 1 – 74, 2016.

[20] T. Hatsuda, "Lattice quantum chromodynamics and baryon-baryon interactions," *Frontiers of Physics*, vol. 13, no. 6, p. 132105, 2018.

[21] S. Weinberg, "Phenomenological Lagrangians," *Physica A: Statistical Mechanics and its Applications*, vol. 96, no. 1, p. 327, 1979.

[22] R. Machleidt, "Nuclear forces from chiral effective field theory," tech. rep., 2007.

[23] J. Goldstone, "Field theories with Superconductor solutions," *Il Nuovo Cimento*, vol. 19, pp. 154–164, Jan 1961.

[24] S. Weinberg, "Three-body interactions among nucleons and pions," *Physics Letters B*, vol. 295, no. 1, pp. 114 – 121, 1992.

[25] E. Epelbaum and U.-G. Meißner, "Chiral Dynamics of Few- and Many-Nucleon Systems," *Annual Review of Nuclear and Particle Science*, vol. 62, no. 1, pp. 159–185, 2012.

[26] K. Hebeler, J. Holt, J. Menendez, and A. Schwenk, "Nuclear Forces and Their Impact on Neutron-Rich Nuclei and Neutron-Rich Matter," *Annual Review of Nuclear and Particle Science*, vol. 65, no. 1, pp. 457–484, 2015.

[27] P. Bortignon, A. Bracco, and R. Broglia, *Giant Resonances: Nuclear Structure at Finite Temperature*. Harwood Academic Publisher, 1998.

[28] H. De Vries, C. De Jager, and C. De Vries, "Nuclear charge-density-distribution parameters from elastic electron scattering," *Atomic Data and Nuclear Data Tables*, vol. 36, no. 3, pp. 495–536, 1987.

[29] M. Bender, P.-H. Heenen, and P.-G. Reinhard, "Self-consistent mean-field models for nuclear structure," *Rev. Mod. Phys.*, vol. 75, pp. 121–180, 2003.

[30] G. Colo, L. Cao, N. V. Giai, and L. Capelli, "Self-consistent rpa calculations with skyrme-type interactions: The skyrme_rpa program," *Computer Physics Communications*, vol. 184, no. 1, pp. 142 – 161, 2013.

[31] G. Colò, "Density functional theory (dft) for atomic nuclei: A simple introduction," in *Proceedings of the International School of Physics "Enrico Fermi". Volume 201: Nuclear Physics with Stable and Radioactive Ion Beams*, pp. 95–128, Amsterdam: IOS Press, 2019.

[32] T. Nakatsukasa, K. Matsuyanagi, M. Matsuo, and K. Yabana, "Time-dependent density-functional description of nuclear dynamics," *Rev. Mod. Phys.*, vol. 88, p. 045004, 2016.

[33] D. Davesne, J. Navarro, J. Meyer, K. Bennaceur, and A. Pastore, "Two-body contributions to the effective mass in nuclear effective interactions," *Phys. Rev. C*, vol. 97, p. 044304, Apr 2018.

[34] P. Hohenberg and W. Kohn, "Inhomogeneous Electron Gas," *Phys. Rev.*, vol. 136, pp. B864–B871, 1964.

[35] N. Schunck, ed., *Energy Density Functional Methods for Atomic Nuclei*. IoP Publishing, 2019.

[36] G. Colò, "Nuclear density functional theory," *Advances in Physics: X*, vol. 5, no. 1, p. 1740061, 2020.

[37] A. Bohr, B. R. Mottelson, and D. Pines, "Possible analogy between the excitation spectra of nuclei and those of the superconducting metallic state," *Phys. Rev.*, vol. 110, pp. 936–938, 1958.

[38] J. Li, G. Colò, and J. Meng, "Microscopic linear response calculations based on the skyrme functional plus the pairing contribution," *Phys. Rev. C*, vol. 78, p. 064304, 2008.

[39] M. N. Harakeh and A. van der Woude, *Giant Resonances. Fundamental High-Frequency Modes of Nuclear Excitation*. Oxford University Press, 2001.

[40] R. Broglia, G. Coló, G. Onida, and H. Roman, *Solid State Physics of Finite Systems: Metal Clusters, Fullerenes, Atomic Wires*. Advanced Texts in Physics, Springer Berlin Heidelberg, 2004.

[41] P. A. Butler and W. Nazarewicz, "Intrinsic reflection asymmetry in atomic nuclei," *Rev. Mod. Phys.*, vol. 68, pp. 349–421, Apr 1996.

[42] P. Ring and P. Schuck, *The Nuclear Many-Body Problem.* Springer, 1980.

[43] J. M. Eisenberg and W. Greiner, *Excitation Mechanisms of the Nucleus. Electromagnetic and Weak Interaction.* North-Holland, 1979.

[44] J. D. Walecka, *Theoretical Nuclear and Subnuclear Physics.* World Scientific, 2004.

[45] C. A. Bertulani, *Nuclear Physics in a Nutshell.* Princeton University Press, 2007.

[46] N. K. Glendenning, *Direct Nuclear Reactions.* World Scientific, 2004.

[47] W. Cottingham and D. Greenwood, *An introduction to nuclear physics.* Cambridge University Press, 1986.

[48] S. N. Ghoshal, "An experimental verification of the theory of compound nucleus," *Phys. Rev.*, vol. 80, pp. 939–942, 1950.

[49] A. Bohr and B. R. Mottelson, *Nuclear Structure*, vol. I. Benjamin, New York, 1969.

[50] C. Bertulani, M. Hussein, and G. Münzenberg, *Physics of radioactive Beams.* Nova Science Publishers, 2001.

[51] H. A. Bethe and C. L. Critchfield, "The formation of deuterons by proton combination," *Phys. Rev.*, vol. 54, pp. 248–254, 1938.

[52] B. P. Abbott, R. Abbott, T. D. Abbott, F. Acernese, K. Ackley, C. Adams, T. Adams, P. Addesso, R. X. Adhikari, V. B. Adya, C. Affeldt, M. Afrough, B. Agarwal, M. Agathos, K. Agatsuma, N. Aggarwal, O. D. Aguiar, L. Aiello, A. Ain, P. Ajith, B. Allen, G. Allen, A. Allocca, M. A. Aloy, P. A. Altin, A. Amato, A. Ananyeva, S. B. Anderson, W. G. Anderson, S. V. Angelova, S. Antier, S. Appert, K. Arai, M. C. Araya, J. S. Areeda, N. Arnaud, K. G. Arun, S. Ascenzi, G. Ashton, M. Ast, S. M. Aston, P. Astone, D. V. Atallah, P. Aufmuth, C. Aulbert, K. AultONeal, C. Austin, A. Avila-Alvarez, S. Babak, P. Bacon, M. K. M. Bader, S. Bae, P. T. Baker, F. Baldaccini, G. Ballardin, S. W. Ballmer, S. Banagiri, J. C. Barayoga, S. E. Barclay, B. C. Barish, D. Barker, K. Barkett, F. Barone, B. Barr,

L. Barsotti, M. Barsuglia, D. Barta, J. Bartlett, I. Bartos, R. Bassiri, A. Basti, J. C. Batch, M. Bawaj, J. C. Bayley, M. Bazzan, B. Bécsy, C. Beer, M. Bejger, I. Belahcene, A. S. Bell, B. K. Berger, G. Bergmann, J. J. Bero, C. P. L. Berry, D. Bersanetti, A. Bertolini, J. Betzwieser, S. Bhagwat, R. Bhandare, I. A. Bilenko, G. Billingsley, C. R. Billman, J. Birch, R. Birney, O. Birnholtz, S. Biscans, S. Biscoveanu, A. Bisht, M. Bitossi, C. Biwer, M. A. Bizouard, J. K. Blackburn, J. Blackman, C. D. Blair, D. G. Blair, R. M. Blair, S. Bloemen, O. Bock, N. Bode, M. Boer, G. Bogaert, A. Bohe, F. Bondu, E. Bonilla, R. Bonnand, B. A. Boom, R. Bork, V. Boschi, S. Bose, K. Bossie, Y. Bouffanais, A. Bozzi, C. Bradaschia, P. R. Brady, M. Branchesi, J. E. Brau, T. Briant, A. Brillet, M. Brinkmann, V. Brisson, P. Brockill, J. E. Broida, A. F. Brooks, D. A. Brown, D. D. Brown, S. Brunett, C. C. Buchanan, A. Buikema, T. Bulik, H. J. Bulten, A. Buonanno, D. Buskulic, C. Buy, R. L. Byer, M. Cabero, L. Cadonati, G. Cagnoli, C. Cahillane, J. C. Bustillo, T. A. Callister, E. Calloni, J. B. Camp, M. Canepa, P. Canizares, K. C. Cannon, H. Cao, J. Cao, C. D. Capano, E. Capocasa, F. Carbognani, S. Caride, M. F. Carney, J. C. Diaz, C. Casentini, S. Caudill, M. Cavaglià, F. Cavalier, R. Cavalieri, G. Cella, C. B. Cepeda, P. Cerdá-Durán, G. Cerretani, E. Cesarini, S. J. Chamberlin, M. Chan, S. Chao, P. Charlton, E. Chase, E. Chassande-Mottin, D. Chatterjee, K. Chatziioannou, B. D. Cheeseboro, H. Y. Chen, X. Chen, Y. Chen, H.-P. Cheng, H. Chia, A. Chincarini, A. Chiummo, T. Chmiel, H. S. Cho, M. Cho, J. H. Chow, N. Christensen, Q. Chu, A. J. K. Chua, S. Chua, A. K. W. Chung, S. Chung, G. Ciani, R. Ciolfi, C. E. Cirelli, A. Cirone, F. Clara, J. A. Clark, P. Clearwater, F. Cleva, C. Cocchieri, E. Coccia, P.-F. Cohadon, D. Cohen, A. Colla, C. G. Collette, L. R. Cominsky, M. C. Jr., L. Conti, S. J. Cooper, P. Corban, T. R. Corbitt, I. Cordero-Carrión, K. R. Corley, N. Cornish, A. Corsi, S. Cortese, C. A. Costa, M. W. Coughlin, S. B. Coughlin, J.-P. Coulon, S. T. Countryman, P. Couvares, P. B. Covas, E. E. Cowan, D. M. Coward, M. J. Cowart, D. C. Coyne, R. Coyne, J. D. E. Creighton, T. D. Creighton, J. Cripe, S. G. Crowder, T. J. Cullen, A. Cumming, L. Cunningham, E. Cuoco, T. D. Canton, G. Dálya, S. L. Danilishin, S. D'Antonio, K. Danzmann, A. Dasgupta, C. F. D. S. Costa, V. Dattilo, I. Dave, M. Davier, D. Davis, E. J. Daw, B. Day, S. De, D. DeBra, J. Degallaix, M. D. Laurentis, S. Deléglise, W. D. Pozzo, N. Demos, T. Denker, T. Dent, R. D. Pietri, V. Dergachev, R. D. Rosa, R. T. DeRosa, C. D. Rossi, R. DeSalvo, O. de Varona, J. De-

venson, S. Dhurandhar, M. C. Díaz, L. D. Fiore, M. D. Giovanni, T. D. Girolamo, A. D. Lieto, S. D. Pace, I. D. Palma, F. D. Renzo, Z. Doctor, V. Dolique, F. Donovan, K. L. Dooley, S. Doravari, I. Dorrington, R. Douglas, M. D. Álvarez, T. P. Downes, M. Drago, C. Dreissigacker, J. C. Driggers, Z. Du, M. Ducrot, P. Dupej, S. E. Dwyer, T. B. Edo, M. C. Edwards, A. Effler, H.-B. Eggenstein, P. Ehrens, J. Eichholz, S. S. Eikenberry, R. A. Eisenstein, R. C. Essick, D. Estevez, Z. B. Etienne, T. Etzel, M. Evans, T. M. Evans, M. Factourovich, V. Fafone, H. Fair, S. Fairhurst, X. Fan, S. Farinon, B. Farr, W. M. Farr, E. J. Fauchon-Jones, M. Favata, M. Fays, C. Fee, H. Fehrmann, J. Feicht, M. M. Fejer, A. Fernandez-Galiana, I. Ferrante, E. C. Ferreira, F. Ferrini, F. Fidecaro, D. Finstad, I. Fiori, D. Fiorucci, M. Fishbach, R. P. Fisher, M. Fitz-Axen, R. Flaminio, M. Fletcher, H. Fong, J. A. Font, P. W. F. Forsyth, S. S. Forsyth, J.-D. Fournier, S. Frasca, F. Frasconi, Z. Frei, A. Freise, R. Frey, V. Frey, E. M. Fries, P. Fritschel, V. V. Frolov, P. Fulda, M. Fyffe, H. Gabbard, B. U. Gadre, S. M. Gaebel, J. R. Gair, L. Gammaitoni, M. R. Ganija, S. G. Gaonkar, C. Garcia-Quiros, F. Garufi, B. Gateley, S. Gaudio, G. Gaur, V. Gayathri, N. Gehrels, G. Gemme, E. Genin, A. Gennai, D. George, J. George, L. Gergely, V. Germain, S. Ghonge, A. Ghosh, A. Ghosh, S. Ghosh, J. A. Giaime, K. D. Giardina, A. Giazotto, K. Gill, L. Glover, E. Goetz, R. Goetz, S. Gomes, B. Goncharov, G. González, J. M. G. Castro, A. Gopakumar, M. L. Gorodetsky, S. E. Gossan, M. Gosselin, R. Gouaty, A. Grado, C. Graef, M. Granata, A. Grant, S. Gras, C. Gray, G. Greco, A. C. Green, E. M. Gretarsson, P. Groot, H. Grote, S. Grunewald, P. Gruning, G. M. Guidi, X. Guo, A. Gupta, M. K. Gupta, K. E. Gushwa, E. K. Gustafson, R. Gustafson, O. Halim, B. R. Hall, E. D. Hall, E. Z. Hamilton, G. Hammond, M. Haney, M. M. Hanke, J. Hanks, C. Hanna, M. D. Hannam, O. A. Hannuksela, J. Hanson, T. Hardwick, J. Harms, G. M. Harry, I. W. Harry, M. J. Hart, C.-J. Haster, K. Haughian, J. Healy, A. Heidmann, M. C. Heintze, H. Heitmann, P. Hello, G. Hemming, M. Hendry, I. S. Heng, J. Hennig, A. W. Heptonstall, M. Heurs, S. Hild, T. Hinderer, D. Hoak, D. Hofman, K. Holt, D. E. Holz, P. Hopkins, C. Horst, J. Hough, E. A. Houston, E. J. Howell, A. Hreibi, Y. M. Hu, E. A. Huerta, D. Huet, B. Hughey, S. Husa, S. H. Huttner, T. Huynh-Dinh, N. Indik, R. Inta, G. Intini, H. N. Isa, J.-M. Isac, M. Isi, B. R. Iyer, K. Izumi, T. Jacqmin, K. Jani, P. Jaranowski, S. Jawahar, F. Jiménez-Forteza, W. W. Johnson, N. K. Johnson-

McDaniel, D. I. Jones, R. Jones, R. J. G. Jonker, L. Ju, J. Junker, C. V. Kalaghatgi, V. Kalogera, B. Kamai, S. Kandhasamy, G. Kang, J. B. Kanner, S. J. Kapadia, S. Karki, K. S. Karvinen, M. Kasprzack, W. Kastaun, M. Katolik, E. Katsavounidis, W. Katzman, S. Kaufer, K. Kawabe, F. Kéfélian, D. Keitel, A. J. Kemball, R. Kennedy, C. Kent, J. S. Key, F. Y. Khalili, I. Khan, S. Khan, Z. Khan, E. A. Khazanov, N. Kijbunchoo, C. Kim, J. C. Kim, K. Kim, W. Kim, W. S. Kim, Y.-M. Kim, S. J. Kimbrell, E. J. King, P. J. King, M. Kinley-Hanlon, R. Kirchhoff, J. S. Kissel, L. Kleybolte, S. Klimenko, T. D. Knowles, P. Koch, S. M. Koehlenbeck, S. Koley, V. Kondrashov, A. Kontos, M. Korobko, W. Z. Korth, I. Kowalska, D. B. Kozak, C. Krmer, V. Kringel, B. Krishnan, A. Królak, G. Kuehn, P. Kumar, R. Kumar, S. Kumar, L. Kuo, A. Kutynia, S. Kwang, B. D. Lackey, K. H. Lai, M. Landry, R. N. Lang, J. Lange, B. Lantz, R. K. Lanza, A. Lartaux-Vollard, P. D. Lasky, M. Laxen, A. Lazzarini, C. Lazzaro, P. Leaci, S. Leavey, C. H. Lee, H. K. Lee, H. M. Lee, H. W. Lee, K. Lee, J. Lehmann, A. Lenon, M. Leonardi, N. Leroy, N. Letendre, Y. Levin, T. G. F. Li, S. D. Linker, T. B. Littenberg, J. Liu, R. K. L. Lo, N. A. Lockerbie, L. T. London, J. E. Lord, M. Lorenzini, V. Loriette, M. Lormand, G. Losurdo, J. D. Lough, C. O. Lousto, G. Lovelace, H. Lck, D. Lumaca, A. P. Lundgren, R. Lynch, Y. Ma, R. Macas, S. Macfoy, B. Machenschalk, M. MacInnis, D. M. Macleod, I. M. Hernandez, F. Magaña-Sandoval, L. M. Zertuche, R. M. Magee, E. Majorana, I. Maksimovic, N. Man, V. Mandic, V. Mangano, G. L. Mansell, M. Manske, M. Mantovani, F. Marchesoni, F. Marion, S. Márka, Z. Márka, C. Markakis, A. S. Markosyan, A. Markowitz, E. Maros, A. Marquina, F. Martelli, L. Martellini, I. W. Martin, R. M. Martin, D. V. Martynov, K. Mason, E. Massera, A. Masserot, T. J. Massinger, M. Masso-Reid, S. Mastrogiovanni, A. Matas, F. Matichard, L. Matone, N. Mavalvala, N. Mazumder, R. McCarthy, D. E. McClelland, S. McCormick, L. McCuller, S. C. McGuire, G. McIntyre, J. McIver, D. J. McManus, L. McNeill, T. McRae, S. T. McWilliams, D. Meacher, G. D. Meadors, M. Mehmet, J. Meidam, E. Mejuto-Villa, A. Melatos, G. Mendell, R. A. Mercer, E. L. Merilh, M. Merzougui, S. Meshkov, C. Messenger, C. Messick, R. Metzdorff, P. M. Meyers, H. Miao, C. Michel, H. Middleton, E. E. Mikhailov, L. Milano, A. L. Miller, B. B. Miller, J. Miller, M. Millhouse, M. C. Milovich-Goff, O. Minazzoli, Y. Minenkov, J. Ming, C. Mishra, S. Mitra, V. P. Mitrofanov, G. Mitselmakher, R. Mittleman, D. Moffa, A. Moggi, K. Mo-

gushi, M. Mohan, S. R. P. Mohapatra, M. Montani, C. J. Moore, D. Moraru, G. Moreno, S. R. Morriss, B. Mours, C. M. Mow-Lowry, G. Mueller, A. W. Muir, A. Mukherjee, D. Mukherjee, S. Mukherjee, N. Mukund, A. Mullavey, J. Munch, E. A. Muñiz, M. Muratore, P. G. Murray, K. Napier, I. Nardecchia, L. Naticchioni, R. K. Nayak, J. Neilson, G. Nelemans, T. J. N. Nelson, M. Nery, A. Neunzert, L. Nevin, J. M. Newport, G. Newton, K. K. Y. Ng, T. T. Nguyen, D. Nichols, A. B. Nielsen, S. Nissanke, A. Nitz, A. Noack, F. Nocera, D. Nolting, C. North, L. K. Nuttall, J. Oberling, G. D. O'Dea, G. H. Ogin, J. J. Oh, S. H. Oh, F. Ohme, M. A. Okada, M. Oliver, P. Oppermann, R. J. Oram, B. O'Reilly, R. Ormiston, L. F. Ortega, R. O'Shaughnessy, S. Ossokine, D. J. Ottaway, H. Overmier, B. J. Owen, A. E. Pace, J. Page, M. A. Page, A. Pai, S. A. Pai, J. R. Palamos, O. Palashov, C. Palomba, A. Pal-Singh, H. Pan, H.-W. Pan, B. Pang, P. T. H. Pang, C. Pankow, F. Pannarale, B. C. Pant, F. Paoletti, A. Paoli, M. A. Papa, A. Parida, W. Parker, D. Pascucci, A. Pasqualetti, R. Passaquieti, D. Passuello, M. Patil, B. Patricelli, B. L. Pearlstone, M. Pedraza, R. Pedurand, L. Pekowsky, A. Pele, S. Penn, C. J. Perez, A. Perreca, L. M. Perri, H. P. Pfeiffer, M. Phelps, O. J. Piccinni, M. Pichot, F. Piergiovanni, V. Pierro, G. Pillant, L. Pinard, I. M. Pinto, M. Pirello, M. Pitkin, M. Poe, R. Poggiani, P. Popolizio, E. K. Porter, A. Post, J. Powell, J. Prasad, J. W. W. Pratt, G. Pratten, V. Predoi, T. Prestegard, M. Prijatelj, M. Principe, S. Privitera, G. A. Prodi, L. G. Prokhorov, O. Puncken, M. Punturo, P. Puppo, M. Prrer, H. Qi, V. Quetschke, E. A. Quintero, R. Quitzow-James, F. J. Raab, D. S. Rabeling, H. Radkins, P. Raffai, S. Raja, C. Rajan, B. Rajbhandari, M. Rakhmanov, K. E. Ramirez, A. Ramos-Buades, P. Rapagnani, V. Raymond, M. Razzano, J. Read, T. Regimbau, L. Rei, S. Reid, D. H. Reitze, W. Ren, S. D. Reyes, F. Ricci, P. M. Ricker, S. Rieger, K. Riles, M. Rizzo, N. A. Robertson, R. Robie, F. Robinet, A. Rocchi, L. Rolland, J. G. Rollins, V. J. Roma, R. Romano, C. L. Romel, J. H. Romie, D. Rosińska, M. P. Ross, S. Rowan, A. Rdiger, P. Ruggi, G. Rutins, K. Ryan, S. Sachdev, T. Sadecki, L. Sadeghian, M. Sakellariadou, L. Salconi, M. Saleem, F. Salemi, A. Samajdar, L. Sammut, L. M. Sampson, E. J. Sanchez, L. E. Sanchez, N. Sanchis-Gual, V. Sandberg, J. R. Sanders, B. Sassolas, B. S. Sathyaprakash, P. R. Saulson, O. Sauter, R. L. Savage, A. Sawadsky, P. Schale, M. Scheel, J. Scheuer, J. Schmidt, P. Schmidt, R. Schnabel, R. M. S. Schofield, A. Schnbeck, E. Schreiber, D. Schuette, B. W.

Schulte, B. F. Schutz, S. G. Schwalbe, J. Scott, S. M. Scott, E. Seidel, D. Sellers, A. S. Sengupta, D. Sentenac, V. Sequino, A. Sergeev, D. A. Shaddock, T. J. Shaffer, A. A. Shah, M. S. Shahriar, M. B. Shaner, L. Shao, B. Shapiro, P. Shawhan, A. Sheperd, D. H. Shoemaker, D. M. Shoemaker, K. Siellez, X. Siemens, M. Sieniawska, D. Sigg, A. D. Silva, L. P. Singer, A. Singh, A. Singhal, A. M. Sintes, B. J. J. Slagmolen, B. Smith, J. R. Smith, R. J. E. Smith, S. Somala, E. J. Son, J. A. Sonnenberg, B. Sorazu, F. Sorrentino, T. Souradeep, A. P. Spencer, A. K. Srivastava, K. Staats, A. Staley, M. Steinke, J. Steinlechner, S. Steinlechner, D. Steinmeyer, S. P. Stevenson, R. Stone, D. J. Stops, K. A. Strain, G. Stratta, S. E. Strigin, A. Strunk, R. Sturani, A. L. Stuver, T. Z. Summerscales, L. Sun, S. Sunil, J. Suresh, P. J. Sutton, B. L. Swinkels, M. J. Szczepańczyk, M. Tacca, S. C. Tait, C. Talbot, D. Talukder, D. B. Tanner, M. Tápai, A. Taracchini, J. D. Tasson, J. A. Taylor, R. Taylor, S. V. Tewari, T. Theeg, F. Thies, E. G. Thomas, M. Thomas, P. Thomas, K. A. Thorne, K. S. Thorne, E. Thrane, S. Tiwari, V. Tiwari, K. V. Tokmakov, K. Toland, M. Tonelli, Z. Tornasi, A. Torres-Forné, C. I. Torrie, D. Tyr, F. Travasso, G. Traylor, J. Trinastic, M. C. Tringali, L. Trozzo, K. W. Tsang, M. Tse, R. Tso, L. Tsukada, D. Tsuna, D. Tuyenbayev, K. Ueno, D. Ugolini, C. S. Unnikrishnan, A. L. Urban, S. A. Usman, H. Vahlbruch, G. Vajente, G. Valdes, N. van Bakel, M. van Beuzekom, J. F. J. van den Brand, C. V. D. Broeck, D. C. Vander-Hyde, L. van der Schaaf, J. V. van Heijningen, A. A. van Veggel, M. Vardaro, V. Varma, S. Vass, M. Vasúth, A. Vecchio, G. Vedovato, J. Veitch, P. J. Veitch, K. Venkateswara, G. Venugopalan, D. Verkindt, F. Vetrano, A. Viceré, A. D. Viets, S. Vinciguerra, D. J. Vine, J.-Y. Vinet, S. Vitale, T. Vo, H. Vocca, C. Vorvick, S. P. Vyatchanin, A. R. Wade, L. E. Wade, M. Wade, R. Walet, M. Walker, L. Wallace, S. Walsh, G. Wang, H. Wang, J. Z. Wang, W. H. Wang, Y. F. Wang, R. L. Ward, J. Warner, M. Was, J. Watchi, B. Weaver, L.-W. Wei, M. Weinert, A. J. Weinstein, R. Weiss, L. Wen, E. K. Wessel, P. Weßels, J. Westerweck, T. Westphal, K. Wette, J. T. Whelan, S. E. Whitcomb, B. F. Whiting, C. Whittle, D. Wilken, D. Williams, R. D. Williams, A. R. Williamson, J. L. Willis, B. Willke, M. H. Wimmer, W. Winkler, C. C. Wipf, H. Wittel, G. Woan, J. Woehler, J. Wofford, K. W. K. Wong, J. Worden, J. L. Wright, D. S. Wu, D. M. Wysocki, S. Xiao, H. Yamamoto, C. C. Yancey, L. Yang, M. J. Yap, M. Yazback, H. Yu, H. Yu, M. Yvert, A. Zadrożny, M. Zanolin, T. Zelenova, J.-P. Zendri, M. Zevin, L. Zhang, M. Zhang,

T. Zhang, Y.-H. Zhang, C. Zhao, M. Zhou, Z. Zhou, S. J. Zhu, X. J. Zhu, A. B. Zimmerman, M. E. Zucker, J. Zweizig, E. Burns, P. Veres, D. Kocevski, J. Racusin, A. Goldstein, V. Connaughton, M. S. Briggs, L. Blackburn, R. Hamburg, C. M. Hui, A. von Kienlin, J. McEnery, R. D. Preece, C. A. Wilson-Hodge, E. Bissaldi, W. H. Cleveland, M. H. Gibby, M. M. Giles, R. M. Kippen, S. McBreen, C. A. Meegan, W. S. Paciesas, S. Poolakkil, O. J. Roberts, M. Stanbro, V. Savchenko, C. Ferrigno, E. Kuulkers, A. Bazzano, E. Bozzo, S. Brandt, J. Chenevez, T. J.-L. Courvoisier, R. Diehl, A. Domingo, L. Hanlon, E. Jourdain, P. Laurent, F. Lebrun, A. Lutovinov, S. Mereghetti, L. Natalucci, J. Rodi, J.-P. Roques, R. Sunyaev, P. Ubertini, , and and, "Gravitational Waves and Gamma-Rays from a Binary Neutron Star Merger: GW170817 and GRB 170817a," *The Astrophysical Journal*, vol. 848, p. L13, oct 2017.

[53] R. R. Silbar and S. Reddy, "Neutron stars for undergraduates," 2003.

[54] J. Rikovska Stone, J. C. Miller, R. Koncewicz, P. D. Stevenson, and M. R. Strayer, "Nuclear matter and neutron-star properties calculated with the skyrme interaction," *Phys. Rev. C*, vol. 68, p. 034324, 2003.

[55] N. Chamel and P. Haensel, "Physics of Neutron Star Crusts," *Living Reviews in Relativity*, vol. 11, no. 10, p. 10, 2008.

[56] C. J. Pethick, "Dense matter and neutron stars: Some basic notions," 2019.

[57] C. Y. Wong, "Interaction barrier in charged-particle nuclear reactions," *Phys. Rev. Lett.*, vol. 31, pp. 766–769, 1973.

[58] K. Hagino, "Sub-barrier fusion reactions, to be published in "Handbook of Nuclear Physics", Springer (2022)," 2022.

[59] N. Bohr and J. A. Wheeler, "The mechanism of nuclear fission," *Phys. Rev.*, vol. 56, pp. 426–450, 1939.

[60] M. S. Plesset, "On the classical model of nuclear fission," *American Journal of Physics*, vol. 9, no. 1, pp. 1–10, 1941.